UC Berkeley
SEMM Reports Series

Title
Durability and Integrity of Marble

Permalink
https://escholarship.org/uc/item/6r23x6bw

Authors
Monteiro, Paulo
Cohen, Julie

Publication Date
1993-12-01

eScholarship.org Powered by the California Digital Library
University of California

REPORT NO.
UCB/SEMM-93/13

STRUCTURAL ENGINEERING
MECHANICS AND MATERIALS

LOAN COPY
PLEASE RETURN TO
NISEE/Computer Applications
404A Davis Hall
Univ. of California, Berkeley 94720

DURABILITY AND INTEGRITY OF MARBLE

by

PAULO J. M. MONTEIRO

and

JULIE MARK COHEN

December 1993

DEPARTMENT OF CIVIL ENGINEERING
UNIVERSITY OF CALIFORNIA
BERKELEY, CALIFORNIA

ACKNOWLEDGMENTS

We thank the National Science Foundation (grant no. 8912224), the Marble Institute of America and the Masonry Institute of America for the financial support. We particularly wish the acknowledge the help and support given by Dr. K. Chong during this research .

Many researchers participated in the experimental work. Dr. Tarcisio Celestino developed and implemented the modified "Brazilian test" to obtain fracture mechanics properties. Dr. R. Piltner made the finite element simulations for this test. The following Ph.D. students actively participated in the research work: C.T Chang, K. Folliard, K. Nemati and U. Nilsen. As usual, the experimental program was easier to implement due to the diligent efforts of Mr. Jon G. Asselanis and William G. MacCracken at the UCB Civil Engineering Materials Lab.

One of the goals of this research was to obtain results of marble that is currently used in engineering construction. We thank the following individuals and companies for their generous donations: Ms. Barbara E. Cohen of the Domestic Marble & Stone Corporation for the white carrara marble specimens, Ms. Cynthia Ramage of C. Melchers & Co. America, Inc. for the Chinese marble samples, Mr. E. William Richardson from the Vermont Marble Company and Mr. George E. Duncan from Georgia Marble Company for the marble slabs.

ABSTRACT

This report present the experimental results from a comprehensive research on the mechanical and durability behavior of marble. A new test method for the measurement of the fracture toughness of different types of marble was suggested. The test is based on the traditional "Brazilian" or splitting test performed under constant strain rate. The experimental procedure is extremely simple and it does not require polishing of the sample. Four types of marble (Georgia, Vermont, Italian and Chinese) were tested in a Brazilian test under controlled strain rate. The test was fully controlled as it can be observed by the stable crack growth that originates the strain softening once the maximum load is achieved. Using the results obtained from the finite element methods it was possible to compute the fracture toughness of the various types of marble. It was found that there is an inverse relationship between fracture toughness and crystal size.

The sensitivity of marble samples to slow crack growth was also studied. The fundamental equation relating strength and load rate was derived for the four types of marble studied. It was found that there is a correlation between the constant n (of the equation $S_f^{N+1} + B\,\dot{\sigma}\,S_f^{N-2} = B\,\dot{\sigma}\,S_f^{N-2}$) and the crystal size of the marble.

The preservation of stress-induced structure and the identification of cracks induced by loading and unloading are important to understand the mechanisms for the generation, propagation and interaction of stress-induced microcracks in complex systems such as marble. To preserve the microstructure in marble specimens under load, the voids were filled with a liquid metal alloy called "Wood's metal" during loading, and the alloy was solidified in place before unloading. Such a technique not only allows one to observe the microcracks as they exist under load, but also facilitates observing the microcracks in three dimensions . A comprehensive image analysis was performed on the cracking pattern developed in the marble samples. Also the propagation of the cracking process was modeled using discontinuous deformation analysis with finite element mesh. The discontinuous approach provides another way to understand the postfailure effect and global stability of the structure system.

This report presents experimental results on the effects on marble specimens when submerged in a sodium sulfate solution that was cycled across the crystallization temperature for mirabilite. The samples were periodically weighted (wet weight) to monitor deterioration. The marble samples were not affected by sodium sulfate. Even after 77 cycles, the weight of original samples were unchanged. It was interesting that the marble samples with crack induced by external mechanical load were not affected by sodium sulfate even after 52 cycles. The amount of damage is a function of the permeability of the samples.

Table of Contents

CHAPTER 1

INTRODUCTION

Technological changes and increased knowledge in the field of structural engineering over the past century have led to changes in the use of masonry and natural stone cladding in building construction. Prior to 1900, masonry was used as load bearing walls that were often more than sixteen inches thick. With the development of reinforced concrete and steel skeleton frame buildings and taller buildings, the use of masonry shifted away from load bearing walls. After World War II, there was a trend towards the use of thin curtain walls for which masonry and natural stone were used for their aesthetic and *assumed* durability qualities (see Moore, et al. [1980]). It should be noted that the use of thinner panels was not justified by any new knowledge about the material properties of masonry and natural stones used as exterior panels.

Marble is a nontraditional cladding material for high-rise buildings. During recent years, improvements in the cutting process have allowed panel thicknesses to decrease markedly. This has led to a dramatic increase in the use of this form of natural stone cladding and to a concern raised by Monk [1985]: "At what point is thin, too thin?" It has also led to recent nation-wide problems with some marble cladding on buildings that are no more than twenty years old. In addition to disastrous economic consequences for the building owners and the marble and curtain wall industries, there are potential risks to life associated with the use of thin marble panels on high-rise construction that may be dangerously increased in the future.

Observed problems of marble cladding include severe and permanent bowing of the material. One example is shown in Fig. 1. Another classic example is found in the graveyards of New Orleans, Louisiana, where the thin, rectangular marble slabs, supported vertically on the top and bottom ends, have bowed outwards at mid-height (see Winkler [1973]). In buildings, this type of deformation may result in the eventual failure of some or all anchorages of the cladding to the structural frame. One of the first buildings for which a solution to excessive bowing was sought is the Lincoln First Tower in Rochester, New York. Unfortunately, the solution was the replacement of all marble with aluminum panels at a cost of about $20 million (Sulzer [1988]). Another more notorious example is the 1,136 foot tall Amoco Building in Chicago clad with 43,000 marble panels each weighing about 275 pounds. Once again, the marble panels will be replaced, but this time with granite and at a cost originally projected to be $20 million (see Trewhitt and Tuchman [1988]), and more recently estimated to be $60 to $80 million (see Arndt [1989]). Obviously, these costs reflect the severity and extent of the litigation involved in trying to resolve the issues of blame and to repair or replace the facade panels.

1.2. BACKGROUND ON THE DURABILITY AND INTEGRITY OF MARBLE CLADDING

1. 2.1 Properties of Marble

Marble is a carbonate rock formed from metamorphic (recrystallized) limestone which is composed principally of crystalline grains of carbonate minerals calcite and dolomite, singly or in combination. (Fig. 2). Grain sizes vary as evidenced by the large crystals in Georgia marble, medium to large crystals in Vermont Danby marble, and the small crystals in Italian white Carrara marble. The grains can be irregular in shape and interlocking (i.e., tightly packed) as in the Georgia and Vermont marbles, or regular in shape and size as the rounded and somewhat spherical grains of the white Carrara marble. The percentage of natural cements between the crystals is a function of the various grain packings.

The scientific research on the properties of marble started last century with the work of many investigators, among them, Bard [1828], Bauschinger [1884] and Johnson [1897]. Bauschinger [1884] was a pioneer in the research of the mechanical properties of building stones and their significance in the design. In 1884, he published a most comprehensive study where the following properties of building stones of Bavaria were determined: modulus of elasticity, modulus of rupture, compressive strength perpendicular and parallel to bed, tensile strength and shearing strength both parallel and perpendicular to bed. In 1911, von Karman used a blue-veined white Carrara marble and a red sandstone from Muttenberg as the materials for the now classic tests on the effect of confining pressures on the mechanical behavior. The results showed that at low confining pressures, marble fails in a brittle manner, but with increasing confining pressures a ductile behavior would manifest.

The degree of anisotropy[1] in marble has prevented the use of new sophisticated methods of modelling materials behavior. A clear indication was the study of Ratigan [1981] on the use of statistical fracture mechanics for the strength of brittle rock, where a

---

[1] An anisotropic (aelotropic) material is one with certain properties varying with direction at any point (see Jumikis [1983])

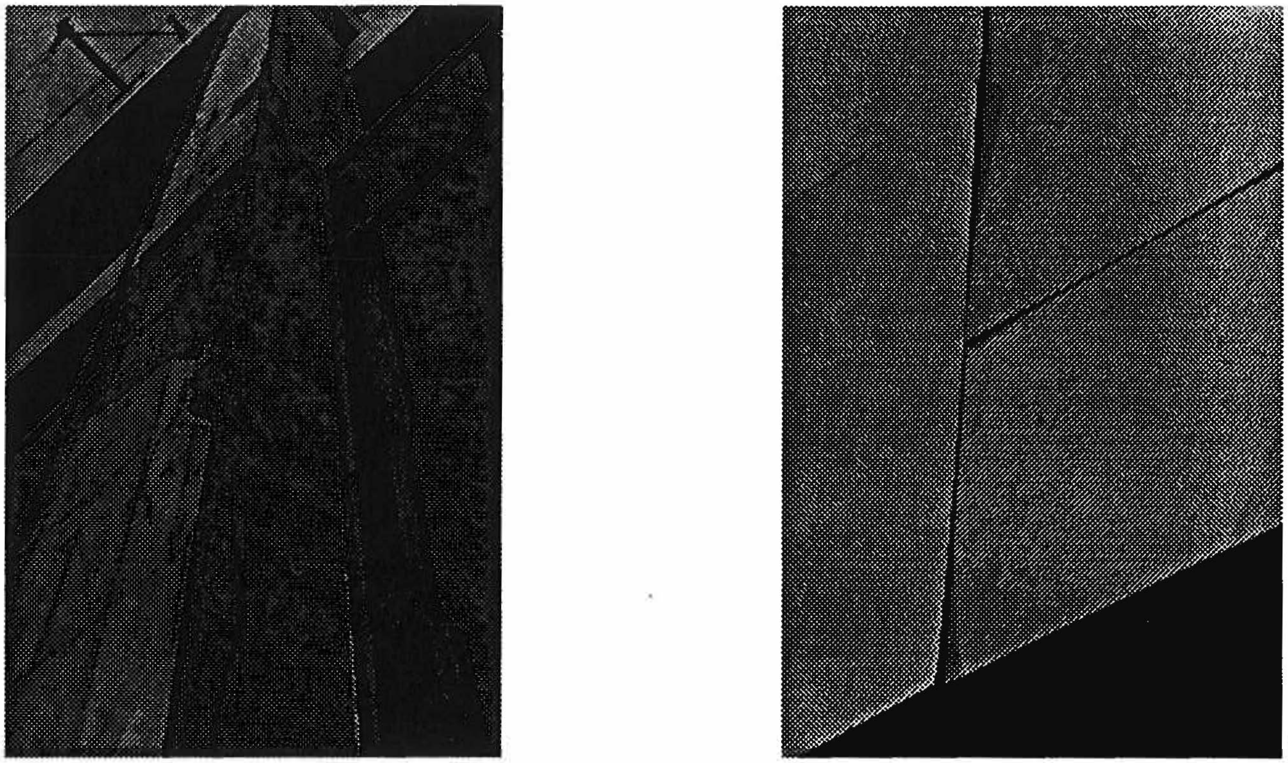

(a) (b)

Fig 1

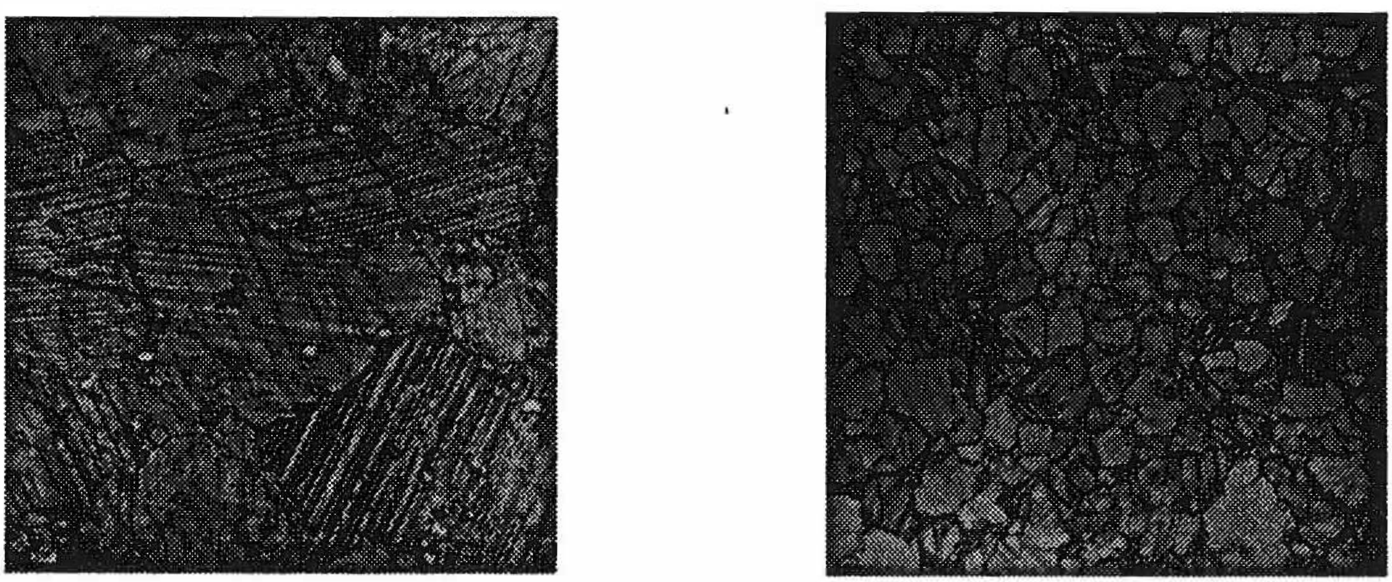

(a) (b)

Fig. 2

three parameter statistical fracture mechanics model with strain energy rate as the variant was successfully used for granite but failed for marble. According to Ratigan, for (Carrara) marble specimens "anisotropy (both in apparent tensile strength and size effect) precludes the use of contemporary statistical fracture mechanics models".

The physical properties of marble recognized in the U.S. by ASTM include compressive strength, flexural strength, shear strength, modulus of elasticity, density, absorption (48 hour soak), thermal conductivity "k", water vapor permeability, coefficient of thermal expansion, and creep deflection (after 24 hours). For the determination of these properties and comparison to physical requirements, the following ASTM Standards and Specifications and Test Methods are used: C503-89, Marble Building Stone (Exterior); C97-83, Absorption and Bulk Specific Gravity of Natural Building Stone; C99-87, Modulus of Rupture of Natural Building Stone; C170-87, Compressive Strength of Natural Building Stone; and C880-89, Flexural Strength of Natural Building Stone. It is interesting to note that, as yet, the ASTM Standards and Test Methods for exterior marble dimensional stone neither recognize nor make any distinction among the marbles and their inherent chemical and microstructural differences, nor offers any time dependent tests such as durability and longer-term creep tests.

The required material properties according to the Manuale dei Marmi Pietre Graniti [1988] are given in Table 1.

TABLE 1

External Agent	**Relevant Material Property**
Wind Action	Elastic Modulus, Flexure Strength
Load on the Structure	Unit Weight
Thermal Insulation	Thermal Expansion Coeff., Frost Resistance
Humidity, Ice	Absorption Coefficient, Frost Resistance
Anchorage System	Flexure Strength, Toughness, Microhardness
Seismic Zone	Compressive and Flexural Strengths, Elastic Modulus
Aggressive Atmosphere	Resistance to chemical agents

1.2.2 Design Guidelines for Marble Cladding

U.S. Handbooks for Specification of Marble Cladding and Attachments

Since there are no nationally available design guidelines for marble cladding, architects use their discretion in choosing the length and width dimensions of panels. They rely upon such references as the Marble Institute of America [1987] and the Masonry Institute of America [1989] for design criteria, as well as the suppliers for advice regarding panel thickness and methods of panel attachments to the structural frame.

The Marble Institute of America [1987] publishes a dimensional stone design manual in which maximum fabricated sizes are specified. Marble classified as Group "A" classification can be used as exterior cladding with maximum sizes of 60" (150 cm) wide by 84" (210 cm) long. Group "A" includes "sound marbles and stones, with uniform and favorable working qualities" for which no specific thicknesses are recommended in correlation with panel width and length dimensions. In a table from ASTM C503-85 for gauged tolerances, the thickness of thin stock ranges from 3/4" (2 cm) to 2" (5 cm). According to the ASTM criteria, the thickness and size of panels required can be found by: (1) determining the design and wind load; (2) obtaining the flexural strength of the marble from ASTM C880 or from the marble supplier; and (3) selecting "the unsupported span for each thickness for which the stress is below the flexural strength of the marble from the appropriate table." A safety factor of 5.0 is recommended based on the use of marble as "an independent unit, curtain wall or veneer."

The Marble Institute of America [1987] contains a table of physical properties of marble from tests of sixteen American marbles. None of the strength and physical requirements for marble necessarily preclude the use of 60" x 70" x 3/4" (150 cm x 210 cm x 2 cm) panels, a panel size which has many disadvantages including fragility during transportation to the site, and erection and attachment to the building.

For the installation of exterior anchors, the Marble Institute of America [1987] provides the following comments: "Anchor sizing is dependent upon materials, codes and physical conditions of the structure. Anchors should be engineered separately for each project... Every construction condition requires engineering based on specific factors for each project - panel weight, wind load, back-up material, structural flexure, seismic conditions, etc. And, ...local codes take precedence. Ask manufacturers of anchoring systems for technical information and engineering formulae." This recommended procedure does not always ensure the preparation of technically competent panel attachment details. In some localities, however, calculations and drawings for anchors must be stamped. In addition, many localities require a controlled engineering inspection during construction. It is noted that there do not seem to be any requirements that a licensed professional engineer stamp and sign the marble panel drawings.

The Masonry Institute of America [1989] provides more detailed information including a chapter on design requirements with the following sections: code requirements, design principles, construction tolerances, loads, selection of gravity and lateral anchors, typical joint design and caulking, flashing, venting of cavity veneer walls, and fabrication of stone panels. The section on design principles include criteria for lateral load, differential movement, thermal movement, deformation, shrinkage, deviations, and freeze/thaw. The referenced technical data, testing and standards are similar to those in the Marble Institute of America [1987].

The Vermont Marble Company [1980] has recognized the material properties and their effect on marble panels in their in-house manual entitled *Exterior Veneer Standards*. Richardson [1989] has offered many valuable comments on the content of these standards. First, the Vermont Marble Company no longer recommends 7/8" (2.2 cm) for any exterior use. (The next increment in thickness is about 1 1/4" (3.2 cm).) Smaller multiples of the slab size of 72" (183 cm) x 86" (218 cm) are promoted. Richardson commented, "The larger the finished size of the piece, the more difficult it is to properly anchor in such a way as to prevent bowing." The manual also contains information pertaining to the number and distribution of anchorages. "For 1 1/4" (3.2 cm) material and thicker, no anchor shall be located farther than 24" (61 cm) from the next nearest anchor. Richardson commented that this is "the real key to resisting bowing... A structural engineer, unfamiliar with the potential for bowing in a thin marble veneer, and designing only for loads that must be resisted by the marble and its anchorage system, would normally consider the total number of anchors we recommend (as) excessive. However, the distribution (or locations) is fully as critical as the number". Additional information is contained within the manual on joints, setting, and building codes.

The Georgia Marble Company has published information pertaining to their Zibell Anchoring System in which they also recognize the importance of specifying both panel sizes and maximum strut spacing for the anchoring system. They recommend 54" (137 cm) as the maximum panel height without the use of intermediate anchors. Even though the manual allows for 7/8" (2.2 cm) thick panels, the panel height of the marble determines the horizontal spacing of the grid struts. As the panel heights increase, the maximum strut spacing decreases, to provide additional stiffness transverse to the panels. However, the maximum strut spacing is smaller for the 1 1/4" (3.2 cm) panel than the

7/8" (2.2 cm) panel. The manual also includes the specifications for exterior marble and an outline procedure for installation.

Dimensions of Marble Used as Cladding

Dimensions of marble used as cladding, including thicknesses which are significantly less than what was used several decades ago, can be found in a summary of the use and failures in the use of natural stone cladding is described by Bortz, et al. [1988]. Bortz, et al., stated that the majority of the buildings using thin panels of limestone, travertine, marble and granite cladding have been constructed during the last twenty-five years, many of which were built in the last decade. "The stone facades being considered are less than 5 cm. thick. Typically, they may range downward in thickness as follows: 5 cm. (1 15/16 in.); 3 cm. (1 3/16 in.); 2.5 cm. (1 in.); and 2.0 cm. (13/16 in.). The maximum size stone is generally not over 20 ft^2 (1.86 m^2), giving rise to the following typical sizes (expressed in feet and meters, respectively): 4 by 5 (1.22 by 1.52); 3 by 6 2/3 (0.92 by 2.03); 2 1/2 by 8 (0.76 by 2.44); 2 by 10 (0.61 by 3.05)." They mentioned that "traditional stone quarrying and fabrication techniques control these limits. The weight of such stones is generally under 600 lb. (1320 kg.) each - down to where two or four men can handle the piece."

"The thinness of stone now in use presents problems which have never before been an issue. ...the strength properties (compression, tension, and shear) are of major concern. Currently, however, the coefficients of thermal and moisture expansion, the effects of repeated temperature variation, permeability of the stone, and the durability and resistance to weathering bear increasing influence as the thickness of stone -sed decreases. Other physical characteristics which become more important are the size of the grain, overall quality, and variability of the specific type of stone to be used on the project" as noted by Cantor and Juda [1988].

1. 2.3 Durability

Durability issues have been raised for each of the many uses of natural stones. In recent years the increase of pollution levels in major industrial centers is causing degradation of structural materials. Marble cladding is particularly susceptible to the acidic atmospheres, which is expected because significant amounts of carbon dioxide (CO_2), sulfur dioxide (SO_2) and nitric acid are present in the pollutants (see Seinfeld [1986]). These gases dissolved in the atmospheric water (creating "acid rain") initiate a series of oxidation reactions in cladding. It should be noted that the solubility of calcite in water is small, however it becomes significant in the presence of carbonic acid, sulfuric and sulfurous acids. The sulfur dioxide can be more deleterious because, if given the adequate environments conditions, it can form sulfuric acid which attacks the marble forming calcium sulfate hydrated (gypsum). The cyclic process of dissolution and precipitation can create greater porosity and cracking in the material.

It is important to realize that the degradation is not only caused by oxidation reaction, but also by physical actions. The main element of this class of deterioration is the differential thermal strain that is originated in the marble due to temperature changes. Calcite crystal has a strong degree of anisotropy, so the coefficient of thermal expansion is not a scalar (as for homogeneous materials), but a vector. Equally important is the frost resistance that the marble must have to support the internal stresses provided by the ice formation inside its porous matrix.

Bauschinger (see Johnson [1897]) was one of the first researchers to propose a freezing test for natural stones. According to his method, the specimens went for 25 cycles of freezing and thawing after which the loss in dry weight and loss of compressive strength were determined. Johnson critique this method because "the loss in weight by this method is so insignificant as to furnish a very small base from which to estimate the relative weathering qualities of the stone..." and ... "the test for strength is also quite as unsatisfactory, since here comparison must be made between specimens of the same stone, and a safe conclusion would have to rest upon average results of a large number of tests, and the results would still be only relative". It should be noted that many researchers still use Bauschinger's freezing test with some modifications to establish the frost resistance of marble.

The scientific study of disintegration of natural stones started at the beginning of the nineteenth century. As early as 1828, Brard proposed a comprehensive methodology of analysis by immersing specimens in a boiling solution of sulfate of soda ($Na_2SO_4.10H_2O$) for some specified time and them removing the batch to let the salt to crystallize. The cycle was done for a week and the weight loss of the specimens were measured.

For marble used as cladding on buildings, an attempt has been made to provide a standard definition of "durability" for dimension stones in ASTM standard C119-87a. Durability is "the measure of the ability of dimension stone to endure and to maintain its essential and distinctive characteristics of strength, resistance to decay, and appearance. Durability is based on the length of time that a stone can maintain its innate characteristics in use. This time will vary depending on the environment and use of the stone in question." Weathering is defined as the "natural alteration by either chemical or mechanical processes due to the action of the constituents of the atmosphere, surface water or ground water, or to temperature change."

However, the ASTM definition of "durability" alone does not serve any practical purpose, since durability problems continue to persist. For example, Bortz, et al. [1988] have stated that "with the advent of exterior thin veneer, weathering deterioration is more critical. Planes of weather weakness may exist along the veins in metamorphic marble stone... The material anomalies were less important in earlier thicker stone uses greater than 3 in. (63.2 mm.) cubic stock. With stone 2 in. (50.8 mm.) and under, planes of weathering weakness can pass through the entire thickness, resulting in potential freeze-thaw damage that can cleave the stone piece into separate parts." They continued, "Bowing of thin marble can occur. This is believed (to be) caused by a permanent hysteresis growth in the stone due to a differential temperature or moisture change through its thickness. Generally convexed outward, the phenomena can be concaved inward depending on boundary and gradient conditions."

Gere [1988] recommended that "an extensive testing program is necessary before ASTM standards can address the durability issue of dimension stone. Research data are needed for the loss in strength of sedimentary, metamorphic, and igneous stones using different types of surface applied finishes (for exterior cladding panels)." He stated that "lately, on a few large jobs, ASTM Test Method for Resistance of Concrete to Rapid Freezing and Thawing (C666-84) has been specified for analyzing the resistance to freeze\thaw cycles of stone. As ASTM C666 does not represent the actual atmospheric and thermal conditions, a special durability test may be desirable." He made no particular recommendations beyond these suggestions.

Some work on the development of durability tests for marble has been done by (forensic) engineering firms involved in investigative testing and research. Thomasen and Ewart [1984] examined and analyzed the durability of thin marble by field examinations and by laboratory testing. Their report covered a broad range of observed problems including: cracking, crushing, buckling and bowing, failure of fastening and anchors, and surface deterioration. They concluded that the "lack of durability and the potential for deterioration in new veneer installations can often be discovered by laboratory tests.

For marble, problems with the durability of ancient sculptures are no exception. In an article by Margolis [1989], the problems of authenticating ancient marbles are discussed. The author pointed out that dolomitic marble of calcium magnesium carbonate is more durable and generally more resistant to weathering then calcitic marble. With reference to a calcite layer on the sculpture under examination, the author points out that "dolomite is well known to change into calcite through weathering. In this process, known as dedolomitization, magnesium atoms in dolomite crystals are slowly replaced by calcium atoms." With reference to sculptures of calcite, he stated, "Calcite is more soluble than dolomite... In weathered calcite the crystal structure changes gradually from micritic calcite at the surface to fresh marble in the interior (of a sculpture)... The exact rate of weathering also depends on such characteristics of the marble as the crystal size and intergranular porosity."

Not all marbles which presently qualify as exterior cladding quality are durable. Even the new 1989 ASTM Test Method C97 for absorption by weight by itself does not necessarily exclude those marbles which have bowed excessively in the recent past. In this standard, the allowable absorption by weight has decreased to a maximum of 0.20% from 0.75% in previous versions of this standard.

The majority of marble cladding problems have been found and may continue to be found in marbles with smaller, more spherical grains which are relatively more loosely packed. This seems to indicate that the volumetric content of the natural cement in marble, as well as the crystal size, may play an important role in the moisture activated bowing of marble cladding panels. The Rilem Committee 25-PEM (Protection et Erosion des Monuments) [1980] proposed a very comprehensive list of tentative recommendation for tests on natural stones. It is hoped that the results of many researchers will allow the establishment of international data basis.

Marble Microstructure and Its Possible Influence on Bowing

Gere [1988] has stated that "Some of the fine-grained *thin* (1 to 1 $^1/2$ in. or 2.54 to 3.81 cm.) crystalline marble slabs, due to thermal expansion and moisture, will release their stress of geological origin and, when cooling off, will not fully return to their original position. Thick marble slabs will resist such volume changes of the minerals on the surface, but thin marble slabs used for cladding can bow unless their anchoring method is designed to resist (this)."

Bain [date unknown] noted "some outstanding instances of warping are reported in the soft or incoherent grades of Carrara. Most West Rutland (Vermont) grades (no longer in use) warp considerably. Cases are infrequent in Pittsford Valley, (Vermont) Danby and Colorado Yule stone." This observation led him to conduct an experimental study that he presented to the Vermont Marble Company. He performed beam tests which he called "creep tests" with and without the application of moisture, seasonal changes in temperature, and sustained loads of various durations to examine strain hysteresis. His study examined the phenomena which cause the bowing deflections which are "not in the direction of a recognized load,... although load may occur due to slight off-vertical setting. The deflection seems to be altogether independent of mechanical stress..."

The general results found by Bain include: "Warping is due partly to movement on the grain boundaries allowing closure of intergranular space on the compression side of a member and opening on the tension side. Such warping is a function of the amount of pore space and grain irregularity... This warping is a direct function of the amount of openings and the presence of a small applied stress. Vibrations, even of sound waves, are adequate stress to cause warping of incompletely supported with large total pore space." He continued, "Warping is also due to unequal moisture absorption such as occurs when one side of a slab is kept dry while the other becomes wet. This sort of warping is independent of total amount of openings and is dependent upon initial dryness of the stone and difference in relative humidity on the two sides of the slab."

Bain concluded that "The first type of warping can be prevented by furnishing adequate support for the marble. Very porous varieties which may warp 3 millimeters out of line in a 500 millimeter distance should be supported at frequent intervals. If this is impossible some other appropriate variety of marble which will warp less than 0.5 millimeters in the same distance should be substituted. Warp is proportional to the difference between total deflection and elastic deflection..." He continued, "The second type of warping can be prevented by equalizing humidity; this requires such ventilation on the two sides of a slab so that one side does not have dry winter air and the other moist summer air. Warping can be prevented also by imposing a counteracting mechanical (resistance); this may be worked into a design in the form of a bracket or a molding which will impose a pressure adequate to cause equal deflection in the opposite direction wherever the free slab begins to warp."

1.3. RESEARCH PROGRAM

"The perils of using thin stone and safeguards against them" were the subject of an article by Wilson [1989]. He concluded his comments by stating, "Testing should be done on stone with the same finish and thickness as that used on the building." Unfortunately, he makes no reference to specific tests. However, there have been many proponents of the development of additional standards to choose and properly design and detail marble for exterior cladding. For example, Cantor and Juda [1988] stated, "Due to the lack of available standards and the natural variability of the material itself, we advise a comprehensive program of stone testing. The standard tests historically preformed to check stone quality are the ASTM tests for absorption, compression strength, abrasion, and modulus of rupture." However, the recent literature supports the belief of the authors that the available ASTM standard tests do *not* provide the basis for a comprehensive testing program. Issues of microstructure and variability of marbles, and time-dependent phenomena are not addressed in these tests. As yet, there are no minimum standards for the flexural strengths of dimensional stones, neither for the initial attachment of the cladding panels to the exterior to the buildings, nor after years in service.

Chapter 2 presents the materials characterization of the marbles studied in this research and Chapter 3 introduces a modified test method for the measurement of the fracture toughness of different types of marble. This test is based on the traditional "Brazilian" or splitting test performed under constant strain rate. The experimental procedure is extremely simple and it does not require polishing of the sample; indeed extracted cores can be tested directly. Chapter 3 also presents the use of the finite element method for the calculation of the stress intensity factors and describes an experimental program developed to calculate the toughness of different types of marble. Chapter 4 investigates the sensitivity of marble samples to slow crack growth since comparatively little study has been performed on the sensitivity of marble and how marbles with different grain size behave under different load rate. Chapter 5 studies the preservation of stress-induced structure and the identification of cracks induced by loading and unloading are important to understand the mechanisms for the generation, propagation and interaction of stress-induced microcracks in complex systems such as marble. To preserve the microstructure in marble specimens under load, the voids were filled with a liquid metal alloy called "Wood's metal" during loading, and the alloy was solidified in place before unloading. A comprehensive image analysis was performed on the cracking pattern developed in the marble samples. Also the propagation of the cracking process was modeled using discontinuous deformation analysis with finite element mesh. Chapter 6 studies the effects of various naturally occurring elements on building materials particularly to sodium sulfate. Tests indicate that the crystallization pressure created when mirabilite forms in solution is the main cause of the deterioration of concrete and other materials. The purpose of this investigation was to determine the effects on marble when submerged in a sodium sulfate solution that was cycled across the crystallization temperature for mirabilite.

REFERENCES

1990 Annual Book of ASTM Standards, Section 4: Construction; Volume 04.08: Soil and Rock, Dimension Stone, Geosynthetics; 1916 Race Street, Philadelphia, PA.

Amrhein, J.E., and Merrigan, M.W. [1986], *Marble and Stone Veneer,* Second Edition, Masonry Institute of America, 2550 Beverly Boulevard, Los Angeles, CA.

Arndt, M. [1989], "Amoco Chucks All the Marble on Its Tower," *Chicago Tribune,* Business Section 3, pp. 1-2, 7 March.

Bain, G.W. [date unknown], "Warping of Marble," a report prepared for the Vermont Marble Company.

Bortz, S.A., Erlin, B., and Monk, C.B. [1988], "Some Field Problems with Thin Veneer Building Stones," *New Stone Technology Design, and Construction for Exterior Wall Systems,* Edited by B. Donaldson, ASTM Special Technical Publication (STP) 996, Philadephia, PA, pp. 11-31.

Bauschinger, J.[1884], Communications, vol. X .

Cantor, I.G., and Juda, M.B. [1988], "The New Stone Age: Overcoming the Structural Stumbling Blocks," *New Stone Technology Design, and Construction for Exterior Wall Systems,* Edited by B. Donaldson, ASTM Special Technical Publication (STP) 996, Philadephia, PA, pp. 3-10.

Consiglio, A. [1972], *A Technical Guide to the Rational Use of Marble, Associazione dell'Industria Marmifera Italiano,* Milano.

Gere, A.S. [1988], "Design Considerations for Using Stone Veneer on High-Rise Buildings," *New Stone Technology Design, and Construction for Exterior Wall Systems,* Edited by B. Donaldson, ASTM Special Technical Publication (STP) 996, Philadephia, PA, pp. 32-46.

Georgia Marble Company [1984], *Handbook of the Structural Division,* Nelson, GA 30151.

Johnson J.B. [1897], *The Materials of Construction,* John Wiley & Sons, New York.

Jumikis A.R.[1983], *Rock Mechanics,* Trans Tech Publications, Federal Republic of Germany.

Kessler, D.W. [1919], *Physical and Chemical Tests on the Commercial Marbles of the United States,* Technological Papers of the Bureau of Standards, Washington, D.C.

Manuale dei Marmi Pietre Graniti [1988], Volume I, Guida Tecnica, E. Corbella and R. Zini, Vallardi Editori, Milano.

Margolis, S.V. [1989], "Authenticating Ancient Marble Sculpture," *Scientific American*, Vol. 260, No. 6, pp. 104-110, June.

Marble Institute of America [1987], *Dimensional Stone, Design Manual III*, 35505 State Street, Farmington, MI 48024.

Monk, C.B. [1985], "The Rational Use of Masonry," *Proc. of the Third N. American Masonry Conference*, Construction Research Center, Civil Engrg. Dept., Univ. of Texas at Arlington, TX, pp. 191-227, 3-5 June.

Moore, W. P., Eberhart, H.D., and Cowan, H.J., Group Editors [1980], Monograph on "Planning and Design of Tall Buildings," *Tall Building Systems and Concepts*, Vol. SC, Ch. SC-5 on Cladding, pp. 191-227.

Ramsey/Sleeper [1988], *Architectural Graphic Standards*, Eighth Edition, J.R. Hoke, Ed., American Institute of Architects, Section 4 on Stone, pp. 196-203.

Ratigan, J.L.[1981], *A Statistical Fracture Mechanics Approach to the Strength of Brittle Rock*, Ph.D. Dissertation, Department of Civil Engineering, University of California at Berkeley.

Rilem Committee 25-PEM Tentative Recommendations [1980], Materiaux et Constructions, No. 75, pp. 175-253.

Richardson, E.W. [1989], Private Correspondence re: *Exterior Veneer Standards* by Vermont Marble Company, April 3.

Seinfeld J.H.[1986], *Air Pollution*, John Wiley.

Sulzer, F. [1988], Private communication re: first draft of NSF Proposal "Durability of Integrity of Marble Cladding for High-Rise Structures," Senior Associate, I.M. Pei & Partners, Architects and Planners, New York City, 30 June.

Thomasen, S.E., and Ewart, C.E. [1984], "Durability of Thin-Set Marble," Presented at the Third Int'l Conference on the Durability of Building Materials and Components, Espoo, Finland.

Trewhitt, J., and Tuchman, J. [1988], "Amoco May Replace Marble on Chicago Headquarters," *ENR*, pp. 11-12, 24 March.

Vermont Marble Company [1980], *Exterior Veneer Standards*, October 1980 Reprinting, Proctor, VT 05765.

von Karman T. [1911], *Festigkei Sveruche Unter Allseitigem Pruck.* Zeitscrift Des Vereins Deutscher Ingenieure 55, pp. 1749-1757

Wilson, F. [1989], "The Perils of Using Thin Stone and Safeguards Against Them," *Architecture*, The AIA Journal, Vol. 78, No. 2, pp. 96-97, Feb.

Winkler, E.M. [1973], *Stone: Properties, Durability in Man's Environment*, Applied Mineralogy 4, Springer-Verlag, NY.

CHAPTER 2

MATERIAL CHARACTERIZATION

2.1. Petrographic Studies

Thin sections of marble were prepared for examination under optical microscope. The thin sections had a thickness of approximately 30 microns to permit a better identification of the crystals. Table 1 shows the average crystal size of the various marble studied. The importance of the typical grain size will become evident in Chapter 4 where the slow crack growth in marble is shown to be dependent on the size of the crystals.

Marble	Crystal Size (mm)
Italian	0.3
Vermont	0.6
Chinese	0.5
Georgia	2.5

Table 1

2.2 Specific Gravity and Absorption

Samples of marble were taken to determine the specific gravity and absorption. The tests were performed according to ASTM C97-83 "Standard Test Method for Natural Building Stone" and the results are shown in Table 2. The importance of the low absorption of all the marble samples will become evident in Chapter 6 where the durability of marble to sulfate attack is studied.

Table 2

Marble Type	Absorption (%)	Spg
Ga	0.08	2.71
Vt	0.08	2.71
It	0.10	2.71
Ch	0.11	2.84

2.3 Elastic Moduli

Four inch diameter and 12 inch tall specimens were cored from 12 inch square cubes. Two specimens were cored parallel to the bedding plane and two perpendicular to the bedding plane.

The modulus of elasticity (E) and Poisson's ratio (ν) were determined by use of an XYY recorder and a computerized data acquisition system employing differential transducers. This arrangement produces a continuous plot of stress versus longitudinal strain and lateral strain versus longitudinal strain from which both the modulus of elasticity and Poisson's ratio were computed and compared with the results obtained from the computerized data acquisition system.

Figures 2.1 and 2.2 show the elastic response of specimens which were loaded parallel and perpendicular to the bedding plane. As expected, the marble is stiffer when loaded parallel to the bedding plane. The same is also indicated in Fig. 2.1b and 2.2 b where the lateral deformations are measured. The observed offsets in Figs. 2.1c-f and 2.2c-f are due to the permanent deformation of the specimen after two cycles. The use of three cycles of stress is recommended by ASTM for concrete specimens. Also, it is recommended that the average values from the the last two cycles be used as the values of Young's modulus and Poisson's ratio. A typical response of these three cycles is shown in Fig. 2.1c for loading perpendicular to the bedding plane. A summary of the results is presented in Table 3.

Table 3

Marble Type	Elastic Modulus (10^6 psi)			Poisson's Ratio		
	#1	#2	Ave.	#1	#2	Ave.
Chinese	8.87	8.42	8.6	0.180	0.187	0.18
Georgia (perp.)	8.06	8.47	8.27	0.119	0.124	0.12
Georgia (parallel)	9.65	9.12	9.36	0.105	0.113	0.11
Italian (fol. I)	7.67	7.35	7.5	0.276	0.269	0.27
Italian (fol. II)	6.93	6.72	6.8	0.269	0.254	0.26
Vermont (perp.)	6.34	5.95	6.15	0.144	0.146	0.15
Vermont (parallel)	7.63	7.27	7.45	0.167	0.175	0.17

Notation:
perp. loaded perpendicular to the bedding plane
parallel: loaded parallel to the bedding plane

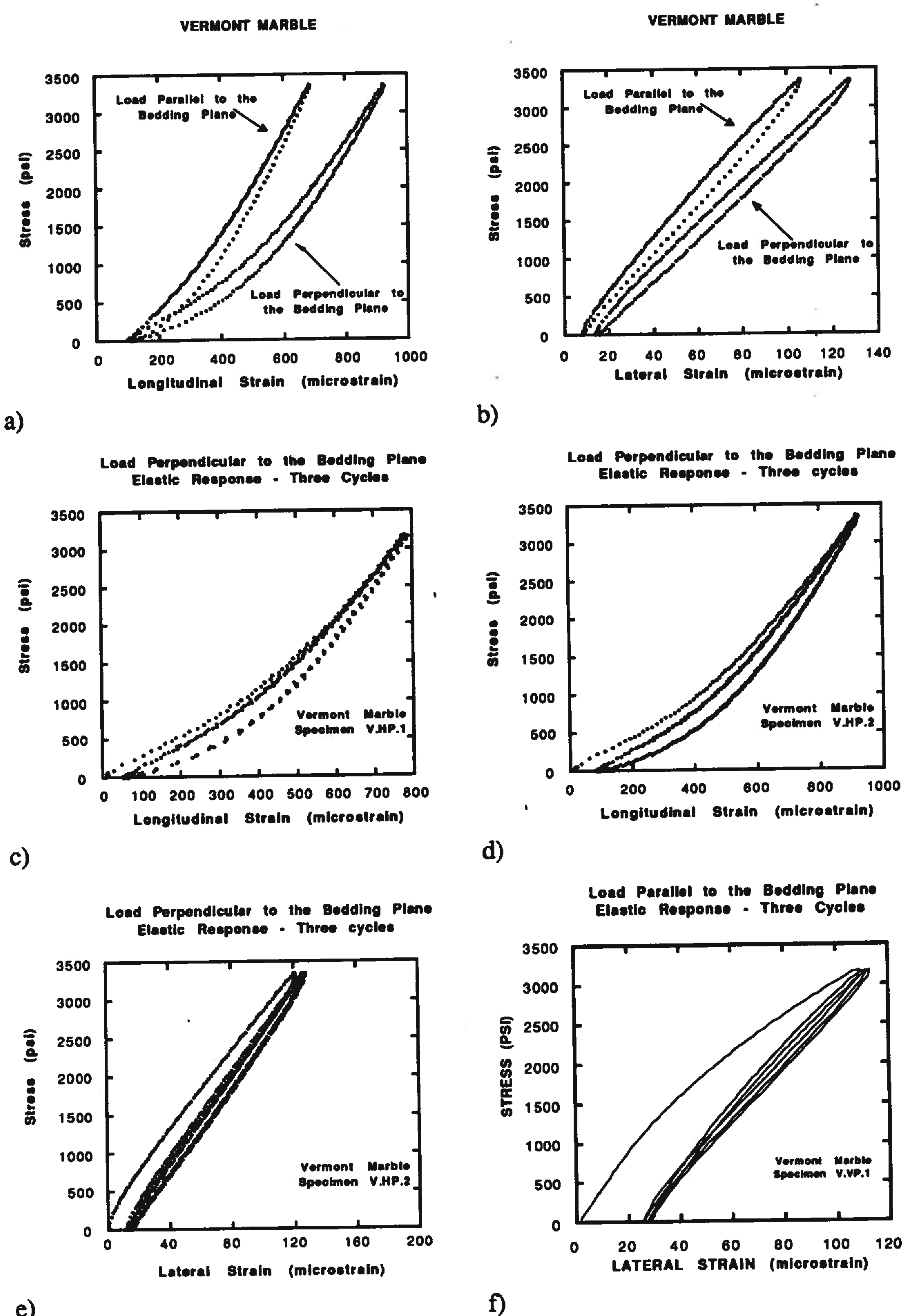

Fig. 2.1
Tests Performed on the Vermont Marble

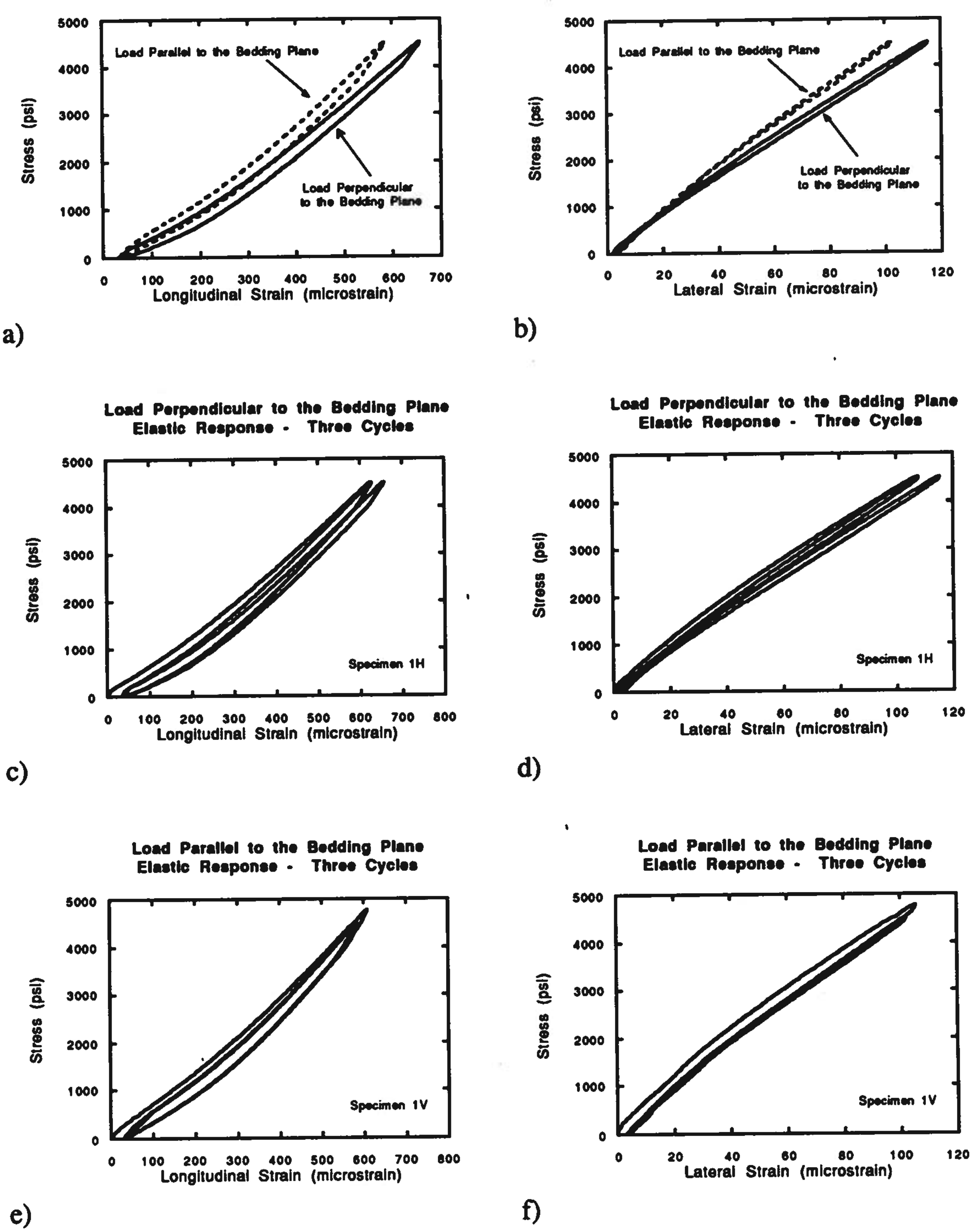

Fig. 2.2
Tests Performed on the Georgia Marble

2.4 Compressive Strength

Compressive Strength. tests were performed according to ASTM C39, "Compressive Strength of Cylindrical Concrete Specimen". Four inch diameter and 12 inch tall specimens were cored from 12 inch square cubes. Three marble specimens were cored parallel to the bedding plane and three perpendicular to the bedding plane.

Figure 2.3a shows the longitudinal compressive strain for two Gerorgia marble specimens which were loaded parallel and perpendicular to the bedding plane up to failure. When tested with the load perpendicular to the bedding plane, a large crack developed at the stress level of 6,000 psi. Figures 2.3 B-C show the lateral and volumetric strains with load parallel to the bedding plane. Figure 2.4 shows the equivalent plots for the georgia marble. The results for the chinese and Itallian marble are presented in Table 4.

Table 4

Marble Type	Strength (psi)	Avg. (psi)
Chinese	17681 17950 15850	17160
Italian fol I	12554 12644 12367	12521
Italian fol II	11594 12799 13083	12492

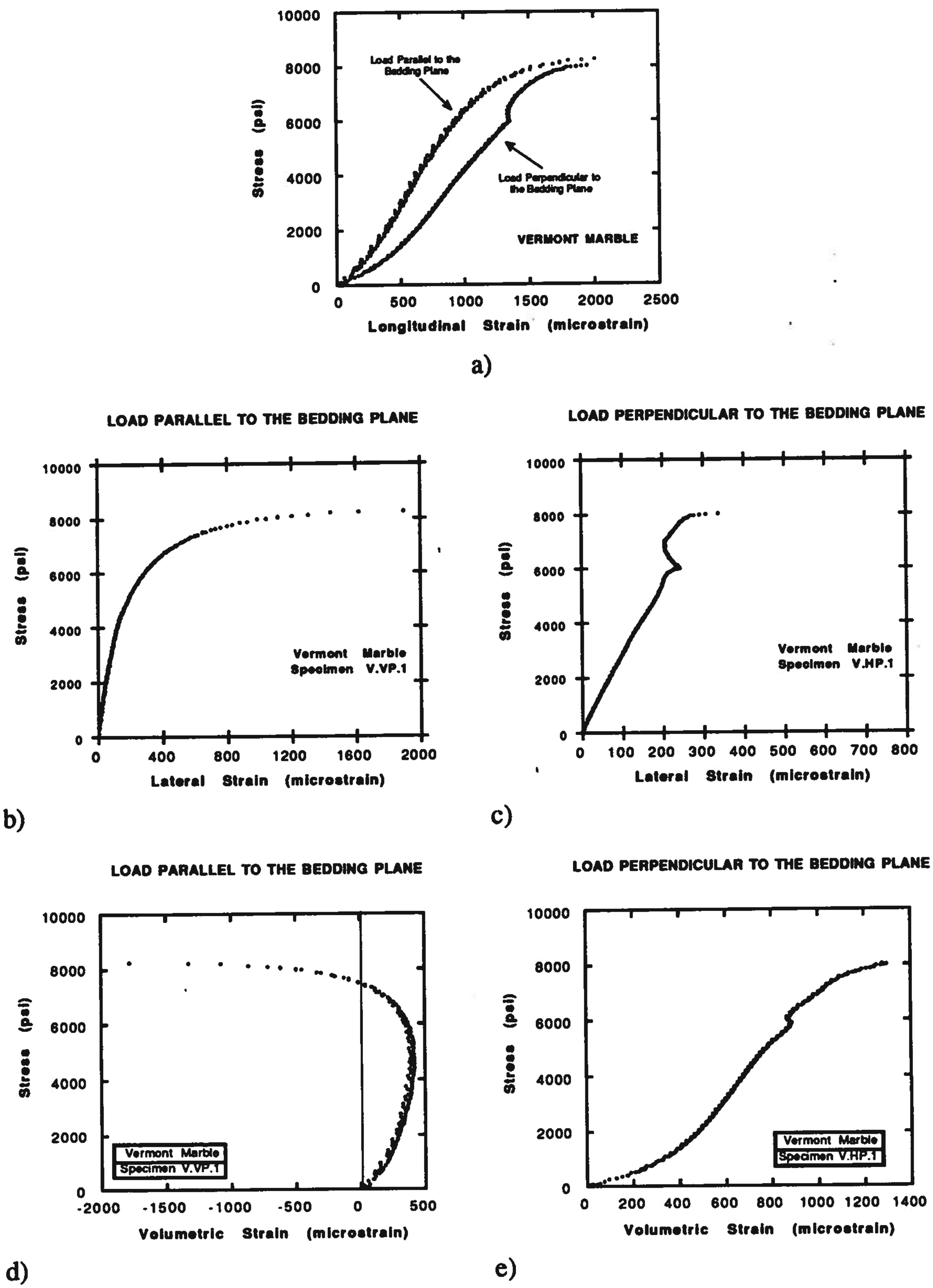

Fig. 2.3

Compression Tests on the Vermont Marble

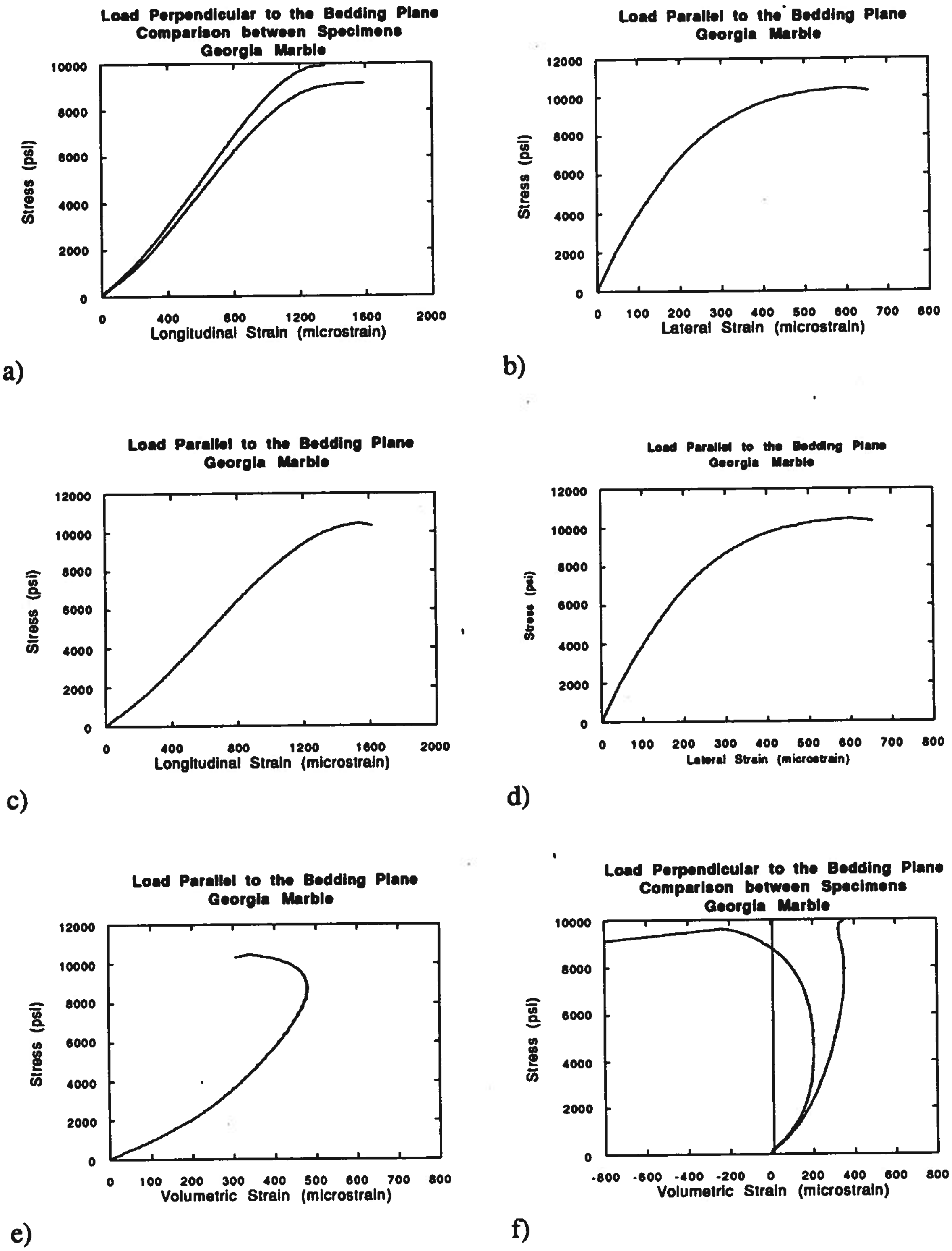

Fig. 2.4

Compression Tests on the Georgia Marble

2.5 Compression Creep

Tests to characterize the short-term creep of marble under compression were undertaken using cylindrical specimens with 4 inch diameters and 12 inch heights. One specimen was compressed under constant stress for approximately 110 hours. The results are given in Figure 2.5 . This test was not successful because no significant creep was measured within this time interval. The investigators are studying a different test procedure including creep under flexure with different levels of stress.

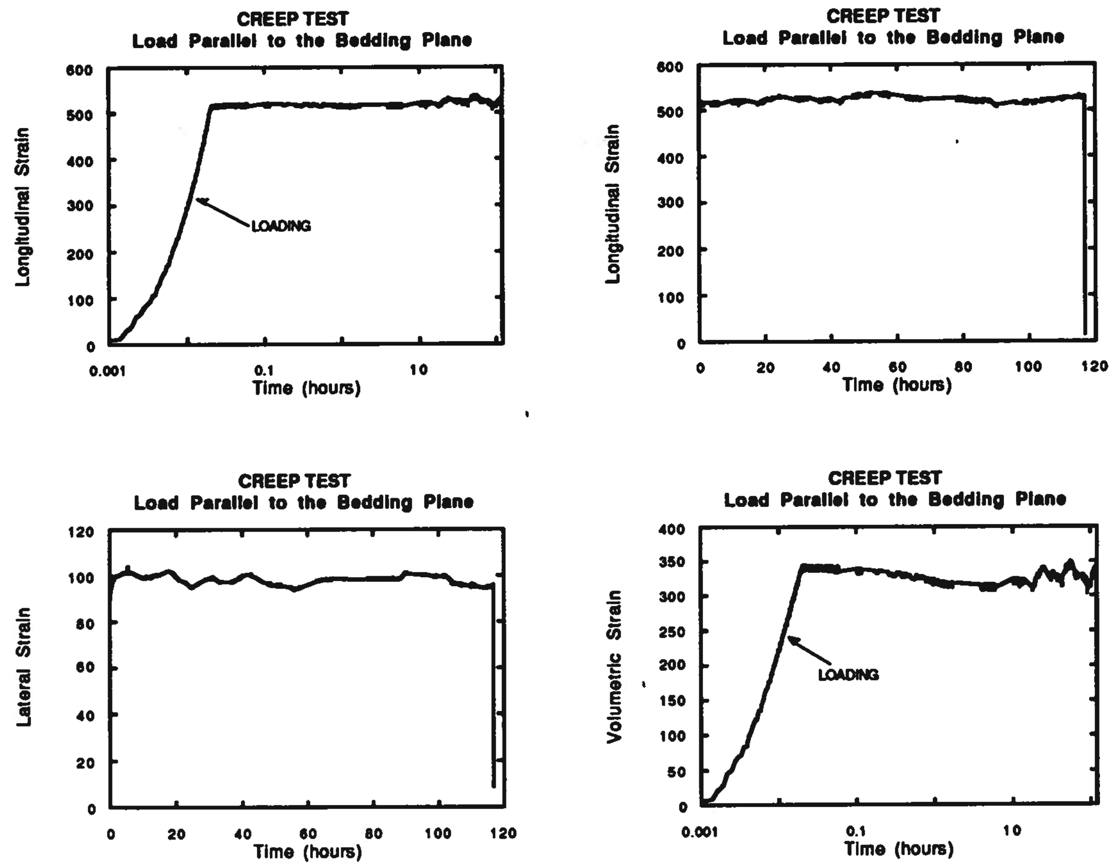

Figure 2.5
Short-Term Compression Creep of Marble

CHAPTER 3

FRACTURE MECHANICS OF MARBLE

3.1 Introduction

The use of fracture mechanics can provide scientific basis for the design of marble elements. Unfortunately, this use is not yet widespread and the design of marble is still based on the strength criteria. The purpose of this chapter is to provide new test method for the measurement of the fracture toughness of different types of marble.

The preparation of marble samples for traditional fracture mechanics test is very elaborated and may introduce flaws or microcracks that were not originally present. Therefore we propose a new test to avoid such limitations. The test is based on the traditional "Brazilian" or splitting test performed under constant strain rate. The experimental procedure is extremely simple and it does not require polishing of the sample; indeed extracted cores can be tested directly. The drawback of the test is that no close form solution for the stress intensity factor is available. This chapter presents the use of the finite element method for the calculation of the stress intensity factors and describes an experimental program developed to calculate the toughness of different types of marble.

3.2 Finite Element Modeling

This section presents how finite elements can be used to determine the stress intensity factors for the splitting test. In order to construct an approximate solution, the domain under consideration is divided into subdomains . For every finite element, linearly independent basis functions can be used in order to approximate the displacement field. Restricting attention to plane problems, the nodal j^{th} values of a finite element are usually chosen to be the displacement components u_j and v_j (Figure 3.1).

The basis functions for standard displacement finite elements consist of shape functions which are multiplied by the unknown nodal values. For the unknown nodal values it is required that the potential energy of the system is minimized and by doing this a set up the system of equations for the unknowns is created. The stresses in standard displacement elements are finite. Therefore, standard displacement elements are not appropriate to approximate the stress singularities at the crack tip. For crack problems special finite elements are needed which include the crack tip singularities in the trial functions. The procedure of coupling a crack element with a standard displacement element is illustrated in Figure 3.2.

For the crack element, displacement trial functions need to be used which have the following properties:

The linearly independent trial functions satisfy the equilibrium equations.

The trial functions satisfy the stress free boundary conditions on the crack surface.

The trial functions for the displacements contain terms which are proportional to $\sqrt{r}$ *so that the associated stresses are proportional to* $1/\sqrt{r}$.

These conditions ensure that the correct form of the singular stress function terms will be used in the finite element approach. From the finite element analysis the coefficients of the singular stress functions for the crack tip are obtained. Apart from a factor, the coefficients of the singular stress functions are the stress intensity factors.

Two points need to be explained in more details : (i) How can we systematically construct linearly independent trial functions for the displacements and stresses with the properties listed above; (ii) How can we compute a stiffness matrix for a crack element when the stresses are singular at one point.

For the construction of linearly independent trial functions a representation of the displacements and stresses in terms of arbitrary functions is helpful. Using two complex functions $\phi(z)$ and $\Psi(z)$ the displacements and stresses can be written in the form[1] :

$$2\mu u = \mathrm{Re}\left[\kappa\,\phi(z) - z\,\overline{\phi'(z)} - \overline{\Psi(z)}\right]$$
$$2\mu v = \mathrm{Im}\left[\kappa\,\phi(z) - z\,\overline{\phi'(z)} - \overline{\Psi(z)}\right]$$
$$\sigma_x = \mathrm{Re}\left[2\,\phi'(z) - \bar{z}\,\phi''(z) - \Psi'(z)\right]$$
$$\sigma_y = \mathrm{Re}\left[2\,\phi'(z) + \bar{z}\,\phi''(z) + \Psi'(z)\right]$$
$$\tau_{xy} = \mathrm{Im}\left[\,\bar{z}\,\phi''(z) + \Psi'(z)\right]$$

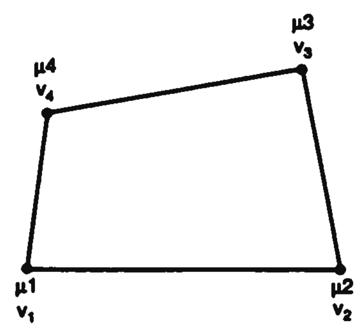

Fig: 3.1

where z=x + iy , f' denotes differentiation with respect to z, $2\mu = E/(1+\nu)$ and $\kappa = (3 - 4\nu)$ for plane strain and $\kappa = (3-\nu)/(1+\nu)$ for plane stress. The advantage of using equation (21) is that for any choice of the functions ϕ and Ψ the equilibrium equations are automatically satisfied. For our crack element we need functions ϕ and Ψ which ensure the satisfaction of the stress free boundary conditions on the crack surfaces. These functions may be represented in the form of a power series as:

---

[1] N. I. Muskhelishvili, *Some Basic Problems of the Mathematical Theory of Elasticity*, Noordhoff, Groningen, Holland, 1953.

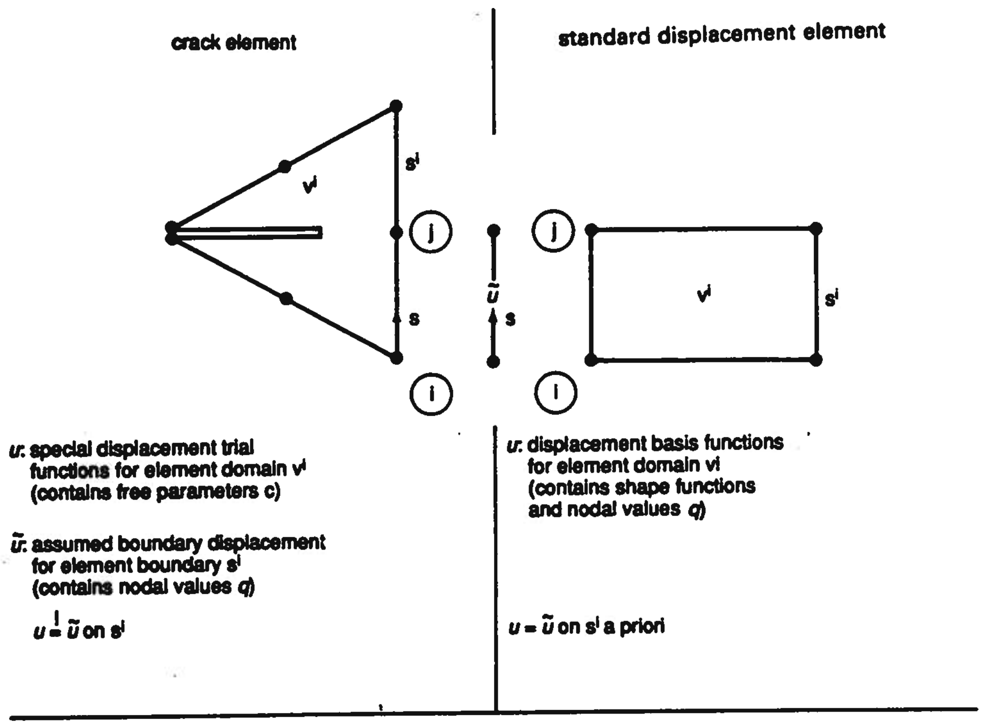

linear $\tilde{u}$ between (i) and (j):

$$\tilde{u} = \begin{bmatrix} (1-\frac{s}{s_{ij}}) & \frac{s}{s_{ij}} & 0 & 0 \\ 0 & 0 & (1-\frac{s}{s_{ij}}) & \frac{s}{s_{ij}} \end{bmatrix} \begin{bmatrix} u_i \\ u_j \\ v_j \\ v_i \end{bmatrix} \quad (0 \leq s \leq s_{ij})$$

Illustration of the coupling between a crack element and a standard displacement element.

Fig: 3.2

$$\phi(z) = \sum_{j=0}^{N} a_j \varsigma^j \tag{3.2}$$

and,

$$\Psi(z) = -\sum_{j=0}^{N} \left[\overline{a_j}(-1)^j + \frac{j}{2} a_j \right] \varsigma^j \tag{3.3}$$

where $a_j = \alpha_j + i\,\beta_j$ and $\varsigma = \sqrt{z}$.

Substituting (3.2, 3.3) into (3.1) gives us the linearly independent real trial functions for our crack element. It should be noted that the terms with the index j=1 give the singular stress terms for mode I and mode II. For example for s_x the singular terms are obtained in the form:

$$\sigma_x = \frac{1}{\sqrt{r}} \cos\frac{\varphi}{2}\left[1 - \sin\frac{\varphi}{2} \sin\frac{3\varphi}{2} \right]\alpha_1 + \frac{1}{\sqrt{r}} \sin\frac{\varphi}{2}\left[2 + \cos\frac{\varphi}{2} \cos\frac{3\varphi}{2} \right]\beta_1 \tag{3.4}$$

The stress intensity factors K_I and K_{II} can be calculated from

$$K_I = \sqrt{2\pi}\,\alpha_1 \tag{3.5}$$

$$K_{II} = -\sqrt{2\pi}\,\beta_1 \tag{3.6}$$

Collecting the unknown coefficients α_j and β_j into a vector $\underline{c}$, the displacements for our crack element can be written in matrix notation as

$$\underline{u} = \underline{U}\,\underline{c} + \underline{u}_p = \underline{u}_h + \underline{u}_p \tag{3.7}$$

where $\underline{u}_p$ is a particular solution involving no unknown coefficients. Only the homogeneous solution $\underline{u}_h$ involves unknown coefficients. Since the unknowns in the vector $\underline{c}$ are not associated with finite element nodal values, the vector $\underline{c}$ is to be related to the vector of nodal displacements $\underline{q}$. The vector $\underline{q}$ contains the nodal values $\underline{u}_j$, $\underline{v}_j$ of the chosen element nodes. In Figure 12-28 a linear variation of the boundary displacements, $[\tilde{u}\ \tilde{v}]^T = \underline{\tilde{u}}$, is assumed between nodes i and j. If we want to couple the crack element with linear standard displacement elements $\tilde{u}$, $\tilde{v}$ are chosen linear between two nodes. If the crack element shall be coupled with quadratic standard elements a quadratic variation of the boundary displacement $\underline{\tilde{u}}$ of the crack element is chosen.

In the first step for the evaluation of a crack element stiffness matrix the vector $\underline{c}$ of the displacement field $\underline{u}$ for the domain V^i of the crack elements is calculated such that an optimal agreement between $\underline{u}$ and $\underline{\tilde{u}}$ is achieved along the boundary of the crack element. This gives a relationship of the form:

$$\underline{c} = G\,\underline{q} + \underline{g} \tag{3.8}$$

so that the unknowns $\underline{c}$ can be eliminated and only the nodal displacements $\underline{q}$ will remain as unknowns of the crack element.

For the evaluation of the crack element stiffness matrix the following displacement functional is used:

$$\Pi^i_H = \Pi^i + \int_{s^i_u} \underline{T}^T (\tilde{\underline{u}} - \underline{u})\, dS^i \tag{3.9}$$

where

$$\Pi^i = \int_{V_i} \left[1/2 \left(\underline{u}^T \underline{D}^T\right) \underline{E} \left(\underline{D}\,\underline{u}\right) - \underline{u}^T \bar{\underline{f}} \right] dV^i - \int_{s^i_u} \underline{u}^T \bar{\underline{T}}\, dS^i \tag{3.10}$$

Where V_i denotes the domain of the finite element. S_i is the boundary of the element and $\underline{T}$ are the tractions along the element boundary. Using the decomposition of the displacements and tractions in the form $\underline{u} = \underline{u}_h + \underline{u}_p$ and $\underline{T} = \underline{T}_h + \underline{T}_p$ the variational formulation is simplified. Since the displacement field for the crack element is constructed such that the governing partial differential equations (Navier-equation in matrix notation):

$$\underline{D}^T \underline{E}\, \underline{D}\, \underline{u} = -\bar{\underline{f}} \qquad \text{in V} \tag{3.11}$$

are satisfied a priori (30), can be simplified to an expression with boundary integrals:

$$\Pi^i = \int_{s^i_u} 1/2\, \underline{u}_h^T \underline{T}_h\, dS^i + \int_{s^i_u} \underline{u}_h^T \underline{T}_p\, dS^i - \int_{s^i_u} \underline{u}_h^T \bar{\underline{T}}\, dS^i + \text{terms without } \underline{u}_h \text{ and } \underline{T}_h \tag{3.12}$$

Using the stiffness matrix of a crack element can be obtained by evaluations of the boundary integrals along the element boundary[2, 3]. It is important that the boundary conditions on the crack surface are satisfied a priori so that all integrals along the crack surface vanish. Therefore, during the calculations of the stiffness matrix we do not need to evaluate stresses at the crack tip and although the stress singularities are included in the model, the evaluation of the stiffness coefficients will not be "polluted" from the presence of the singularities.

Figure 3.3 shows the discretization of the splitting test using a finite element mesh. The numerical values are presented in Table 3.1.

---

[2] R. Piltner, Int. J. Numer. Methods Eng., 21, 1471, 1985

[3] R. Piltner, in Local Effects in the Analysis of Structures, Elsevier, Amsterdam, 299, 1985.

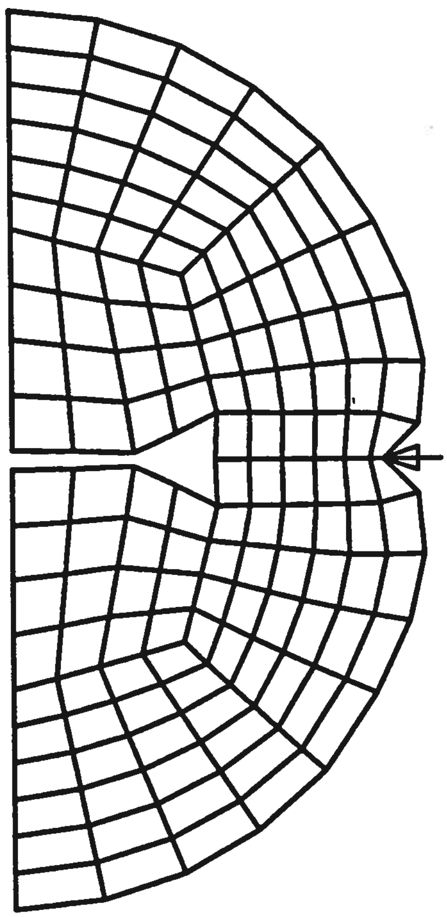

Fig: 3.3(a)

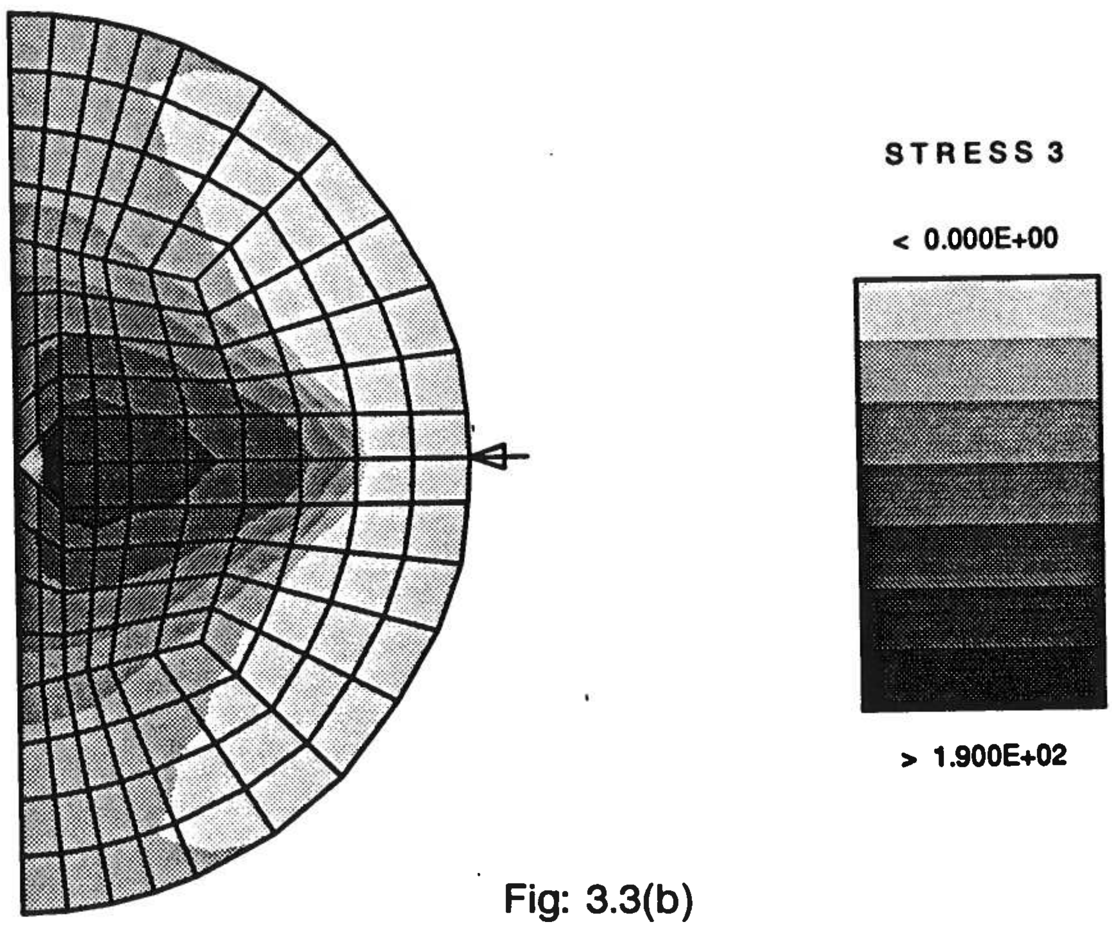

Fig: 3.3(b)

Table 3.1

crack length (cm)	v1 (cm)	2 v* (cm)	K $(N/cm^{3/2})$
0.0000	0	0.00017230	0.0000
0.18000	$1.098\ 10^{-5}$	0.00017360	118.40
0.54000	$3.528\ 10^{-5}$	0.00019180	217.30
0.90000	$6.604\ 10^{-5}$	0.00023320	313.70
1.1700	$9.636\ 10^{-5}$	0.00028220	391.50
1.5750	$1.616.\ 10^{-4}$	0.00040060	537.10
1.6425	$1.76\ 10^{-4}$	0.00042740	565.60
1.7100	$1.916\ 10^{-4}$	0.00045680	596.30
1.9800	$2.704\ 10^{-4}$	0.00060620	747.60

$E = 4.688\ 10^6\ N/cm^2$
$P = 3.6\ 10^3\ N$
t= 2.62 cm thickness
R= 2.7 cm radius

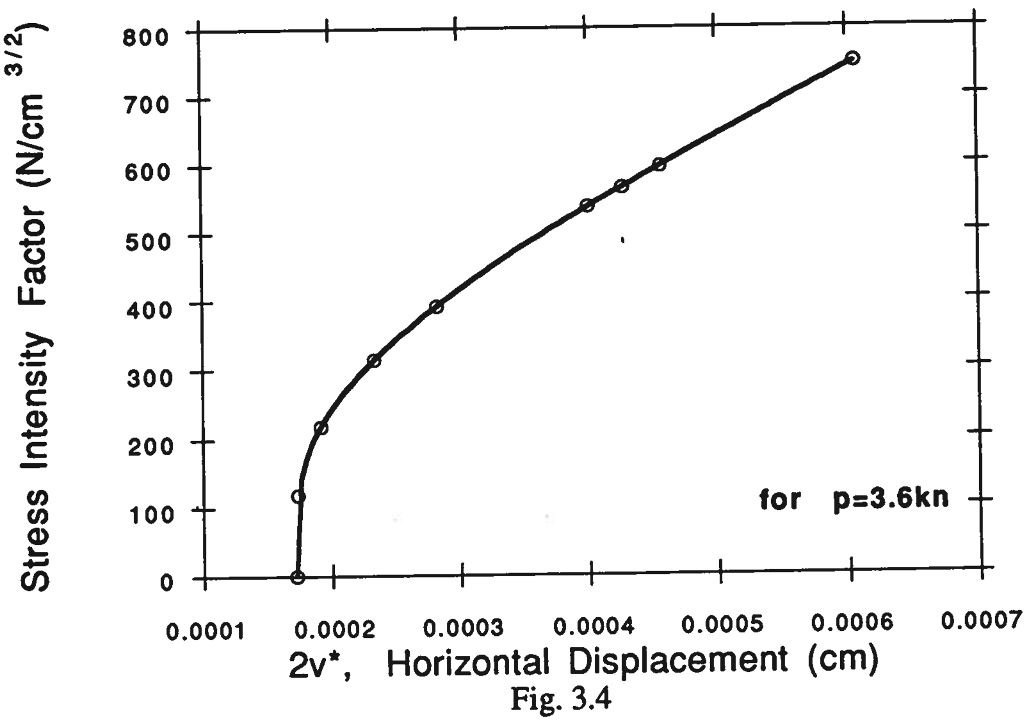

Fig. 3.4

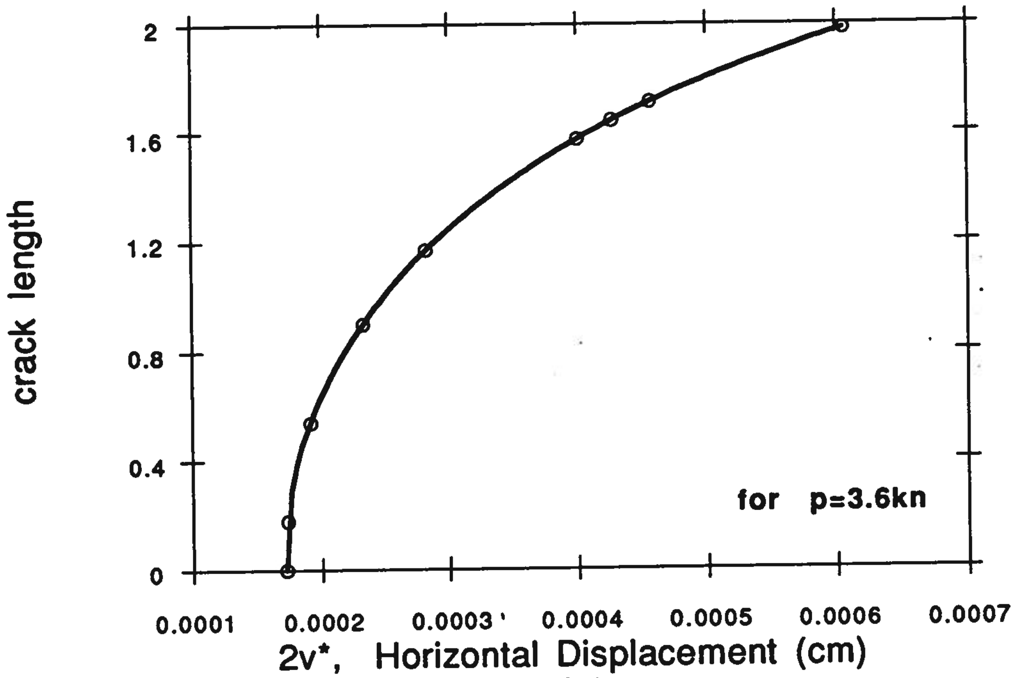
2
1.6
1.2
0.8
0.4
0
crack length
for p=3.6kn
0.0001
0.0002
0.0003
0.0004
0.0005
0.0006
0.0007
2v*, Horizontal Displacement (cm)

Fig. 3.5

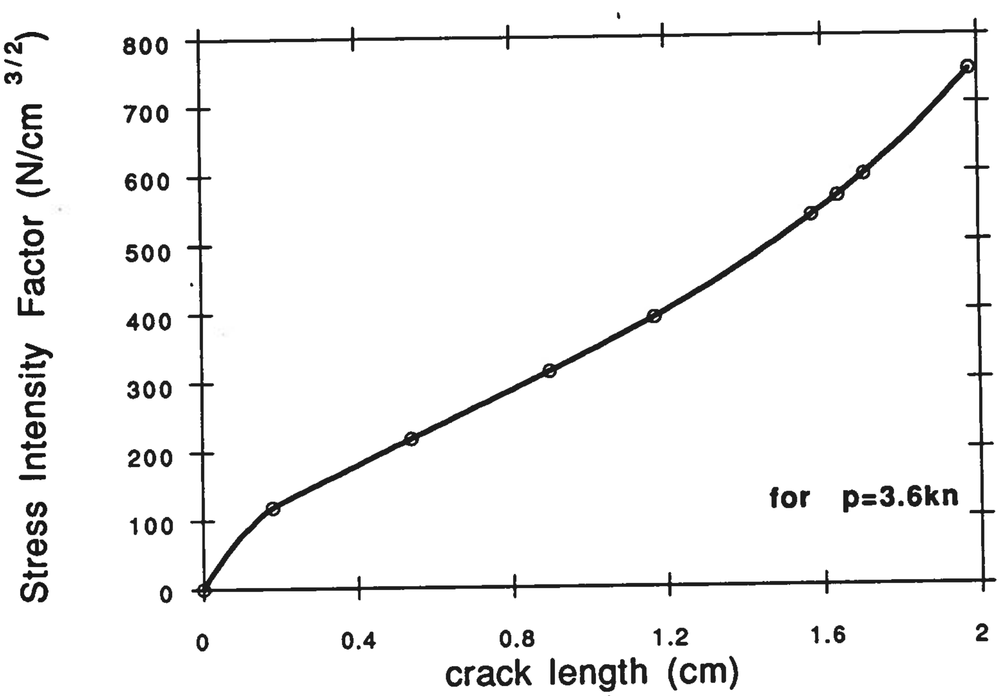
800
700
600
500
400
300
200
100
0
Stress Intensity Factor (N/cm 3/2)
for p=3.6kn
0
0.4
0.8
1.2
1.6
2
crack length (cm)

Fig. 3.6

3.3 Experimental Results

Four types of marble were tested in a Brazilian test under controlled strain rate. The experimetal results are indicated in Figures 3.7 to 3.23. The test was fully controlled as it can be observed by the stable crack growth that originates the strain softeneing once the maximum load is achieved. Using the results obtained in last section using finite element methods it was possible to compute the fracture toughness of the various types of marble, as shown in Table 3.2. As indicated in Fig. 3.23, there is an inverse relationship between fracture toughness and crystal size.

Table 3.2

Type of Marble	**Fracture Toughness** K $(N/cm^{3/2})$	**Crack Length (cm)**	**Crystal Size (mm)**
Italian	1691	1.6	0.3
Chinese	1459	1.2	0.5
Vermont	1496	1.75	0.6
Georgia	1107	1.3	2.5

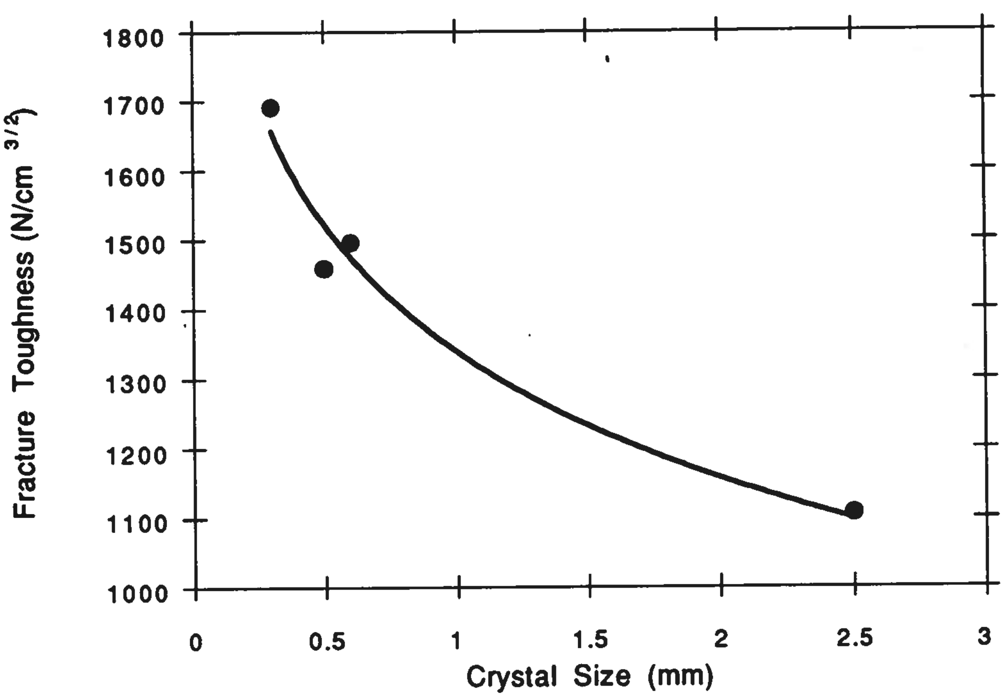

Fig. 3.24

SPECIMEN: ITALIAN MARBLE

LENGTH: 2.62cm

DIAMETER: 5.40cm

DENSITY: 2.65g/cm^3

RADIAL DISPLACEMENT RATE: 0.001/mm/min

GAGE LENGTH: 5.06cm

MAXIMUM LOAD: 10.2kN

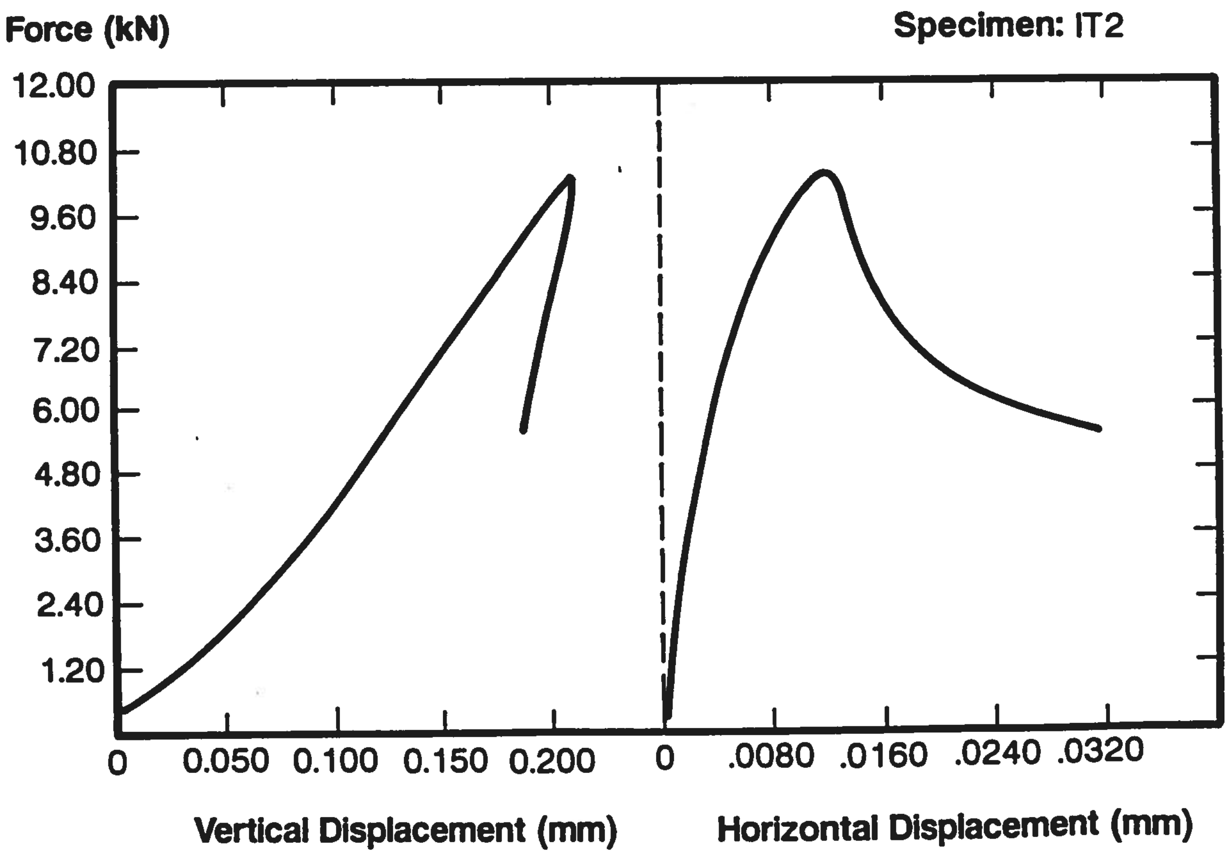

Fig: 3.7

SPECIMEN: ITALIAN MARBLE

LENGTH: 2.58cm

DIAMETER: 5.40cm

DENSITY: 2.68g/cm^3

RADIAL DISPLACEMENT RATE: 0.001/mm/min

GAGE LENGTH: 5.03cm

MAXIMUM LOAD: 10.4kN

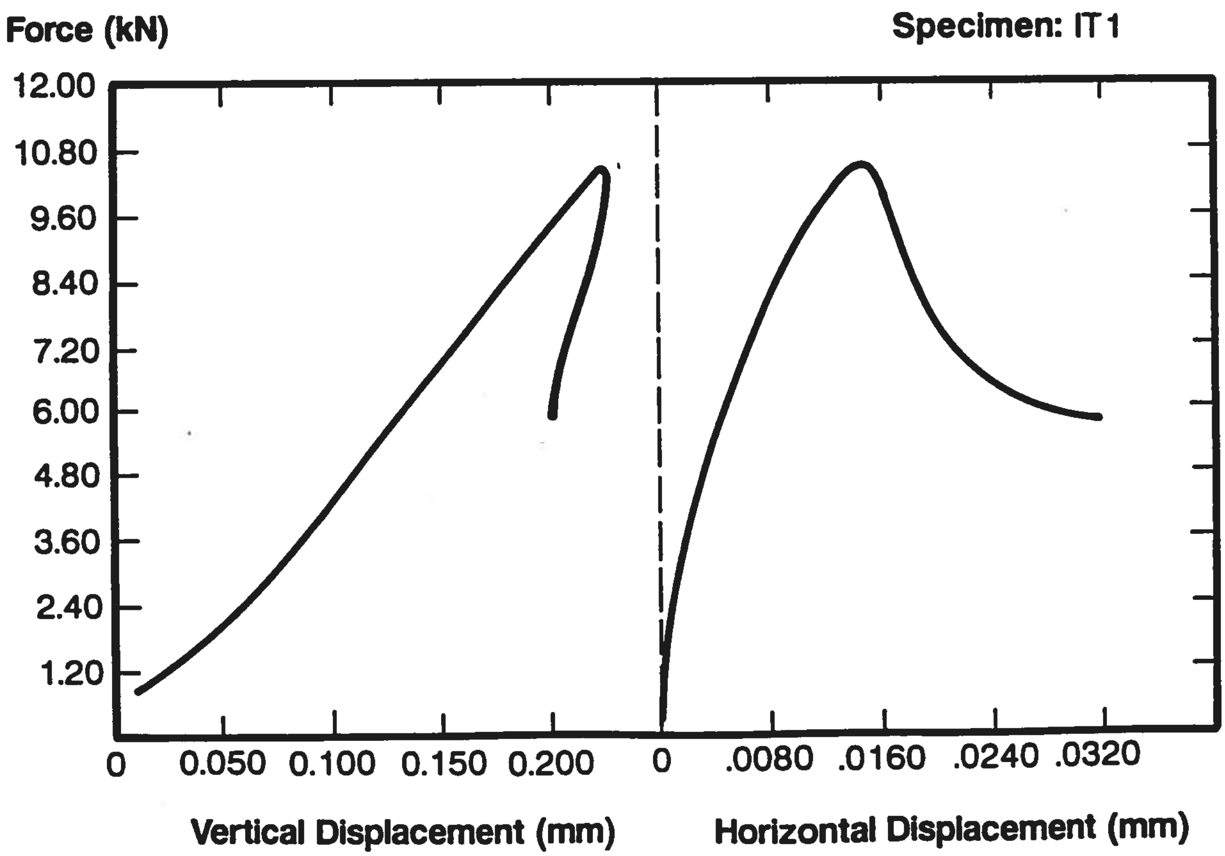

Fig: 3.8

SPECIMEN: ITALIAN MARBLE

LENGTH: 2.55cm

DIAMETER: 5.39cm

DENSITY: 2.68g/cm^3

RADIAL DISPLACEMENT RATE: 0.001/mm/min

GAGE LENGTH: 5.05cm

MAXIMUM LOAD: 11.7kN

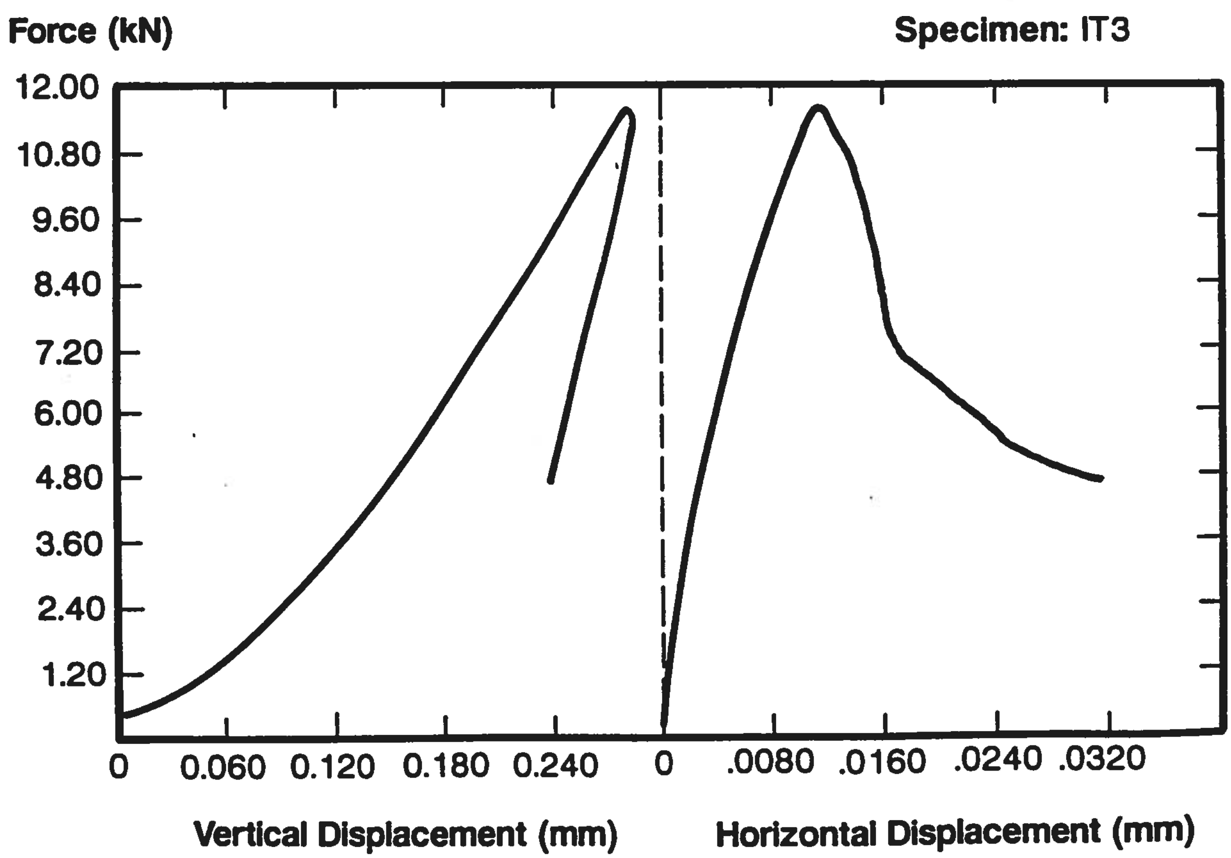

Fig: 3.9

SPECIMEN: VERMONT MARBLE

LENGTH: 2.54cm

DIAMETER: 5.40cm

DENSITY: 2.7g/cm^3

RADIAL DISPLACEMENT RATE: 0.002/mm/min

GAGE LENGTH: 5.09cm

MAXIMUM LOAD: 9.3kN

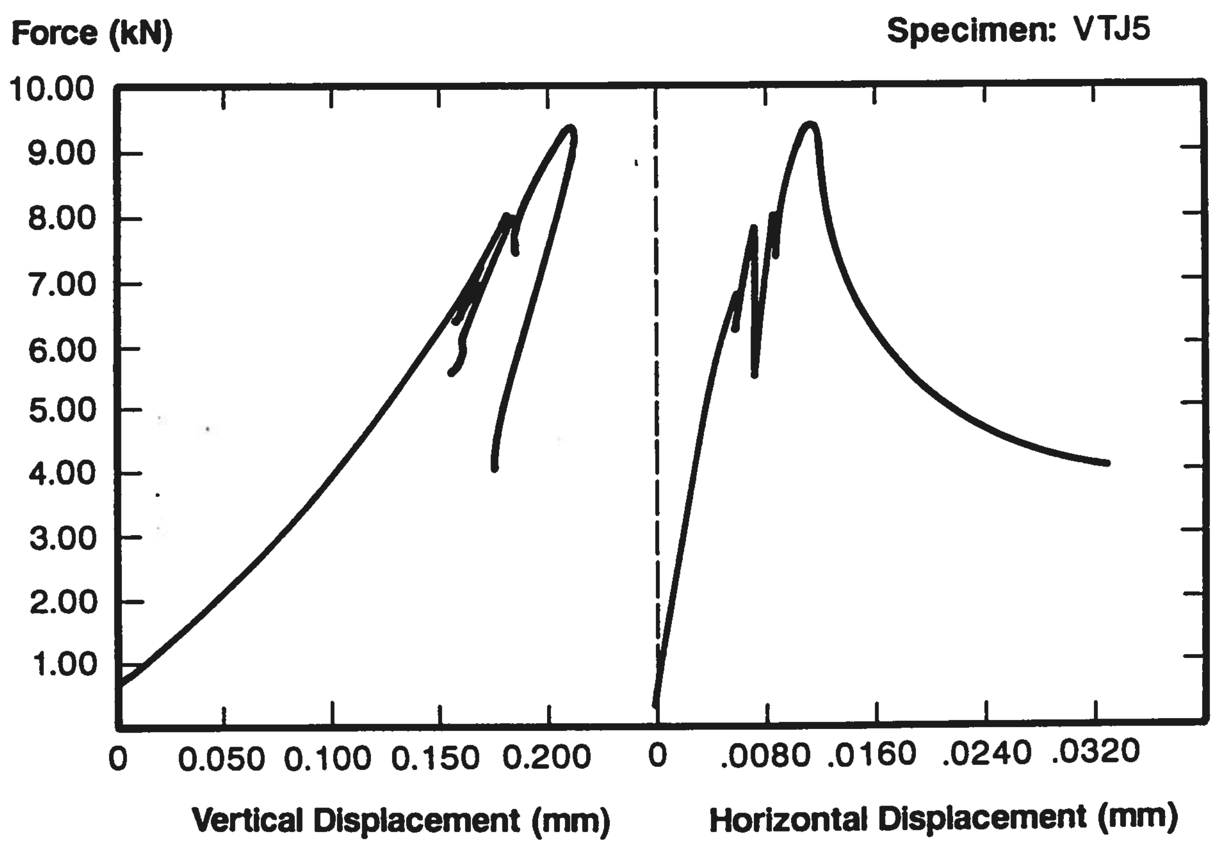

Fig: 3.10

SPECIMEN: VERMONT MARBLE

LENGTH: 2.55cm

DIAMETER: 5.39cm

DENSITY: 2.68g/cm^3

RADIAL DISPLACEMENT RATE: 0.001/mm/min

GAGE LENGTH: 5.00cm

MAXIMUM LOAD: 8.3kN

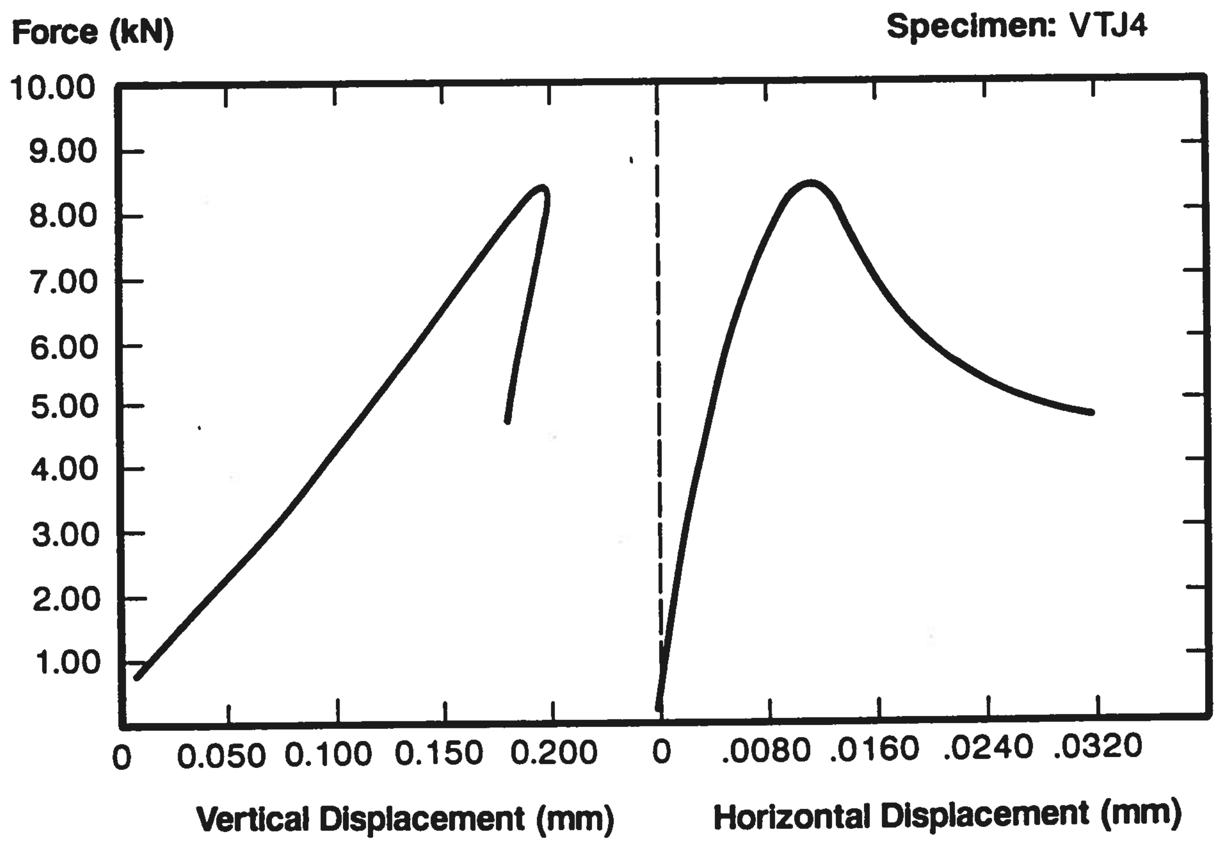

Fig: 3.11

SPECIMEN: VERMONT MARBLE

LENGTH: 2.53cm

DIAMETER: 5.40cm

DENSITY: 2.66g/cm^3

RADIAL DISPLACEMENT RATE: 0.002/mm/min

GAGE LENGTH: 5.00cm

MAXIMUM LOAD: 9.7kN

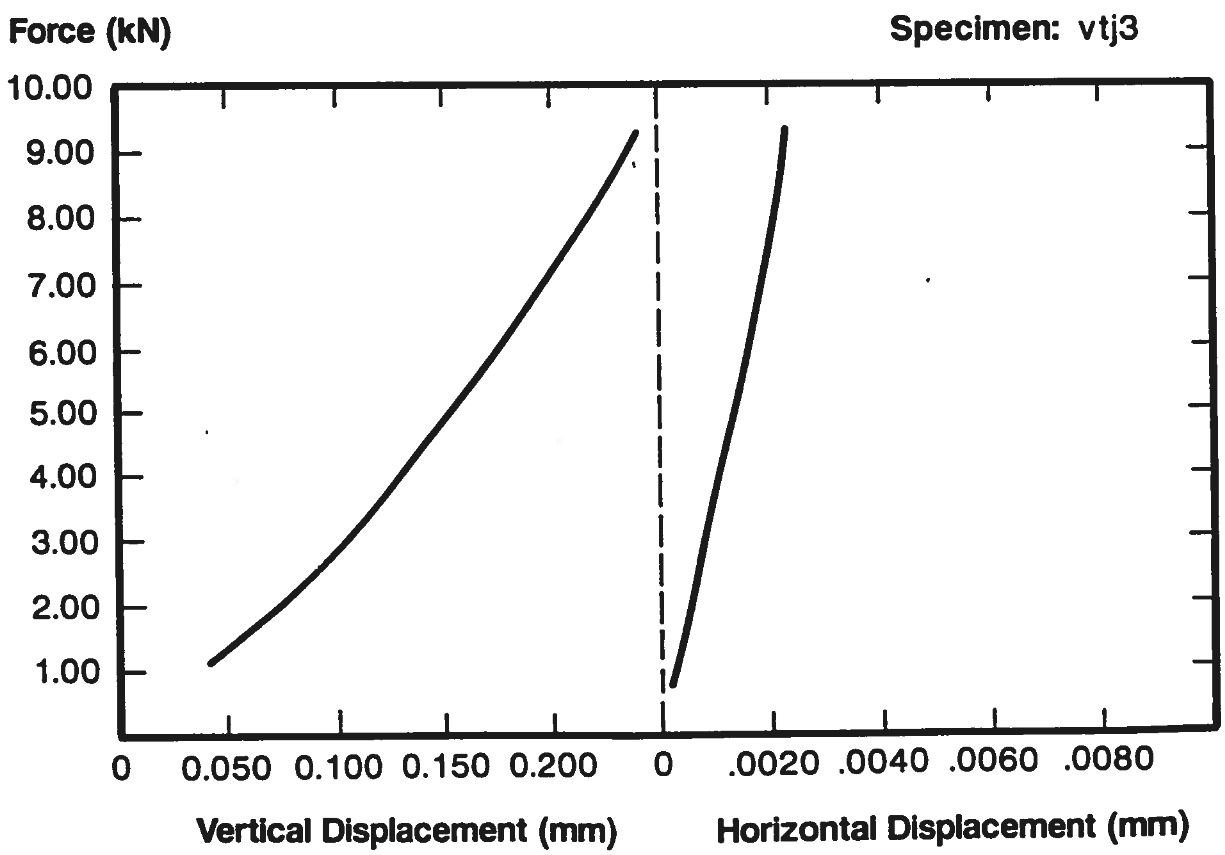

Fig: 3.12

SPECIMEN: VERMONT MARBLE

LENGTH: 2.52cm

DIAMETER: 5.39cm

DENSITY: 2.66g/cm^3

RADIAL DISPLACEMENT RATE: 0.001/mm/min

GAGE LENGTH: 5.00cm

MAXIMUM LOAD: 7.4kN

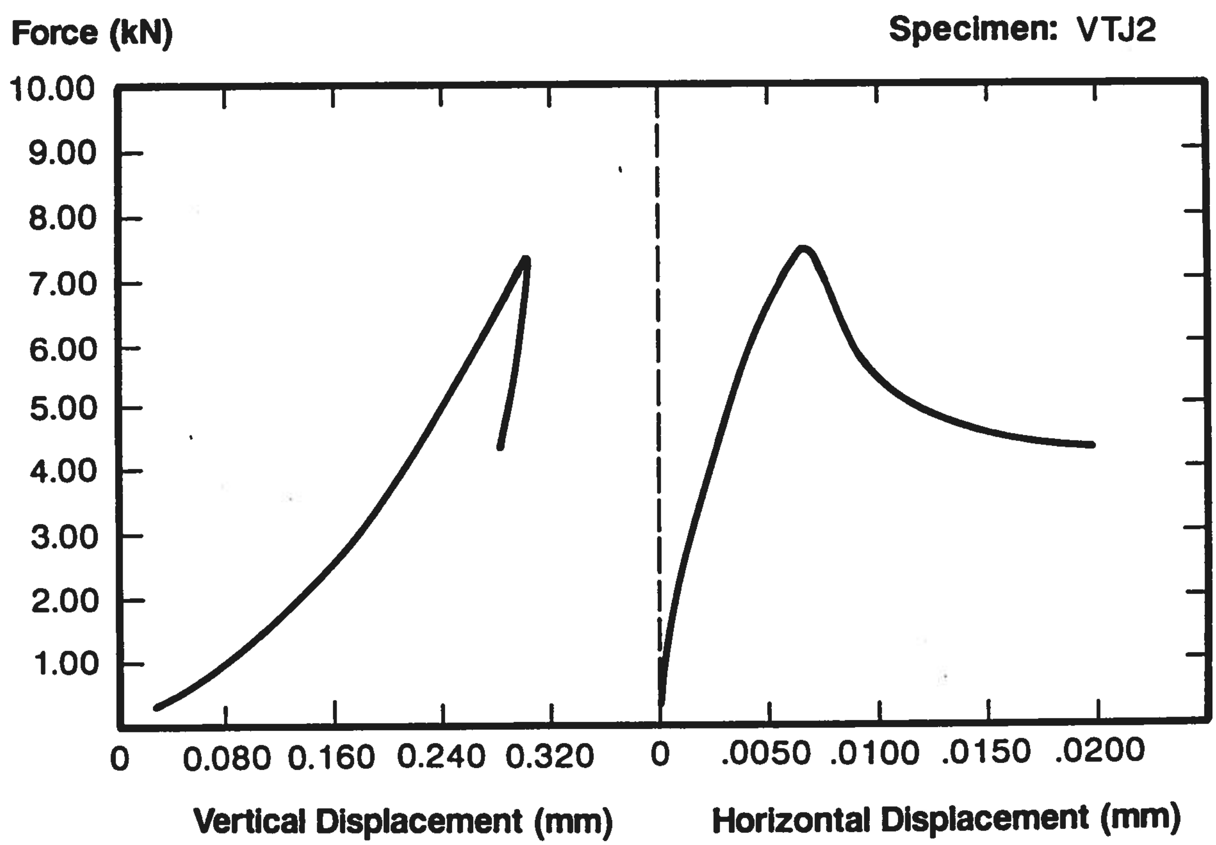

Fig: 3.13

SPECIMEN: VERMONT MARBLE

LENGTH: 2.57cm

DIAMETER: 5.40cm

DENSITY: 2.67g/cm^3

RADIAL DISPLACEMENT RATE: 0.002mm/min

GAGE LENGTH: 5.00cm

MAXIMUM LOAD: 11.7kN

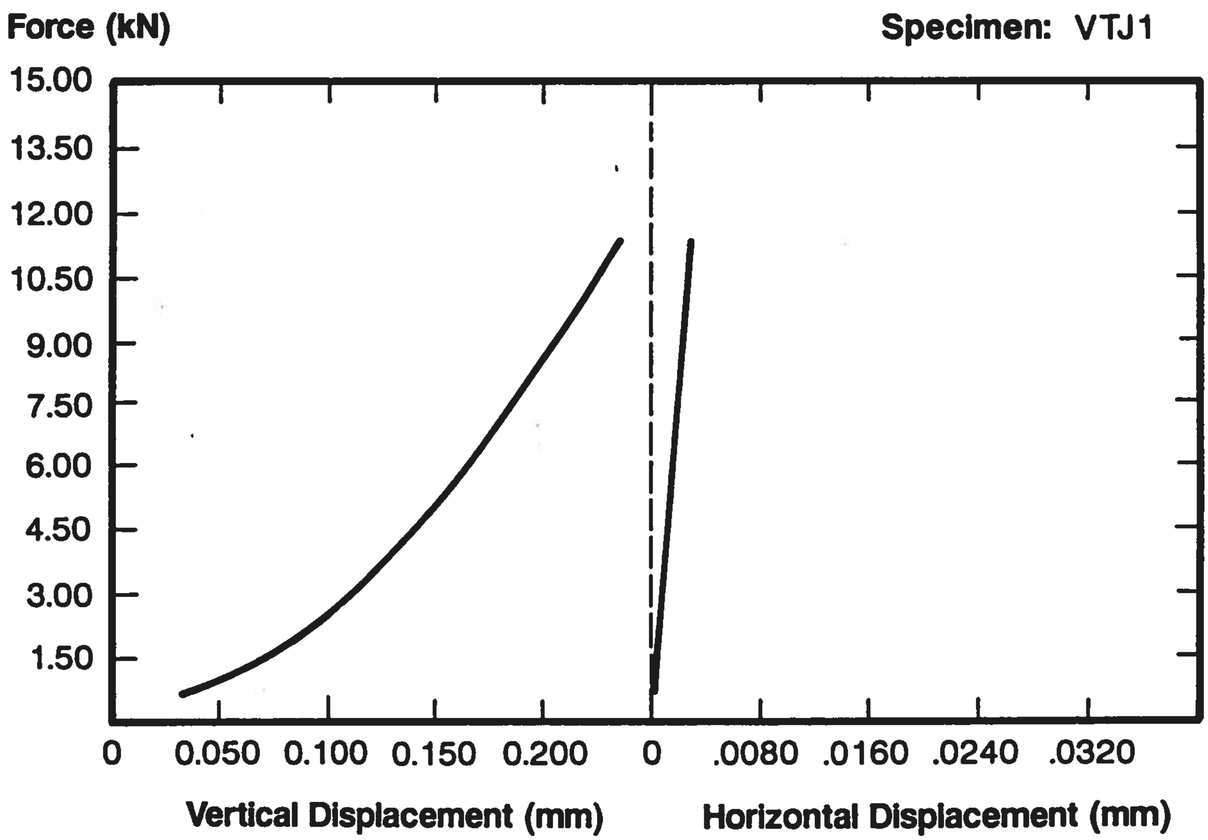

Fig: 3.14

SPECIMEN: GEORGIA MARBLE

LENGTH: 2.53cm

DIAMETER: 5.42cm

DENSITY: 2.65g/cm^3

RADIAL DISPLACEMENT RATE: 0.0005/mm/min

GAGE LENGTH: 5.06cm

MAXIMUM LOAD: 10.6kN

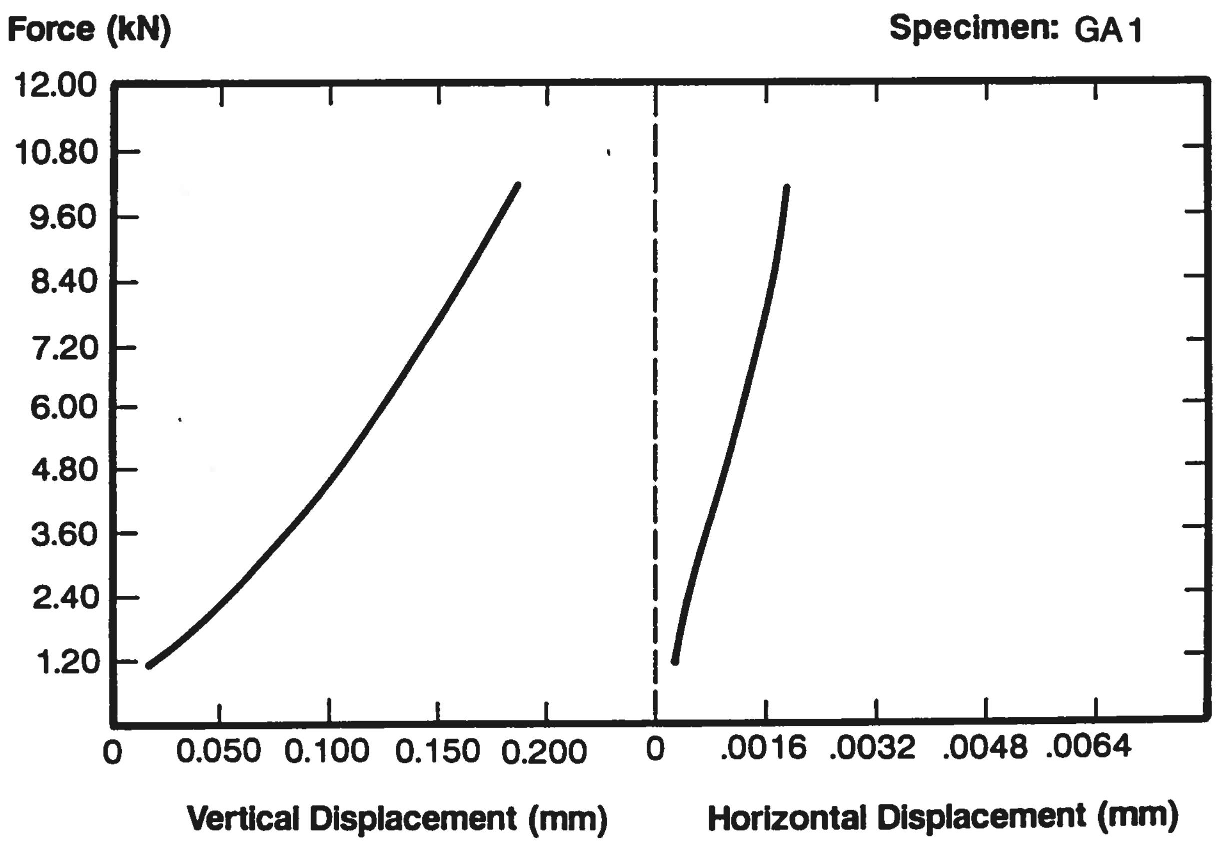

Fig: 3.15

SPECIMEN: GEORGIA MARBLE

LENGTH: 2.55cm

DIAMETER: 5.23cm

DENSITY: 2.71g/cm^3

RADIAL DISPLACEMENT RATE: 0.0005/mm/min

GAGE LENGTH: 4.90cm

MAXIMUM LOAD: 12.86kN

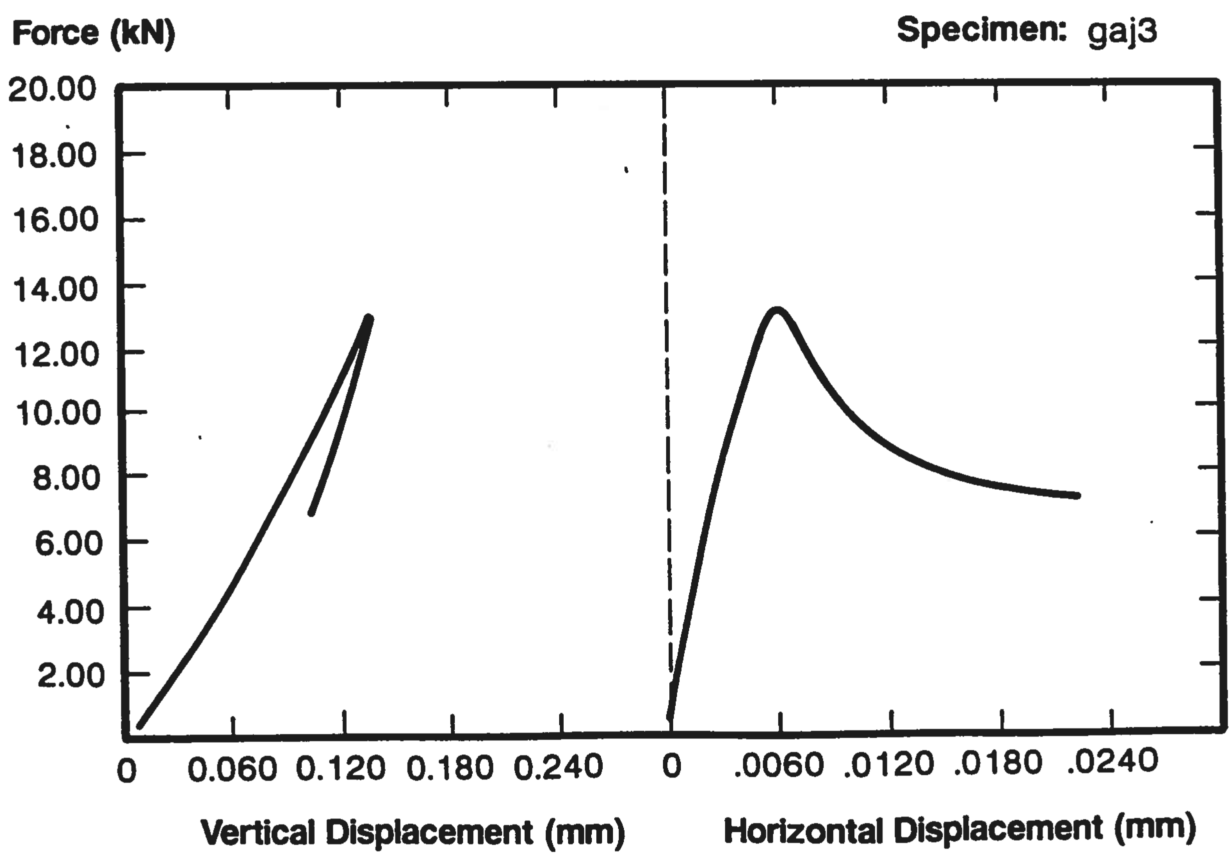

Fig: 3.16

SPECIMEN: GEORGIA MARBLE

LENGTH: 2.41cm

DIAMETER: 5.28cm

DENSITY: 2.69g/cm^3

RADIAL DISPLACEMENT RATE: 0.0005/mm/min

GAGE LENGTH: 4.90cm

MAXIMUM LOAD: 10.4kN

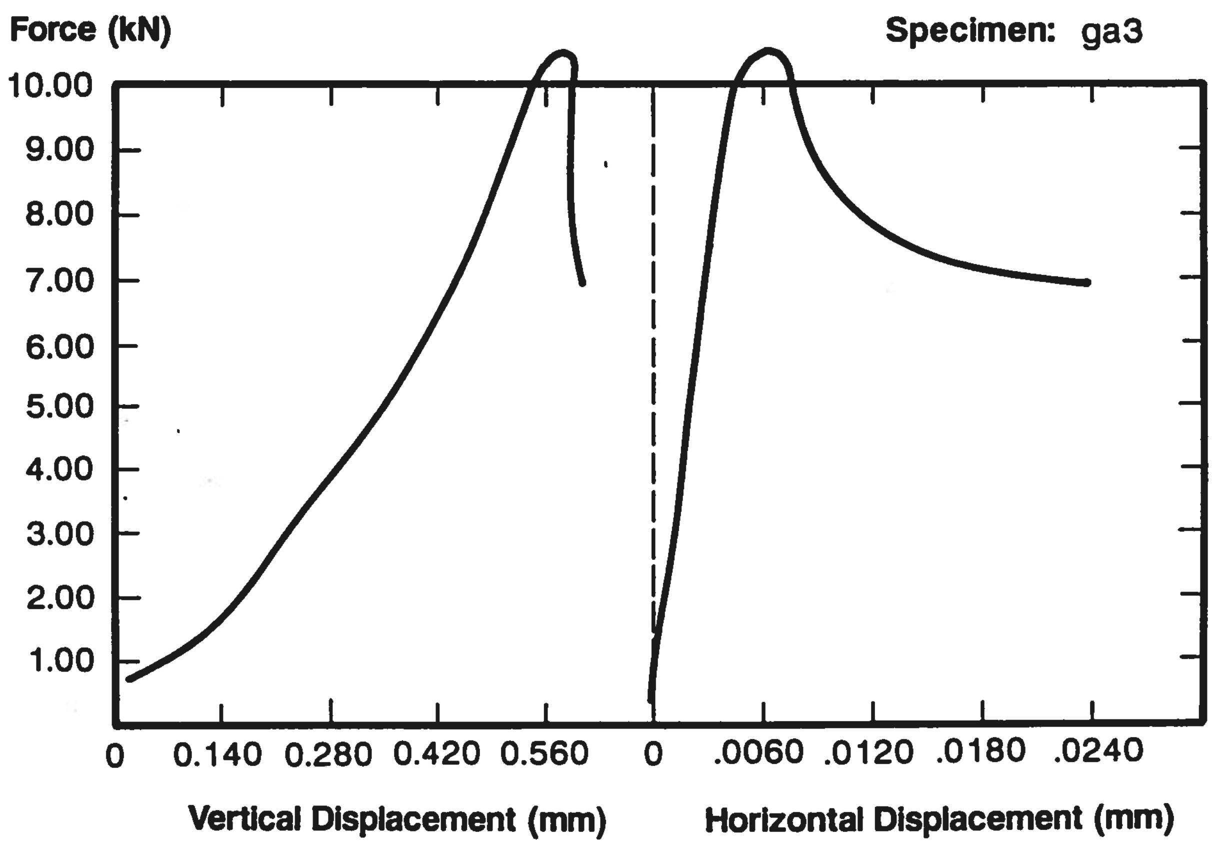

Fig: 3.17

SPECIMEN: GEORGIA MARBLE

LENGTH: 2.45cm

DIAMETER: 5.30cm

DENSITY: 2.69g/cm^3

RADIAL DISPLACEMENT RATE: 0.001/mm/min

GAGE LENGTH: 4.90cm

MAXIMUM LOAD: 12.7kN

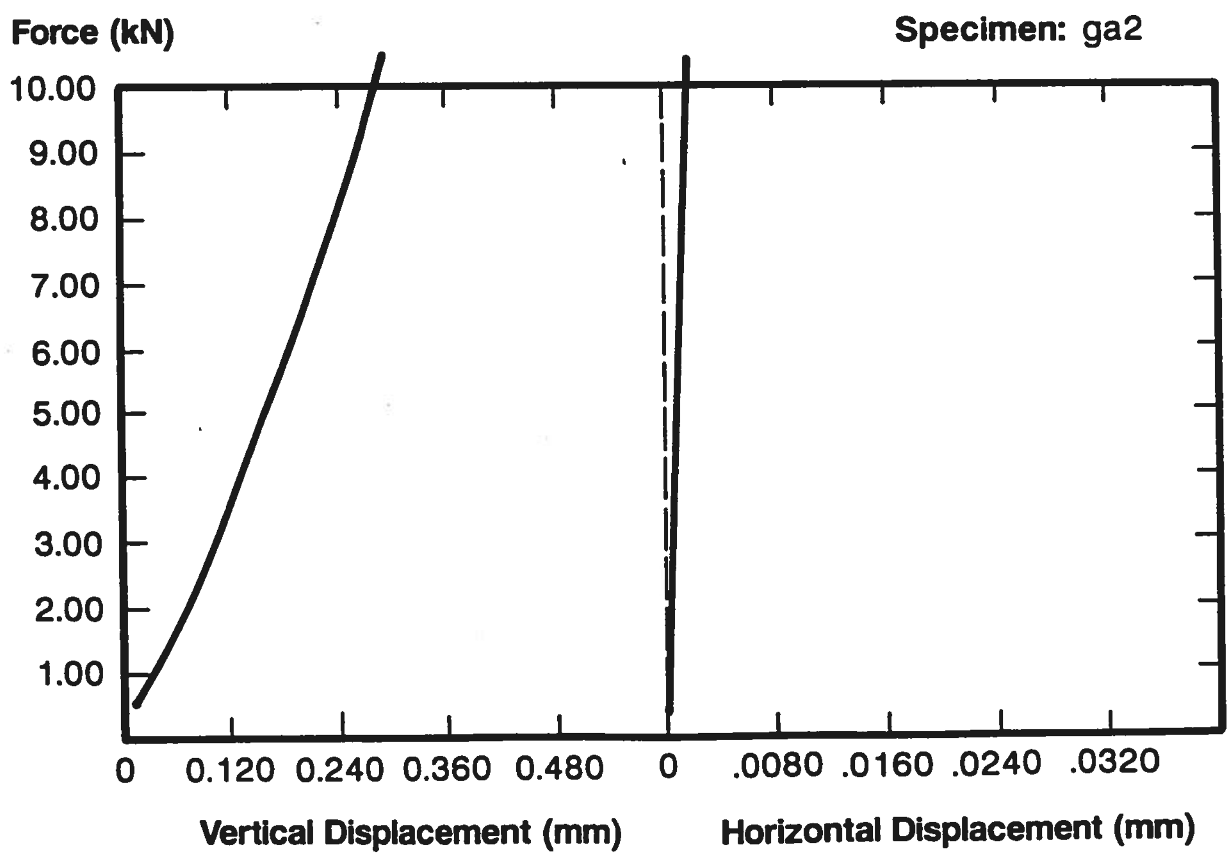

Fig: 3.18

SPECIMEN: GEORGIA MARBLE

LENGTH: 2.44cm

DIAMETER: 5.25cm

DENSITY: 2.69g/cm^3

RADIAL DISPLACEMENT RATE: 0.0005/mm/min

GAGE LENGTH: 4.90cm

MAXIMUM LOAD: 13.3kN

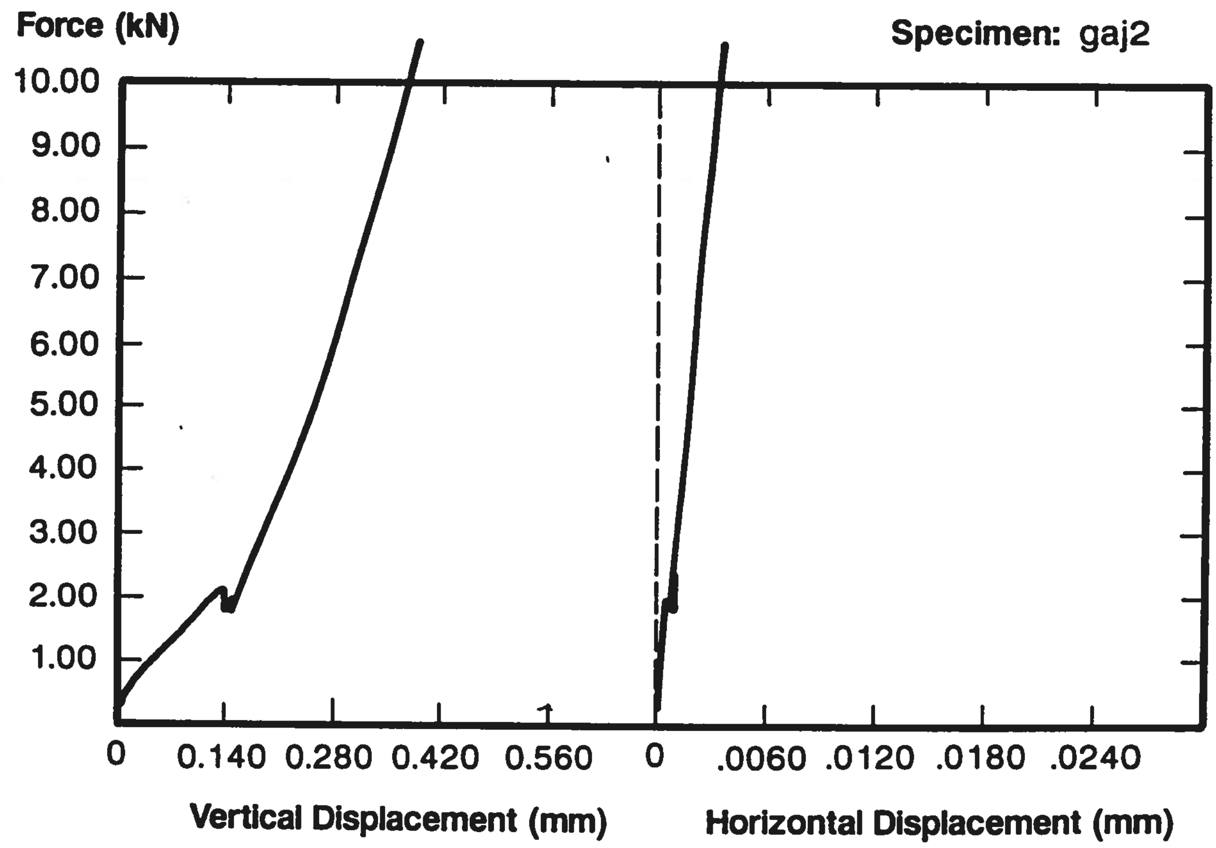

Fig: 3.19

SPECIMEN: CHINESE MARBLE

LENGTH: 2.53cm

DIAMETER: 5.40cm

DENSITY: 2.80g/cm^3

RADIAL DISPLACEMENT RATE: 0.0005/mm/min

GAGE LENGTH: 5.06cm

MAXIMUM LOAD: 13.2kN

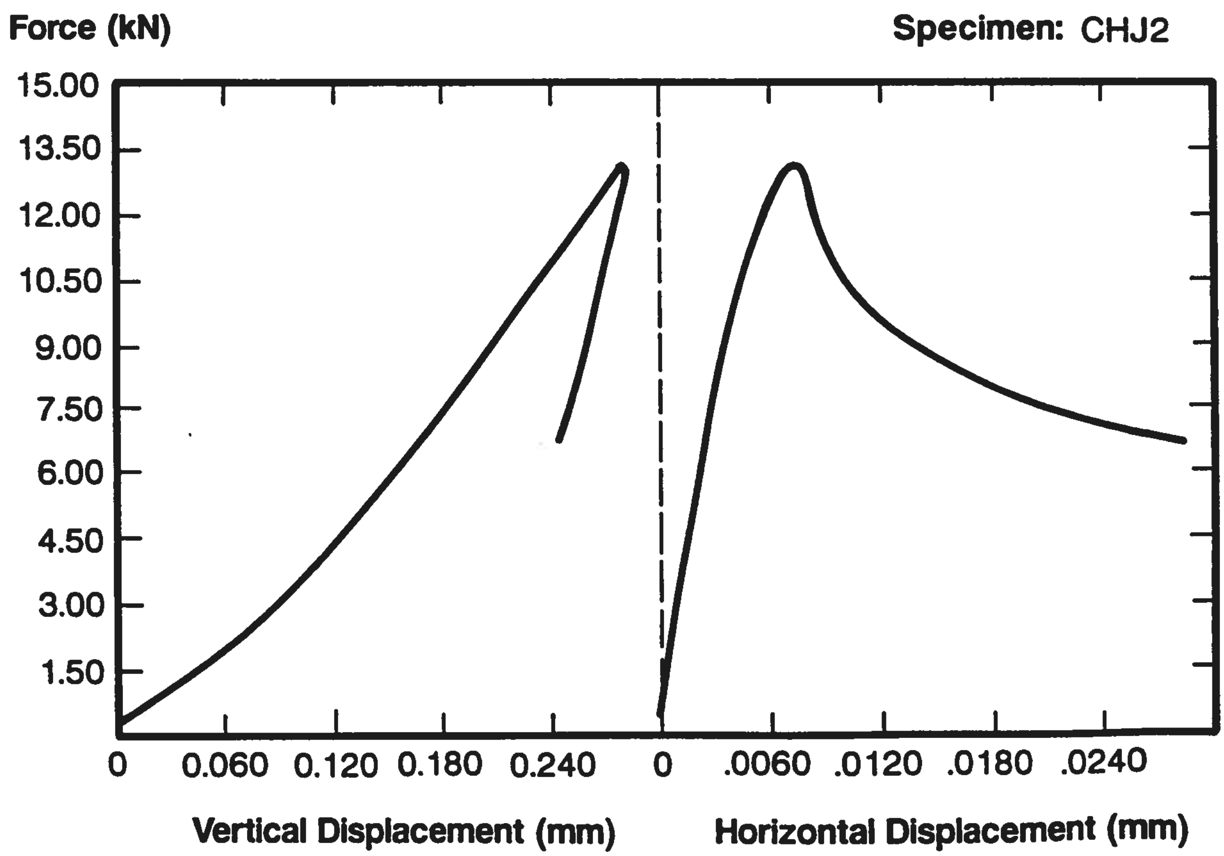

Fig: 3.20

SPECIMEN: CHINESE MARBLE

LENGTH: 2.41cm

DIAMETER: 5.27cm

DENSITY: 2.81g/cm^3

RADIAL DISPLACEMENT RATE: 0.0005/mm/min

GAGE LENGTH: 4.90cm

MAXIMUM LOAD: 13.6kN

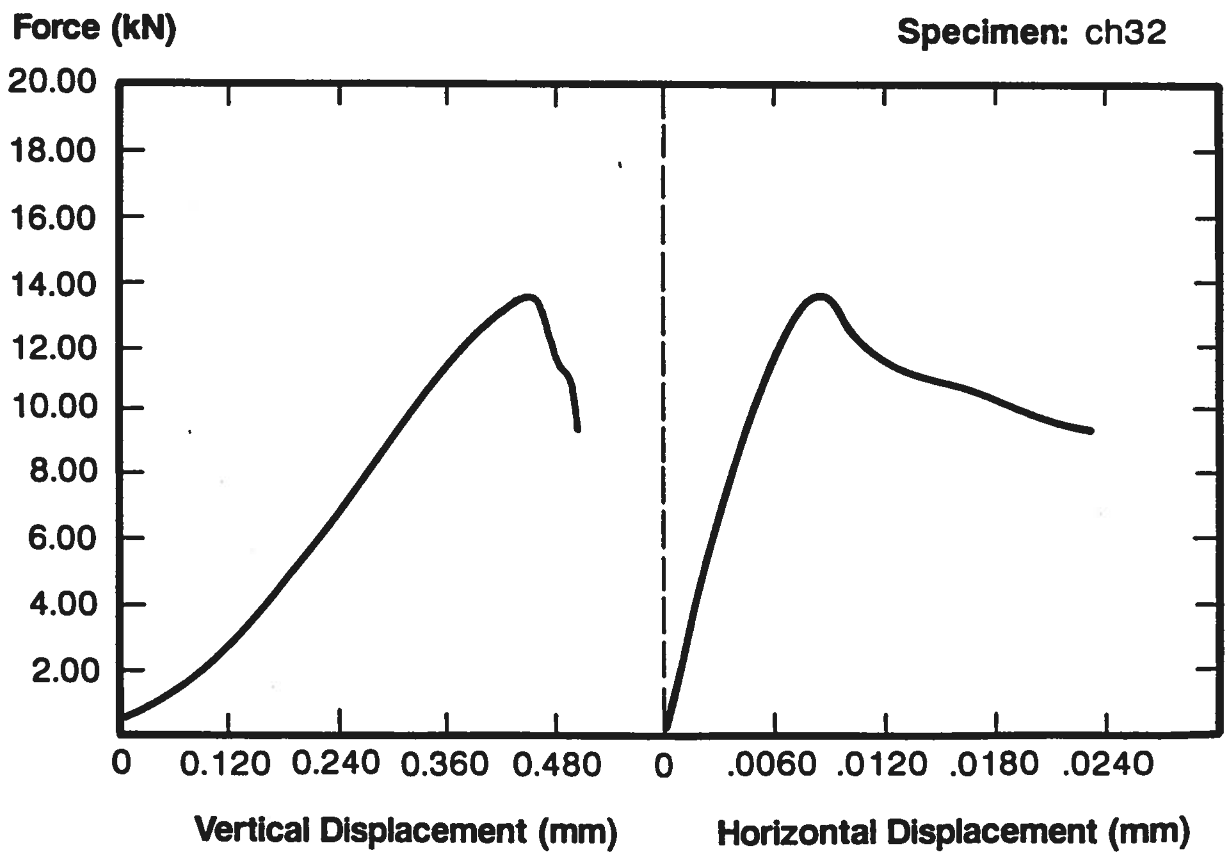

Fig: 3.21

SPECIMEN: CHINESE MARBLE

LENGTH: 2.58cm

DIAMETER: 5.39cm

DENSITY: 2.80g/cm^3

RADIAL DISPLACEMENT RATE: 0.00/mm/min

GAGE LENGTH: 5.06cm

MAXIMUM LOAD: 12.7kN

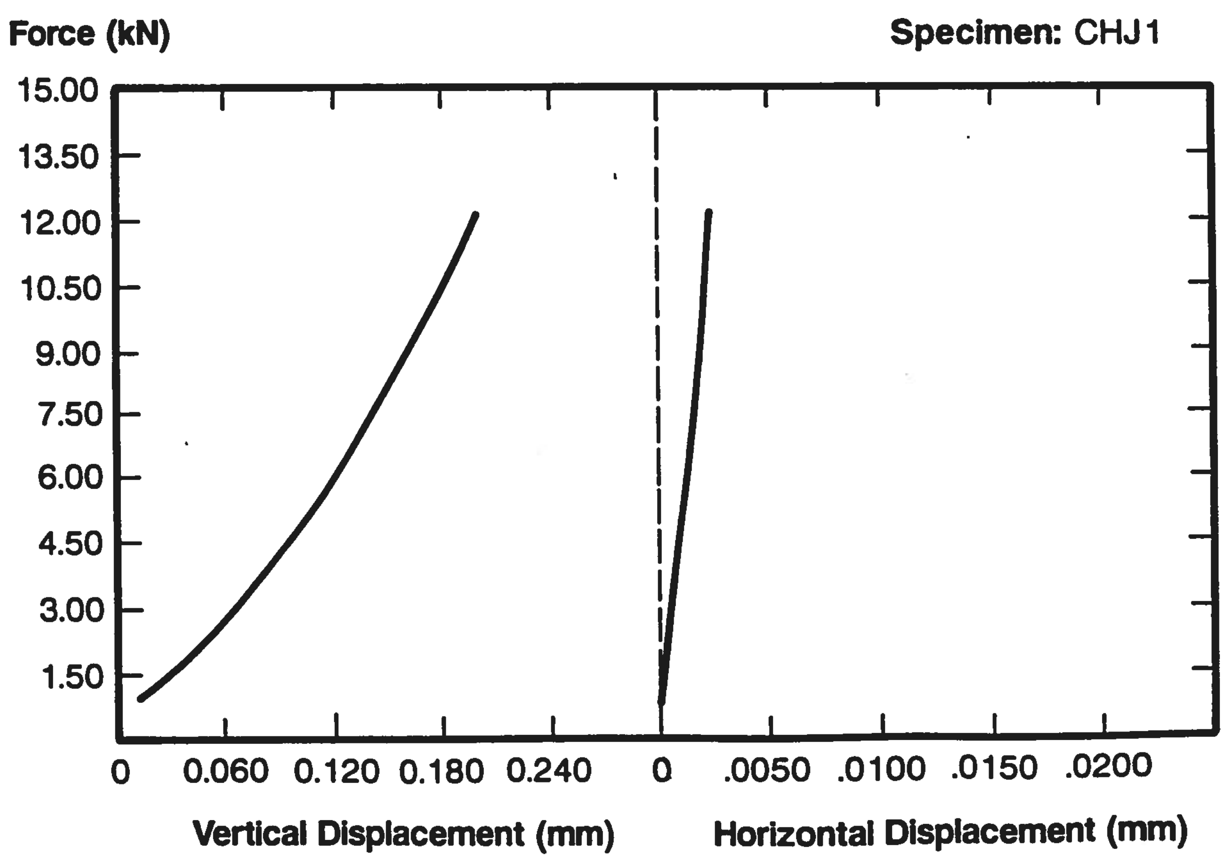

Fig: 3.22

SPECIMEN: CHINESE MARBLE

LENGTH: 2.48cm

DIAMETER: 5.40cm

DENSITY: 2.82g/cm^3

RADIAL DISPLACEMENT RATE: 0.000/mm/min

GAGE LENGTH: 5.06cm

MAXIMUM LOAD: 16.5kN

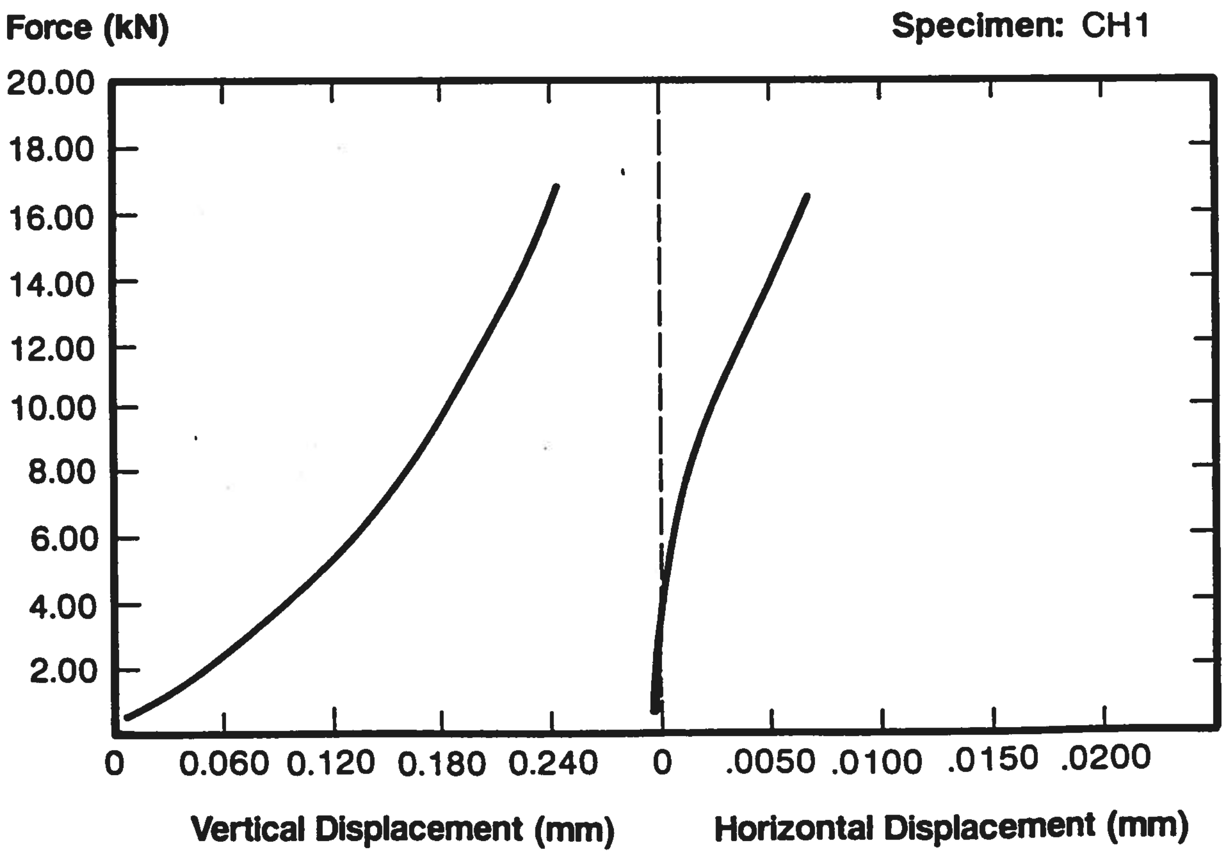

Fig: 3.23

CHAPTER 4

SLOW CRACK GROWTH IN MARBLE

4.1 Introduction

The purpose of this chapter is to investigate the sensitivity of marble samples to slow crack growth. It is well-known that for many structural materials the strength is dependent on how fast the stress is applied. Brittle materials such as glass, mortar, and concretes are very sensitive to the load rate. Comparatively little study has been performed on the sensitivity of marble and how marbles with different grain size behave under different load rate.

Evans[1] , Nadeau et al.[2] developed models for the effect of load rate on brittle materials based on fracture mechanics approach. Here the approach suggested by Nadeau et al is followed. The relationship between the stress intensity factor, K, the applied stress σ and the crack length a is given by:

$$K = Y\sigma\sqrt{a} \tag{4.1}$$

Where Y is a geometric constant. The material breaks when the stress intensity factor reaches an intrinsic material property Kc the fracture toughness. The applied stress at this condition will be associated to the strength of the material S. Equation 2 becomes:

$$K_c = YS\sqrt{a} \tag{4.2}$$

The crack velocity can be expressed as

$$\frac{da}{dt} = A\,K^N \tag{4.3}$$

Where A and N are constants. Combining equations (1) and (3)

$$\frac{da}{dt} = A\,Y^N\,K^N\,a^{n/2} \tag{4.4}$$

[1] A.G. Evans, Int. J. Fract. **10** , 251, (1974)

[2] Nadeau, R. Bennett and E.R. Fuller, Journal of Materials Science 17 2831, (1982)

Substituting the identity

$$\frac{d\sigma}{\dot{\sigma}} = dt \tag{4.5}$$

and integrating equation (4)

$$\int_{a_i}^{a_f} a^{-N/2}\, da \;=\; \left(\frac{A\, Y^N}{\dot{\sigma}}\right) \int \sigma^N\, d\sigma \tag{4.6}$$

or,

$$\frac{2}{(N-2)} \left\{ a_i^{-(N-2)/2} - a_f^{-(N-2)/2} \right\} \;=\; \frac{A\, Y^N}{(N+1)\,\dot{\sigma}}\, \sigma_f^{N+1} \tag{4.7}$$

Where the subscripts i and f corresponds to the initial and final condition. Noting from equation (1) that $a = \frac{K^2}{\sigma^2\, Y^2}$, and that $S_f = \sigma_f$, equation (7) becomes:

$$S_f^{N+1} \;=\; 2\,\dot{\sigma}\, K_c^{2-N}\, (N+1)/AY^2\, (N-2)\, \left(S_i^{N-2} - S_f^{N-2}\right) \tag{4.8}$$

Defining

$$B \equiv 2\;\, K_c^{2-N}\, (N+1)/AY^2\, (N-2) \tag{4.9}$$

gives,

$$S_f^{N+1} + B\,\dot{\sigma}\, S_f^{N-2} \;=\; B\,\dot{\sigma}\, S_f^{N-2} \tag{4.10}$$

Equation 10 can be used directly to determine the initial strength of a specimen once the final strength is known or to determine the final strength for a given load rate once the initial strength is known. It should be noted that the latter condition requires to solve equation 10 numerically. Of course for that the constants N and B should be determined beforehand. In this work the constants were obtained using two methods: (a) develop a non-linear modeling of fitting the experimental results in equation (10), (b) to take the logarithm of equation 10 and assume a linear response which gives that in a plot of ln Sf against ln $\dot{\sigma}$ gives a slope of 1/(N+1) at low values of $\dot{\sigma}$; the intercept of such plot gives the information on B by the relationship: $\log B = (N+1)\log S_{f_0} - (N-2)\log S_i$.

4.2 Experimental

The beams were tested in four point loading, with 248 mm between the supports and 124 mm between the loads. Four different load rates ranging from 0.31 psi/s to 3100 psi/s were used. For the two highest load rates a 220 kN capacity loadcell was used for loading while a 4 kN loadcell was used for reading the load. The 4 kN loadcell was used for load control for the two slower rates. The accuracy of the 4 kN loadcell was better than 0.5 N. Four different marbles were tested.

4.3 Results and Discussions

The experimental results of the effect of load rate on the strength of marble are given in Tables 4.1-4.3. Figures 4.1-4.5 show the plots of log Sf against log $\dot{\sigma}$ used to obtain the material constants, N and B, according to method (b) described above. Table 4.4 summarizes these constants.

Marble	N	B
Italian	45.93	1.21
Georgia (I)	31.26	0.38
Georgia (II)	31.26	1.83
Vermont	28.41	1.74
Chinese	46.62	5.55

Table 4.4

Values of N and B for various types of marble

Non-linear fittings were also performed for the Italian and Georgia Marble. The fundamental equation (10) was derived for the four types of marble studied in this study and they are presented below:

Italian Marble (stresses in Ksi)

linear

$$S_f^{46.93} + 1.21\,\dot{\sigma}\,S_f^{43.93} = 2.99\,10^6\,\dot{\sigma}$$

non-linear

$$S_f^{39.47} + 33.36\,\dot{\sigma}\,S_f^{36.47} = 1.03\,10^6\,\dot{\sigma}$$

Georgia Marble (I)

linear

$$S_f^{33.25} + 0.38\,\dot{\sigma}\,S_f^{29.26} = 1.16\,10^{-4}\,\dot{\sigma}$$

non-linear

$$S_f^{23.60} + 28.42\,\dot{\sigma}\,S_f^{20.60} = 1.14\,10^{-2}\,\dot{\sigma}$$

Georgia Marble (II)

linear

$$S_f^{32.26} + 1.84\,\dot{\sigma}\,S_f^{29.26} = 2.60\,10^{10}\,\dot{\sigma}$$

Vermont Marble

$$S_f^{29.41} + 1.74\,\dot{\sigma}\,S_f^{26.41} = 4.17\,10^{9}\,\dot{\sigma}$$

Chinese

$$S_f^{47.62} + 5.56\,\dot{\sigma}\,S_f^{44.62} = 8.96\,10^{14}\,\dot{\sigma}$$

The above equations permit the computation of the fracture strengh at a given constant loading rate once the initial strength is known. The equations are non-linear so a program was written for Mathematica and the values were computed numerically. Figures 4.6 to 4.10 indicates such relationship. It should be noted that there was not a significant difference from the values obtained using the non-linear fit of the experimental results. Figure 4.11 indicates that there is a correlation between the value n and the crystal size of the marble.

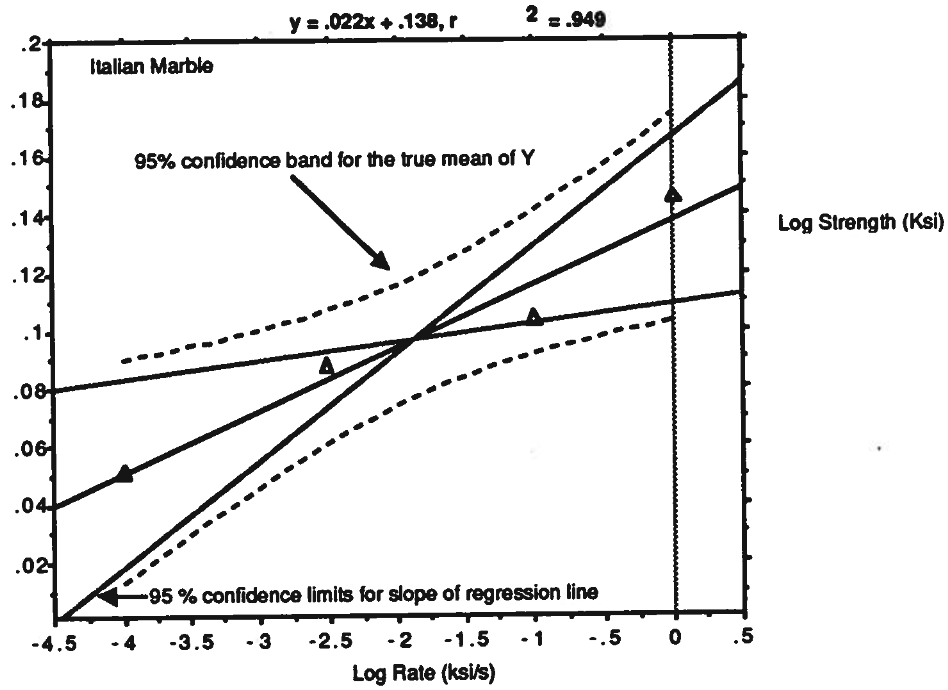

Fig. 4.1

Plot of log Sf against log $\dot{\sigma}$

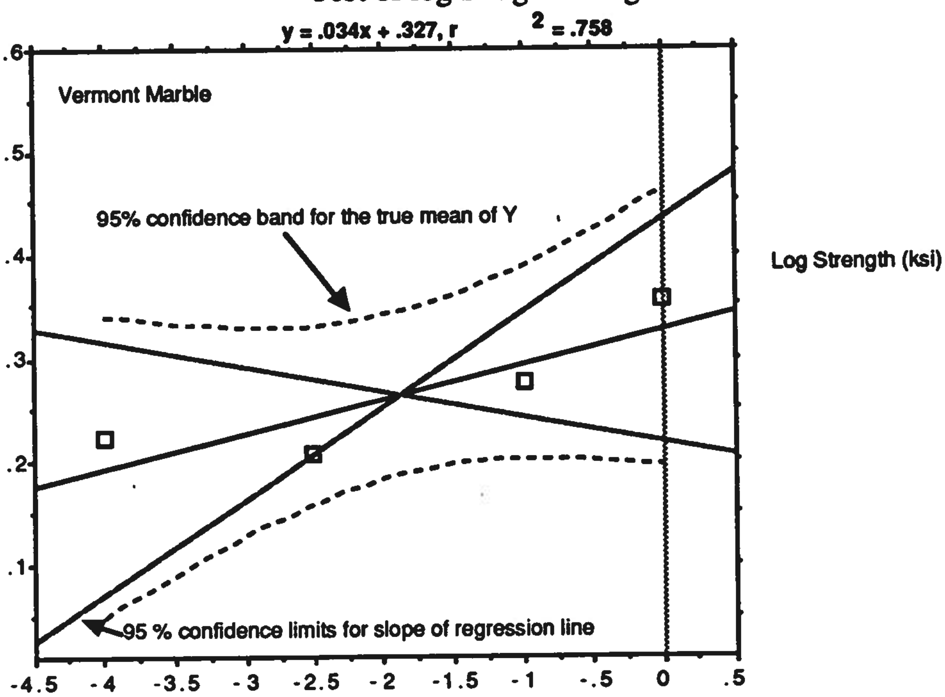

Fig. 4.2

Plot of log Sf against log $\dot{\sigma}$

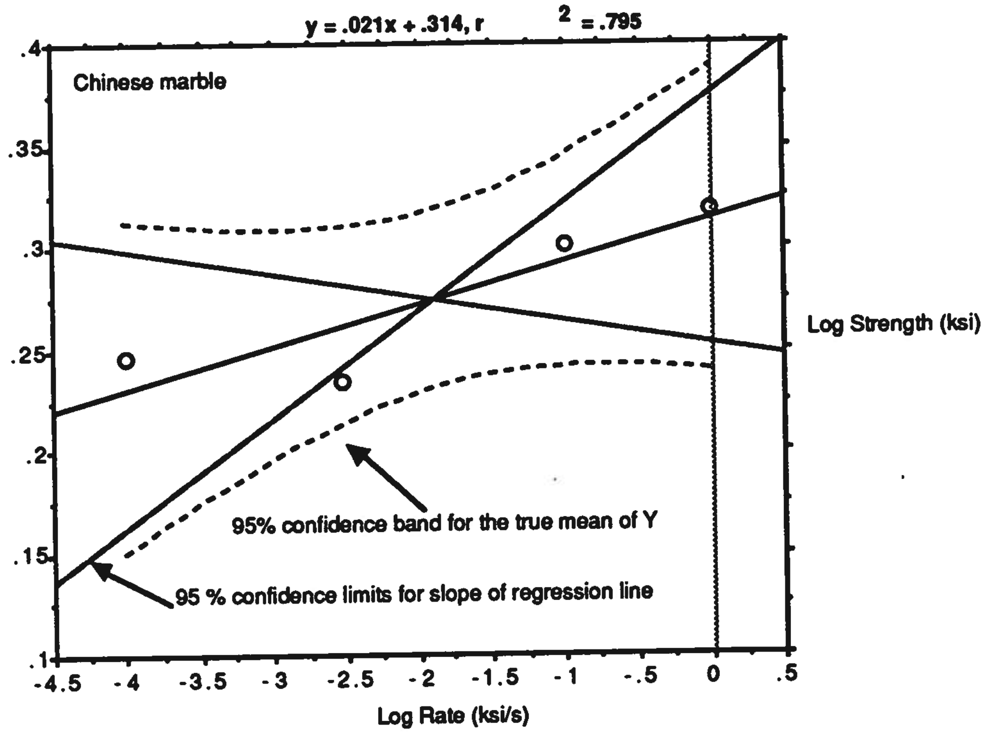

Fig. 4.3

Plot of log Sf against log $\dot{\sigma}$

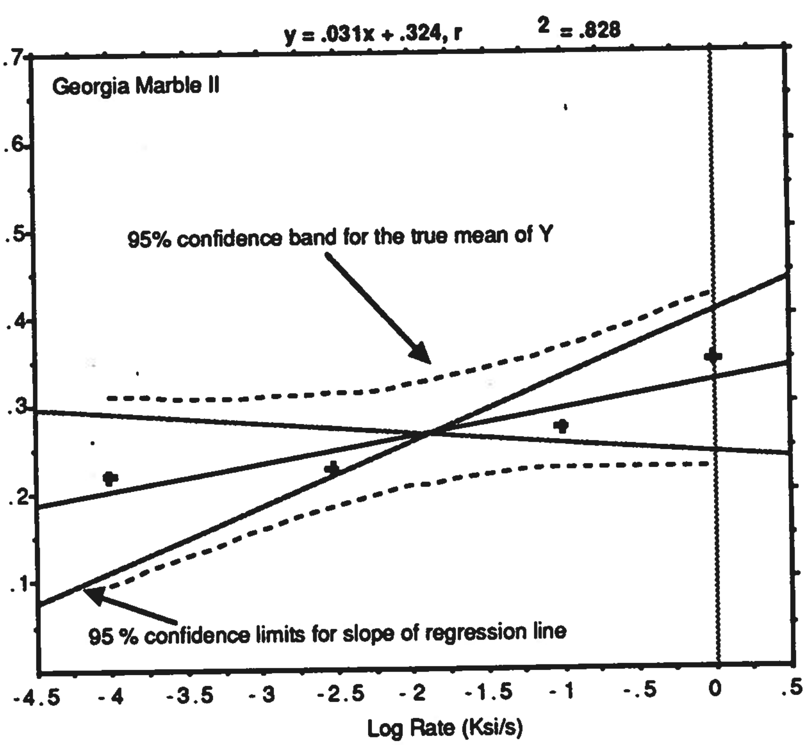

Fig. 4.4

Plot of log Sf against log $\dot{\sigma}$

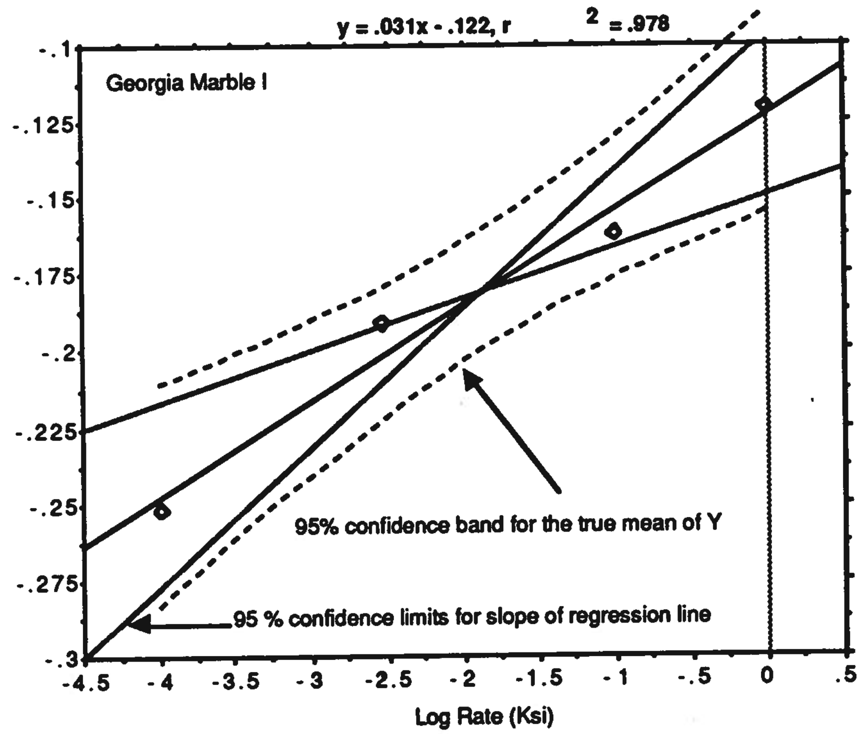

Fig. 4.5

Plot of log Sf against log $\dot{\sigma}$

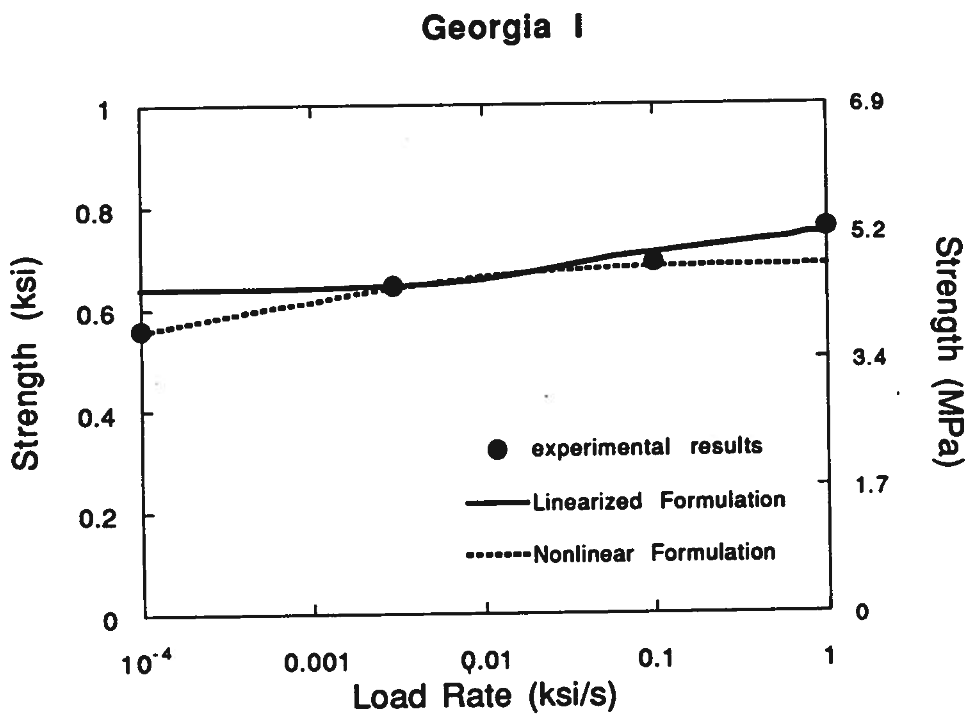

Georgia I
1
0.8
0.6
0.4
0.2
0
Strength (ksi)
6.9
5.2
3.4
1.7
0
Strength (MPa)
experimental results
Linearized Formulation
Nonlinear Formulation
10^{-4}
0.001
0.01
0.1
1
Load Rate (ksi/s)

Fig. 4.6

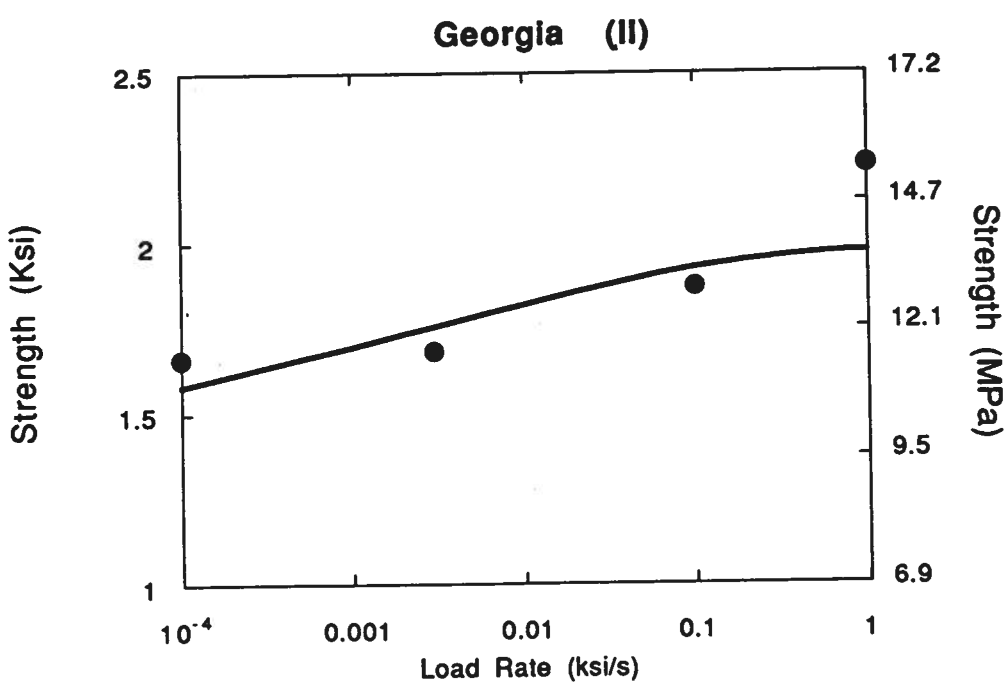

Georgia (II)
2.5
2
1.5
1
Strength (Ksi)
17.2
14.7
12.1
9.5
6.9
Strength (MPa)
10^{-4}
0.001
0.01
0.1
1
Load Rate (ksi/s)

Fig. 4.7

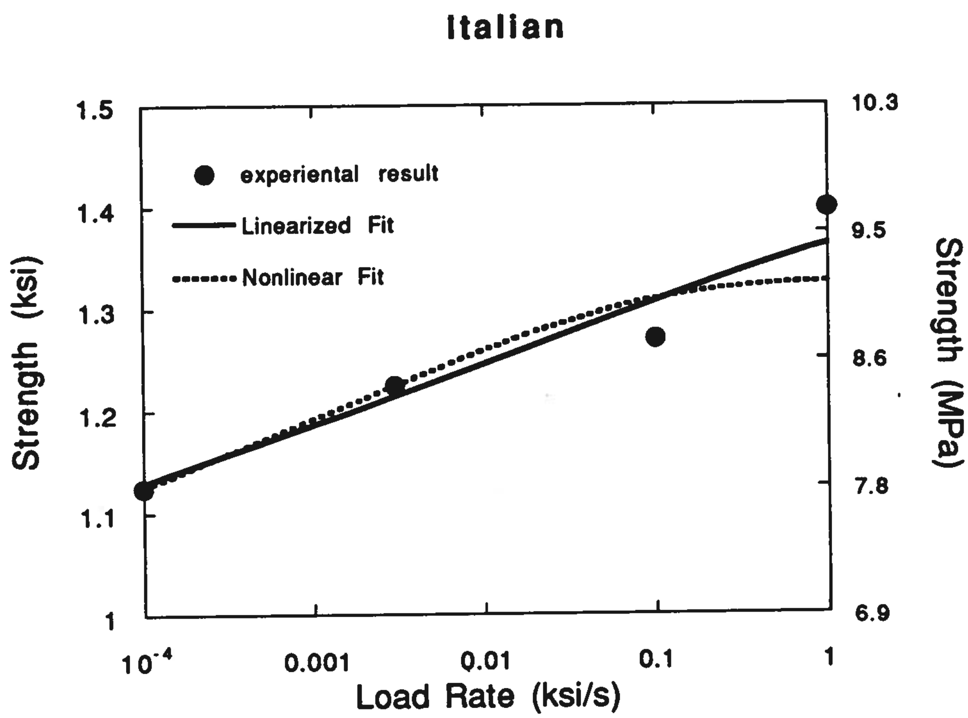
Italian
1.5
1.4
1.3
1.2
1.1
1
10.3
9.5
8.6
7.8
6.9
experiental result
Linearized Fit
Nonlinear Fit
Strength (ksi)
Strength (MPa)
10^-4
0.001
0.01
0.1
1
Load Rate (ksi/s)

Fig. 4.8

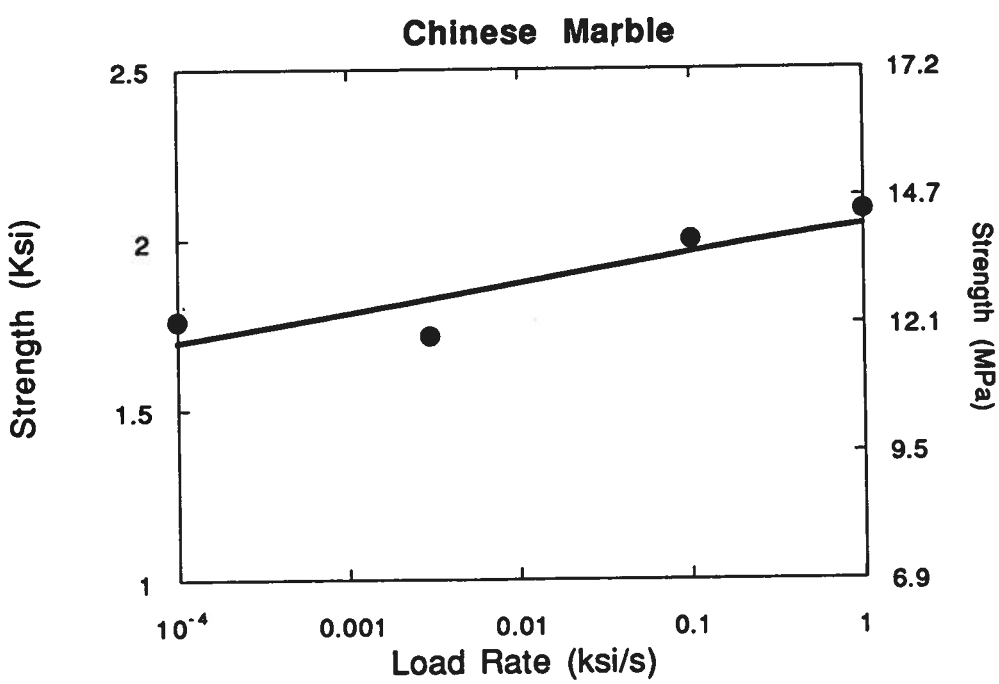
Chinese Marble
2.5
2
1.5
1
17.2
14.7
12.1
9.5
6.9
Strength (Ksi)
Strength (MPa)
10^-4
0.001
0.01
0.1
1
Load Rate (ksi/s)

Fig. 4.9

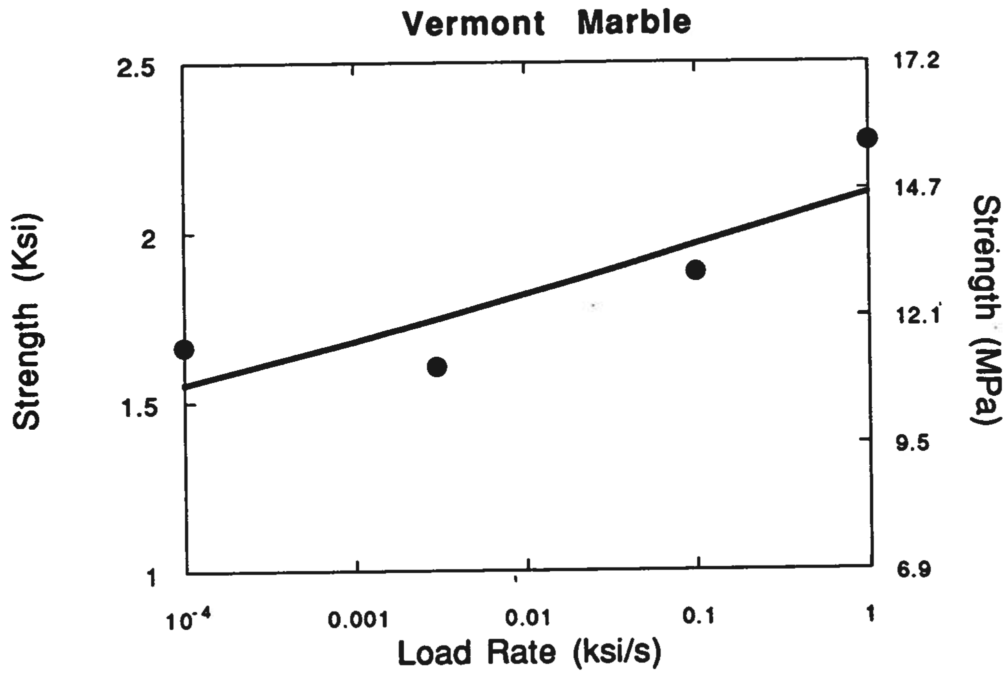

Fig. 4.10

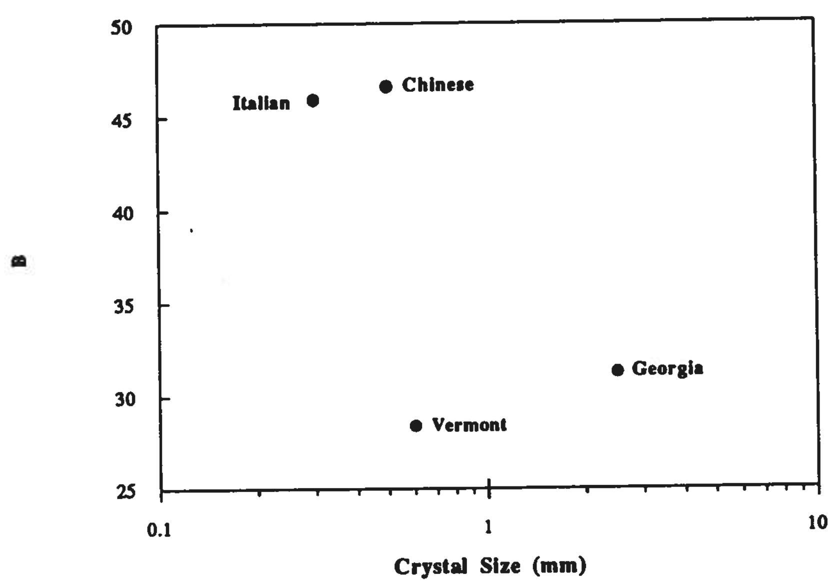

Fig. 4.11

CHINESE MARBLE		ITALIAN MARBLE	
load rate (psi/s)	strength (psi)	load rate (psi/s)	strength (psi)
3100.00	2020.00	3100.0	1501.0
3100.00	1919.00	3100.0	1328.0
3100.00	1887.00	3100.0	1334.0
3100.00	2170.00	3100.0	1316.0
3100.00	2174.00	3100.0	1472.0
3100.00	2320.00	3100.0	1438.0
310.00	2051.00	310.00	1097.0
310.00	2113.00	310.00	1230.0
310.00	2237.00	310.00	1516.0
310.00	1779.00	310.00	1297.0
310.00	1965.00	310.00	1217.0
310.00	1838.00	310.00	1308.0
9.30	1753.00	310.00	1225.0
9.30	1818.00	9.30	1232.0
9.30	1798.00	9.30	1239.0
9.30	1646.00	9.30	1120.0
9.30	1667.00	9.30	1446.0
9.30	1611.00	9.30	1229.0
0.31	1684.00	9.30	1080.0
0.31	1624.00	0.31	1109.0
0.31	1698.00	0.31	1089.0
0.31	2428.00	0.31	1120.0
0.31	1606.00	0.31	1144.0
0.31	1577.00	0.31	1161.0
0.31	1712.00		

Table 4.1

Effect of Load Rate on the Strength

Georgia Marble

FOLIATION II		FOLIATION I	
load rate (psi/s)	strength (psi)	load rate (psi/s)	strength (psi)
3100.0	2003.0	3100.0	880.00
3100.0	2207.0	3100.0	686.00
3100.0	2114.0	3100.0	782.00
3100.0	2164.0	3100.0	685.00
3100.0	2234.0	310.00	728.00
3100.0	2215.0	310.00	737.00
3100.0	1894.0	310.00	680.00
3100.0	3114.0	310.00	612.00
3100.0	2155.0	9.3000	607.00
3100.0	2195.0	9.3000	592.00
310.00	1807.0	9.3000	682.00
310.00	1918.0	9.3000	699.00
310.00	1904.0	0.31000	496.00
310.00	1925.0	0.31000	615.00
310.00	1811.0	0.31000	570.00
9.3000	1610.0		
9.3000	1627.0		
9.3000	1766.0		
9.3000	1815.0		
9.3000	1601.0		
0.31000	1798.0		
0.31000	1474.0		
0.31000	1707.0		
0.31000	1561.0		
0.31000	1767.0		

Table 4.2

Effect of Load Rate on the Strength

Table 4.3 Effect of Load Rate on the Strength of Vermont Marble

load rate (psi/s)	strength (psi)
3100.0	2034.0
3100.0	1984.0
3100.0	2274.0
3100.0	2439.0
3100.0	1924.0
3100.0	2639.0
3100.0	2098.0
3100.0	2311.0
3100.0	2004.0
3100.0	2918.0
3100.0	2287.0
3100.0	2271.0
310.00	1782.0
310.00	1730.0
310.00	2063.0
310.00	1950.0
9.3000	1280.0
9.3000	1744.0
9.3000	1216.0
9.3000	1303.0
9.3000	1779.0
9.3000	1804.0
9.3000	1885.0
9.3000	1822.0
0.31000	2149.0
0.31000	1935.0
0.31000	1904.0
0.31000	1917.0
0.31000	1822.0
0.31000	1281.0
0.31000	1453.0
0.31000	1557.0
0.31000	1186.0
0.31000	1429.0

CHAPTER 5

BEHAVIOR OF MARBLE UNDER COMPRESSION

5. 1 Introduction

The preservation of stress-induced structure and the identification of cracks induced by loading and unloading are important to understand the mechanisms for the generation, propagation and interaction of stress-induced microcracks in complex systems such as marble. To preserve the microstructure in marble specimens under load, the voids were filled with a liquid metal alloy called "Wood's metal" during loading, and the alloy was solidified in place before unloading. Wood's metal is a metal alloy that has a melting point below the boiling point of water. Cylindrical marble specimens were submerged in the molten metal alloy during the test and the alloy was driven into voids and fractures by pore pressure. The alloy could be solidified at any stage of the experiment to preserve the geometry of microcracks as they existed under load and to distinguish them from those generated later. With a surface tension of 400 mN/m, the alloy could penetrate into flat cracks with apertures as fine as 0.08 microns under a pore pressure of 1500 psi. Such a technique not only allows one to observe the microcracks as they exist under load, but also facilitates observing the microcracks in three dimensions . A comprehensive image analysis was performed on the cracking pattern developed in the marble samples. Also the propagation of the cracking process was modeled using discontinuous deformation analysis with finite element mesh

5. 2 Experimental Techniques

The composition of the Wood's metal was: 42.5% Bi, 37.7% Pb, 11.3% Sn, and 8.5% Cd, and had a melting point of approximately 80 C. Cylindrical specimens were submerged in the molten metal alloy during test and the alloy was driven into voids and fractures by pore pressure. The specimens were 4 inches long by 1-inch in diameter. The cylindrical cores were cut and the ends were ground parallel to one another at the required length. The specimens after this stage were ready for uniaxial compression test assembly. The next step was to assemble the specimens into a specially designed vessel for the molten metal injection. After the specimen and the steel-end piece were assembled into the vessel, it was heated up to 100 C with the end cap open. The molten Wood's metal was poured into the vessel to a level above the top end of the specimen, forming a metal reservoir with the specimen totally submerged inside. The top end cap was assembled immediately. The vessel containing the molten metal and the specimen was assembled with loading and measuring apparatus. The LVDT's for the axial displacement measurements were attached to the steel end-piece and LVDT for the radial displacement measurement was attached to a split steel ring. Figure 5.1 shows a schematic set up for the testing. To saturate the specimen with molten metal, nitrogen pressure was applied to the top of molten metal in which the specimen was completely submerged. The nitrogen pressure was controlled by a high pressure regulator on a bottle of nitrogen. An axial stress was applied to the specimen up to 1600 psi, and a pressure of 500 and 1250 psi was applied to the molten metal as the pore pressure. The pore pressure was kept constant throughout the tests and did not alter the effective stresses on the specimens. The axial strain of interest was kept constant for 10 minutes to allow the liquid to penetrate into pores and fractures fully, before the vessel was rapidly cooled down to room temperature. Each test specimen was then sectioned along its axis and across its diameter, ground and polished for microscopic examination and photography.

5.3 Stereology of the Marble Samples

Stereology is the study of the three-dimensional structures of objects and matter that are viewed two-dimensionally in sections. In real structures, the lines in a microsection of a given specimen are usually either isometric or partially oriented. Only in rare cases do completely oriented systems of lines are found. In a partially oriented system of lines in a plane, part of the total length of lines is oriented in a definite direction (or directions). The remaining segments may essentially have a random orientation.

The lines of a partially oriented system of lines in a plane can be divided into elementary straight segments that are very small and of equal length. Some or all segments will lie parallel to one or more definite directions (the orientation axes). The remaining segments are assumed to be oriented randomly, i.e., isometrically. From this point of view, a partially oriented system of lines may be regarded as consisting of two superimposed systems of lines , i.e., an oriented portion and a random portion.

The length of linear elements in a plane is proportional to the number of intersections made with a test line. Using a test array of straight parallel lines, the number of intersections with an oriented system of lines (such as a crack system) will vary with the direction of the test array. The dependence of the number of intersections per unit length with the angle of the test array can be used to characterize the degree and type of orientation of a system of lines in a plane. The equation that relates the length of lineal elements in a plane to their intersection with a test line is

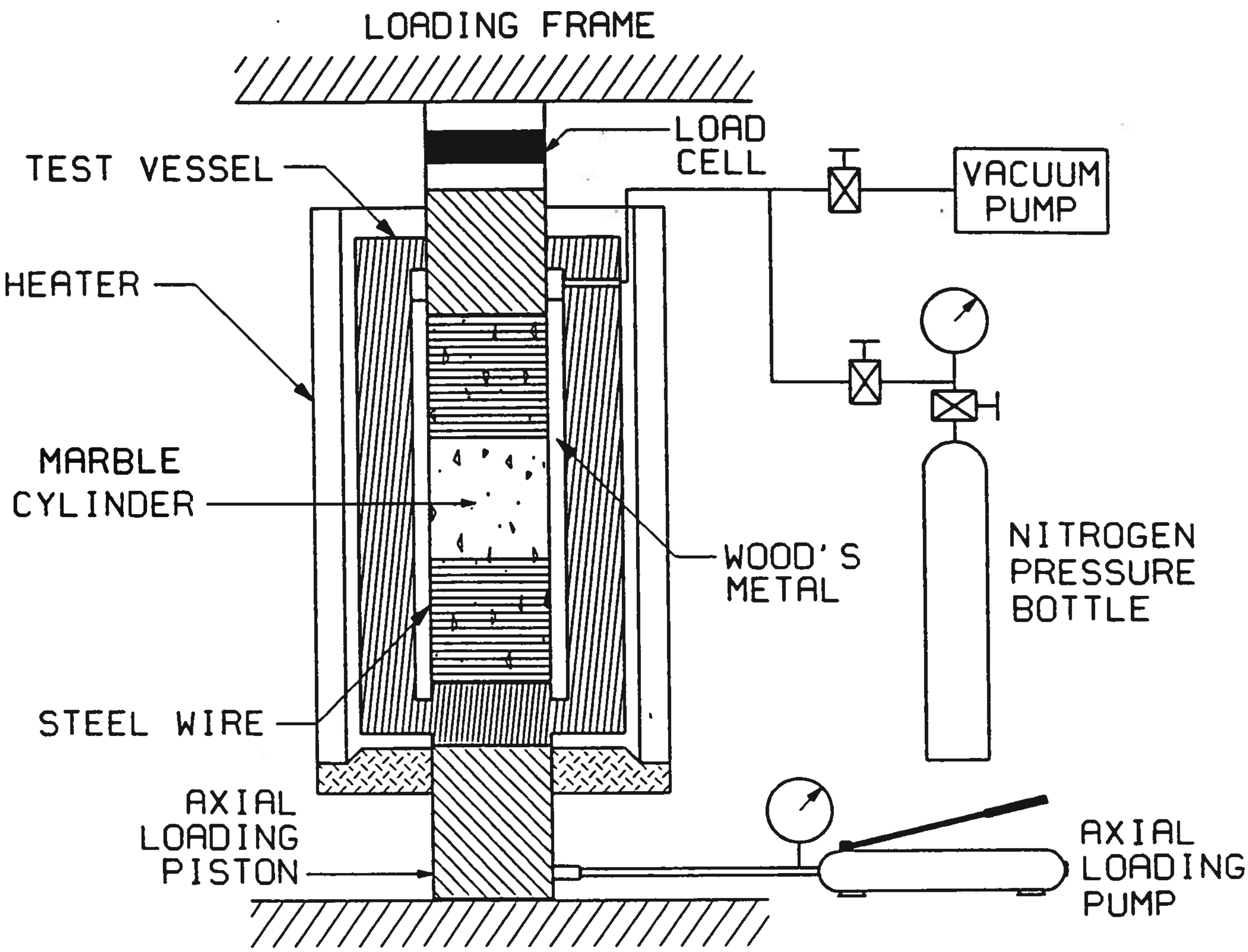
LOADING FRAME
LOAD CELL
TEST VESSEL
VACUUM PUMP
HEATER
MARBLE CYLINDER
WOOD'S METAL
NITROGEN PRESSURE BOTTLE
STEEL WIRE
AXIAL LOADING PISTON
AXIAL LOADING PUMP

Fig: 5.1

$$L_A = \left(\frac{\pi}{2}\right) P_L \qquad \mu m/m^2$$

The quantity L_A is a basic microstructural parameter that serves useful either as is or when manipulated into other forms.

Given a randomly oriented system of lines in a plane, let us consider a square test area A_T of edge length l. A set of N vertical test lines of total length L_T=Nl is passed randomly through the test area, cutting horizontal lines through the square with density N/l. The system of lines is divided into n straight elementary segments of length δL and the total line length in the system is L=n δL. The elementary segments from angle θ_i to the vertical test lines, and the length of projections of the elementary segments on a horizontal line are L sinθ_i. Thus the fraction of test lines intersecting the elementary segments is δLsinθ_i/l.

if P_i is the number of intersections of each elementary segment by the test lines, then the expected value of the total number of intersections with the entire system of lines is

$$E(P) = \sum P_i = N\sum_0^n \delta L \sin\theta_i \;\; /l = (N\delta L/l)\sum_0^n \sin\theta_i \tag{1}$$

Since the elementary systems are oriented randomly each value of the angle i has equal likelihood of existence and $(1/n)^n$ sinθ_i equals the average value, sinθ. Making appropriate substitutions, we obtain

$$E(P) = (\delta\, Ln/l\,)\sin\theta = \left(\frac{L_T}{l^2}\right)\sin\theta \tag{2}$$

The probability that the elementary segments are oriented between θ+dθ is equal to the fraction of the perimeter of a circle that is occupied by this orientation range. From the symmetry involved, only one quadrant of the circle need to be considered, giving for the probability

$$P(\theta)\,d\theta = \left[r\,d\theta/(\pi\,r/2)\right] = \left(\frac{2}{\pi}\right)d\theta$$

Thus the average value of sinθ_i is

$$\sin\theta = \int_0^{\pi/2} P(\theta)\sin\theta\,d\theta = \left(\frac{2}{\pi}\right)\int_0^{\pi/2}\sin\theta\,d\theta = \left(\frac{2}{\pi}\right) \tag{3}$$

Rearrangement of equation (2) gives

$$\frac{L}{A_T} = \left(\frac{\pi}{2}\right) \left[\frac{E(P)}{L_T}\right] \qquad \mu m / m^2 \qquad (4)$$

or in our notation,

$$L_A = \left(\frac{\pi}{2}\right) P_l \qquad (5)$$

In the case of an isometric system, the value of $P_L(\theta)$ is dependent of θ and both sides of equation (5) can be averaged with respect to orientation. The result is an important relationship connecting the length of lineal features in a sampling area, L_A, to the specific surface area or to the number of intersections per unit length of the test line, and averaged with respect to the orientation. Therefore,

$$L_A = \left(\frac{\pi}{2}\right) P_l = \left(\frac{\pi}{4}\right) S_v \qquad (6)$$

Where Sv is the specific surface area.

Applying the method of random secants on a plane to an image of a crack pattern, equation (6) presents simple algebraic relationships to calculate the total crack length per unit area or the specific surface area (of the cracks) per unit volume. The dependence of the number of intersections per unit length with the angle of the test array can be used to characterize the degree and types of orientation of a system of lines in a plane. Saitykov proposes a polar plot of PL with respect to the orientation axis (axes), and calls the resulting curve the *rose of the number of intersections*, or simply the *rose*.

The rose for an oriented system of lines can be easily obtained experimentally. We apply a test array to the system of lines at (equal) angular increments with respect to the orientation axis, and determine PL separately at each angle. The we draw radius vectors on a polar graph paper, plotting PL versus . We connect the ends of the radius vectors by a smooth curve, giving the rose. In case of isometry, the rose will be a circle with its center at the origin of the polar figure. If a preference direction should occur in a crack pattern, the shape of the rose will change.

The stress-induced microcrack system in marble is considered to be a partially oriented as opposed to a completely oriented (idealized) system. Test arrays of equal angular increments were applied to each binary image, and the number of intersections was determined separately at each angle 0. Then the number of intersections was plotted versus 0, creating the "compass rose" pattern diagram.

The rose diagram characterizes the degree of orientation of the cracks, and makes it easier to interpret the data. The rose diagrams were plotted to cover only the range of 0 to 150^{o} (cracks at 0 and 180^{o} have equal lengths) since the range from 180 to 360^{o} is redundant.

5.4 Experimental Results

Figure 5.2 shows the vertical cross section of a marble specimen that has been loaded up to failure. The dark zones indicate where the metal has penetrated the crack induced by the mechanical load. There is a strain localization at the center of the specimen and four major lines of shear failure starting at the edges of the specimen. This image will be used as a starting point for the modeling developed in section 5.5. Figure 5.3 shows an optical image of the center of the specimen where cracking localization developed. Note that besides the major dark lines caused by shear failure, a significant amount of damage was also produced at the individual crystal level. Cracks developed not only at the grain boundaries but also running through the grains. Due to the three-dimensional confinement caused by end effects the amount of damage is not as intense at the extremities of the sample, as indicated by Figure 5.4.

All the quantitative analysis was performed in polished samples of marble and using backscattered electron imaging. Figure 5.4 shows a typical image using such technique. A few samples were exposed to mild acid so the marble would leach away leaving the 3-dimensional framework formed by the cracks filled with Wood's metal. Under secondary electron microscope these samples indicate the complexity of the system of cracks induced by the stress. Figures 5.5 a and b show the three-dimensional crack network . It should be noted that these images, even though useful for visualization, are not quantitative so most of the research effort concentrated on the use of backscattered images. One point that should be addressed is the importance of the crystal orientation on the crack propagation. Little has been done in this area, so preliminary research was performed using the new method of Kikuchi patterns, used in solid state physics. Backscattered Kikuchi patterns were analyzed to determine lattice orientation in small localized regions. When a focused beam of electrons penetrates a crystalline material, backscattered electrons emanate in all directions within a small interaction volume . The energy of these electrons is reduced only slightly from their initial value. Some of these electrons backscatter through the surface, where the flux pattern they form clearly marks bands of electrons diffracted from planes in the crystal lattice. Electron Back Scattered diffraction Patterns, or EBSP'S use a standard scanning electron microscope in

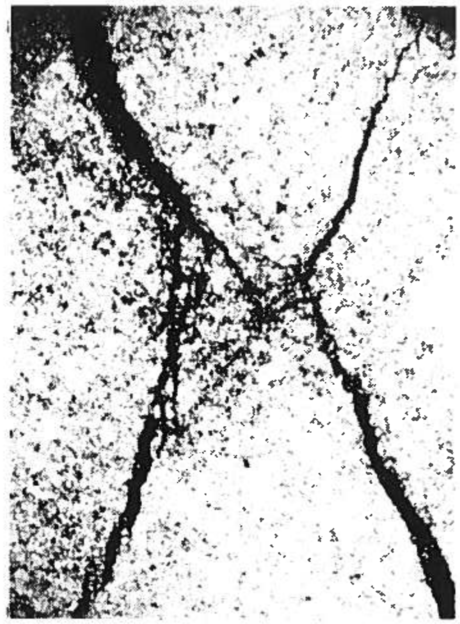

Fig: 5.2

Fig: 5.3(a)

Fig: 5.3(b)

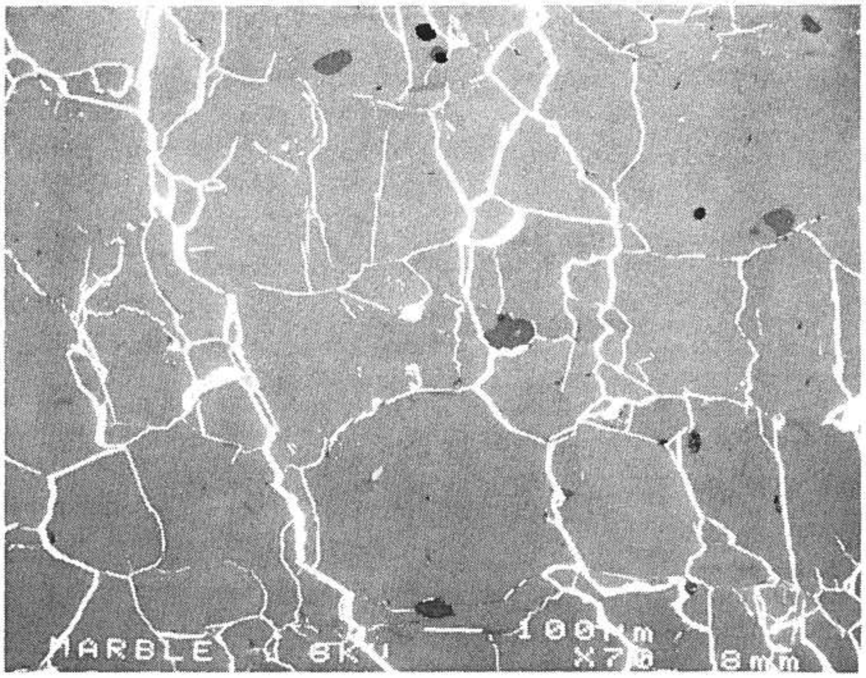

Fig: 5.4

Fig: 5.5(a)

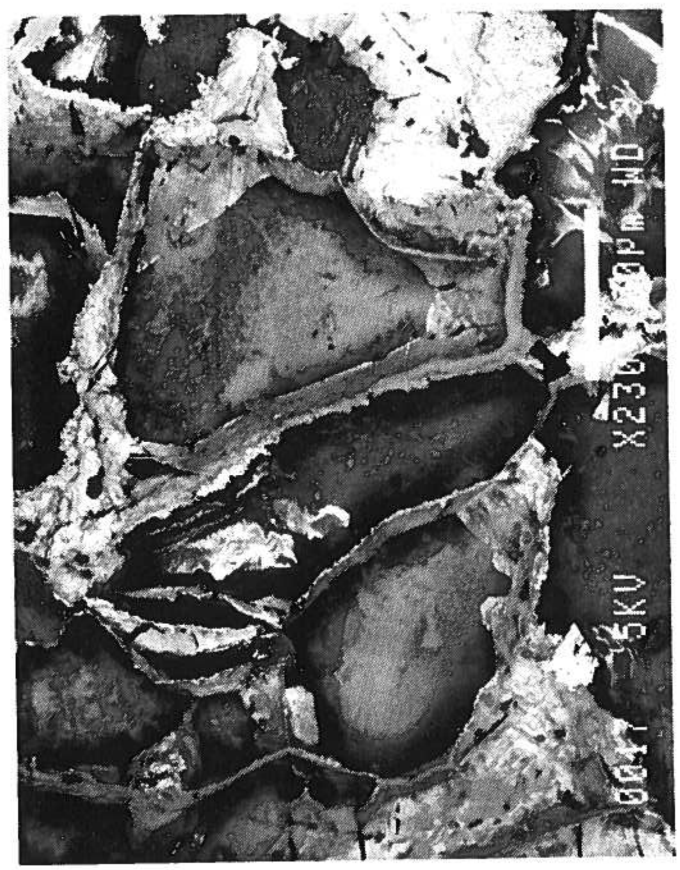

Fig: 5.5(b)

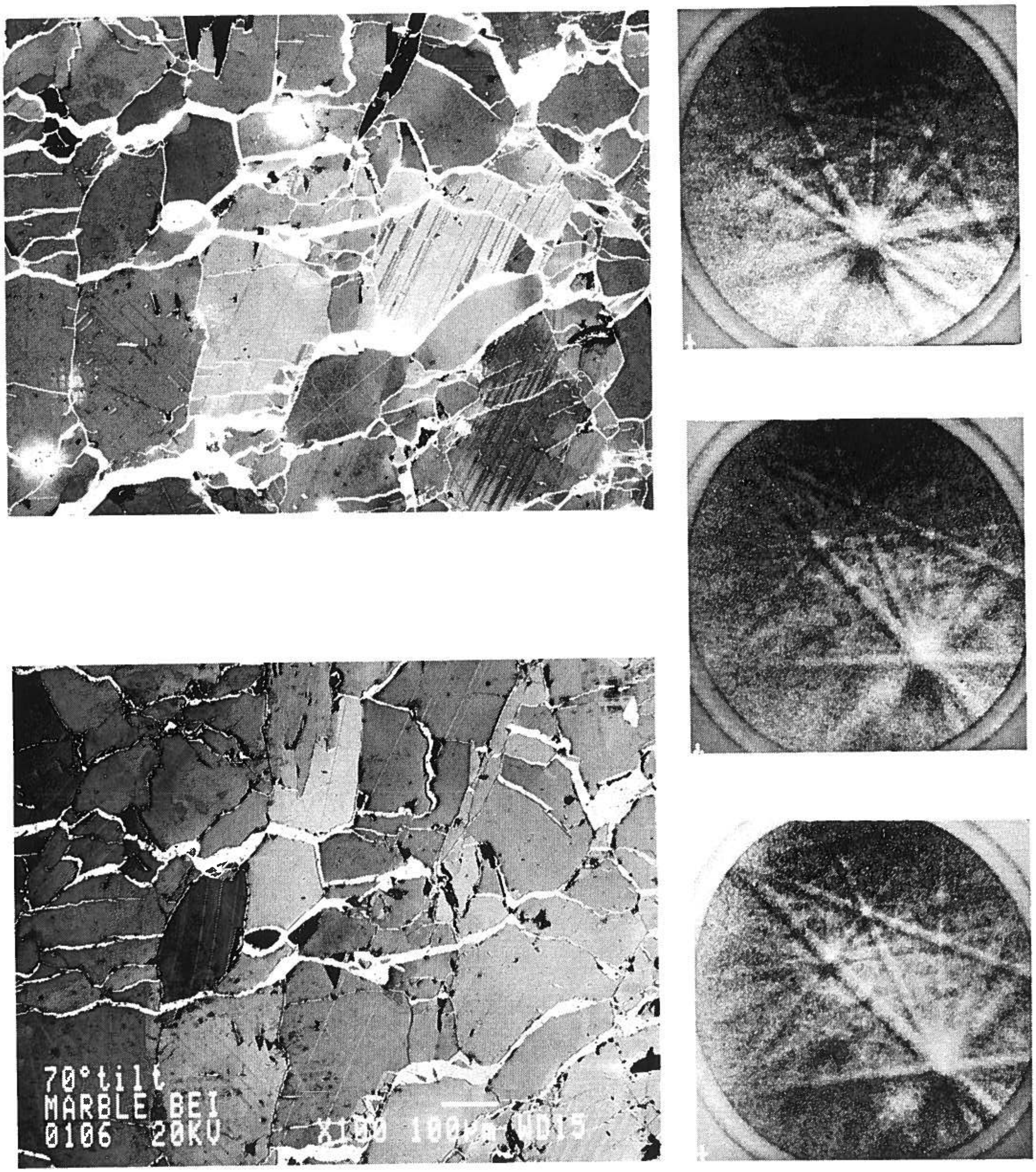

Fig: 5.6

conjunction with high-gain television technology to analyze the flux of backscattered electrons emanating from crystalline regions. Figure 5.6 shows the Kikuchi patterns obtained by Monteiro at SINTEF (Norway) during his sabbatical leave. The technique proved to be extremely powerful in identifying the crystals misorientations and it has the potential to provide meaningful insight on the effect of the misorientations between adjacent crystallites on the cracking mechanism.

Figure 5.7 indicates the sequence of computer image manipulations done on the original image so that meaningful characterization can be determined. Fifty-six images went through such computer manipulations to establish the statistical parameters. Figure 5.8 shows some typical images. For each parameter, an average, standard deviation, standard error, and ratio of standard error over average were calculated. Standard error was calculated as follows:

$$Standard \quad Error = \frac{\sigma}{\sqrt{Number \quad of \quad Images}}$$

The ratio of standard error over the average of 5% is considered to be a good result.

The results are indicated on Tables 5.1 and 5.3. The microcrack density distribution represents the number of microcracks per unit of observation area. Pore spaces are not counted as microcracks. Figure 5.9 shows the number of crack intercepts as a function of line array angles. Together they represent the open version of the rose diagram. These figures indicate that there is a definite crack orientation and that the majority of interceptions are at the 90° lines.

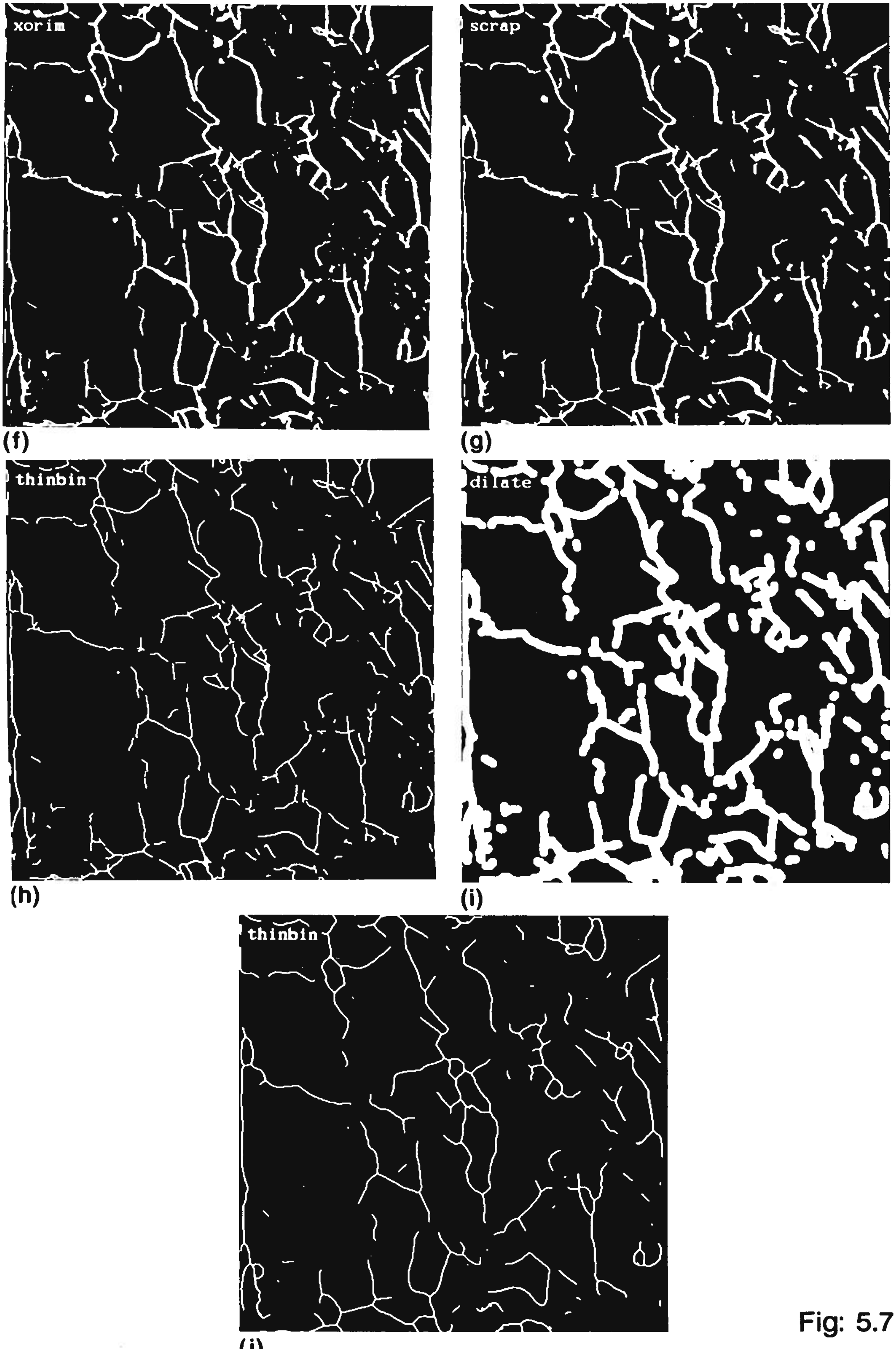

Fig: 5.7

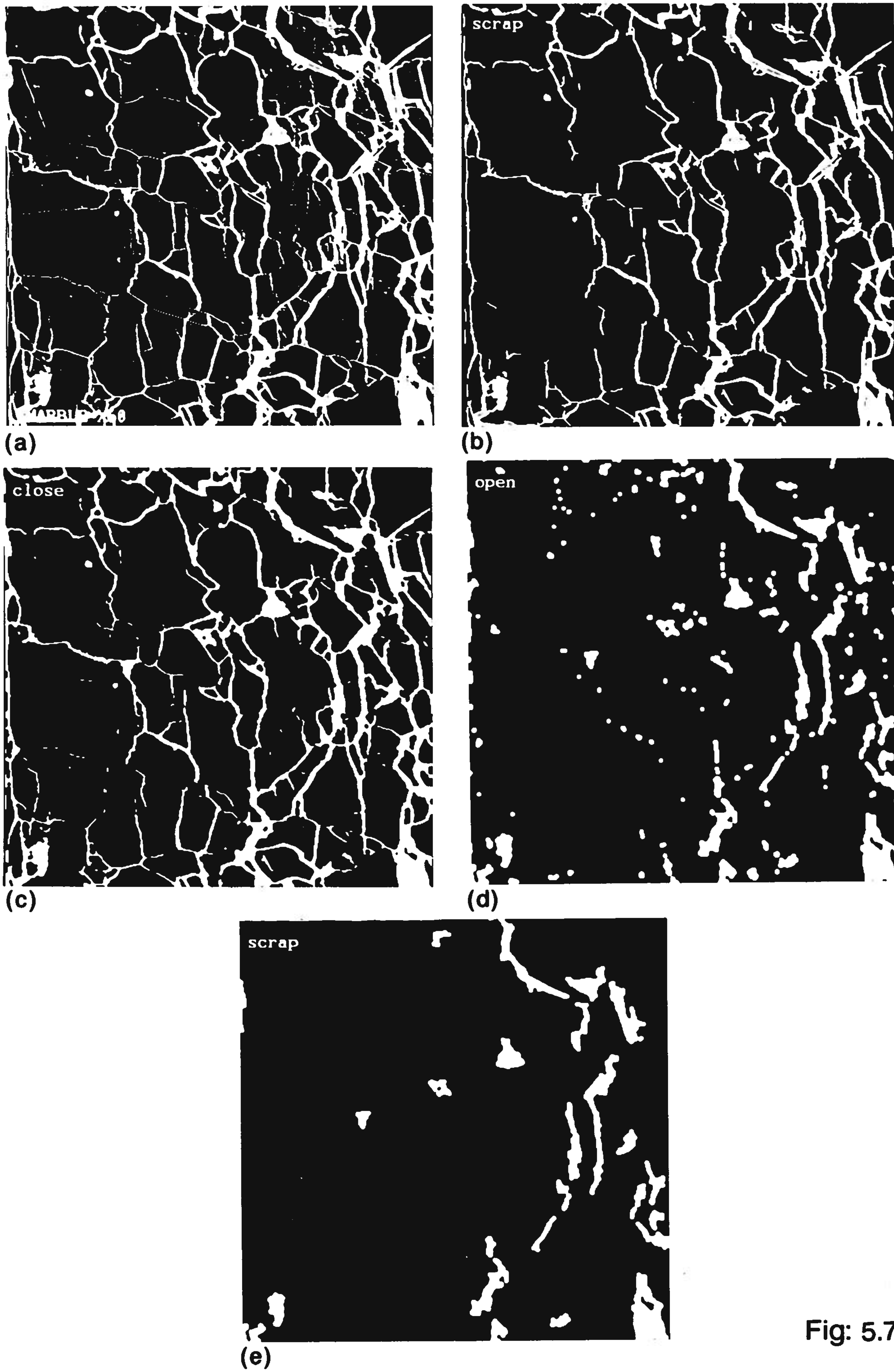

Fig: 5.7

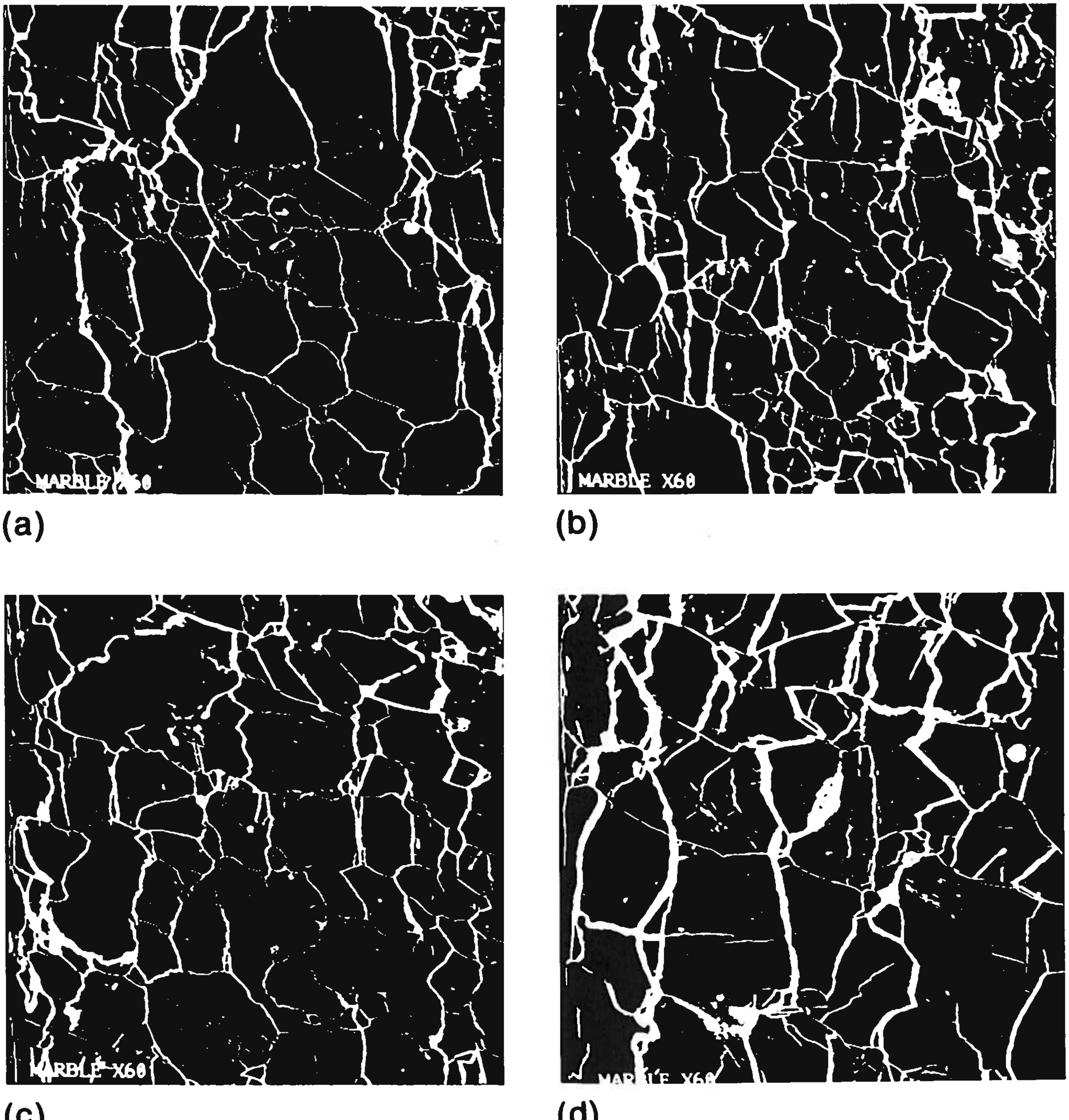

Fig: 5.8

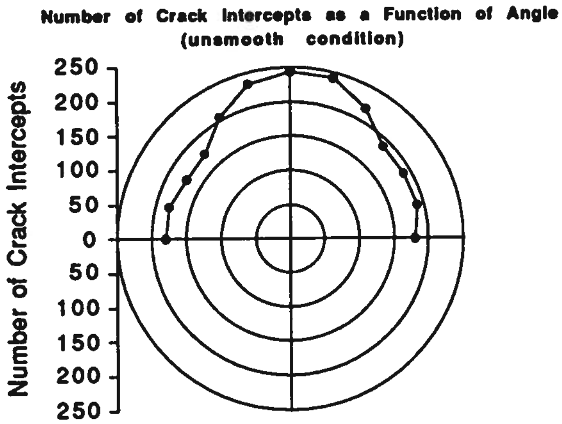

(a)

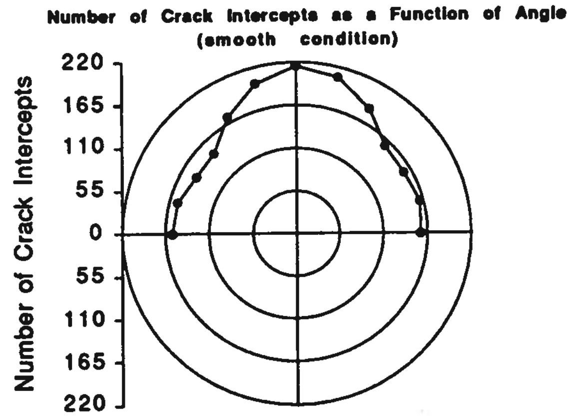

(b)

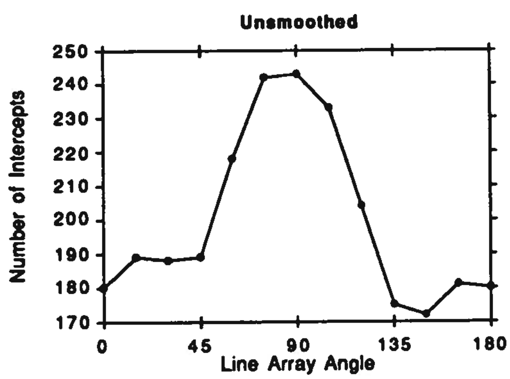

(c)

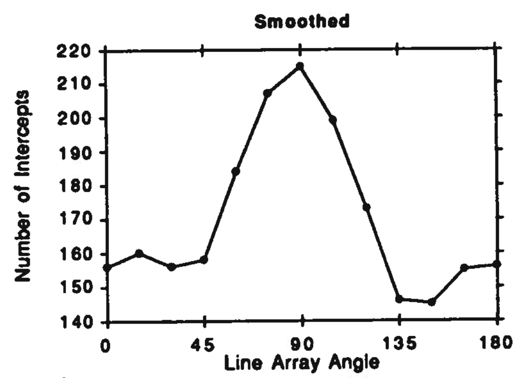

(d)

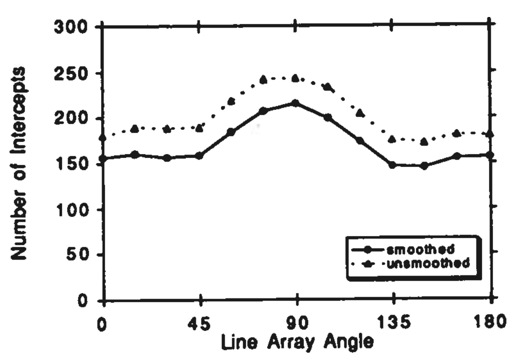

(e)

Fig. 5.9
Number of Crack Intercepts in Function of Line Array Angles

TABLE 5.1 NUMBER OF CRACK INTERCEPTS AT DIFFERENT ANGLES (SMOOTHED)

image	0°	15°	30°	45°	60°	75°	90°	105°	120°	135°	150°	165°	Total	Sv	Nodes
1	106	119	120	116	156	158	163	158	123	113	104	106	1573	0.0049	70
2	137	135	139	141	146	182	182	174	148	127	146	137	1823	0.0056	68
3	106	120	115	104	120	153	147	145	123	101	98	103	1462	0.0045	52
4	186	186	199	190	222	243	252	234	201	190	182	189	2510	0.0078	81
5	182	182	182	175	202	229	229	221	192	154	177	186	2335	0.0072	67
6	109	112	110	108	124	137	140	145	122	96	102	124	1440	0.0045	29
7	217	204	210	206	228	262	271	241	218	189	189	210	2686	0.0083	112
8	223	214	214	220	230	258	273	243	220	200	201	201	2739	0.0085	97
9	148	163	169	167	203	220	236	209	186	153	143	152	2190	0.0068	75
10	174	170	164	156	191	231	229	207	189	161	154	177	2249	0.007	54
11	152	160	155	151	176	188	200	170	155	128	142	163	1978	0.0061	64
12	196	189	179	195	216	236	247	231	206	169	184	187	2476	0.0077	90
13	172	187	174	189	208	241	242	222	219	175	168	178	2421	0.0075	85
14	184	179	181	186	221	256	269	240	220	190	167	176	2510	0.0078	86
15	195	198	184	191	223	226	234	240	202	184	158	178	2460	0.0076	88
16	162	180	185	184	210	221	236	204	182	154	151	178	2288	0.0071	71
17	166	154	178	159	185	201	206	182	159	149	146	157	2073	0.0064	67
18	178	187	177	180	208	236	240	222	182	164	156	178	2337	0.0072	79
19	169	178	192	174	201	216	203	196	184	144	143	176	2203	0.0068	59
20	221	217	208	214	237	279	271	257	229	182	190	204	2738	0.0085	95
21	170	192	184	171	206	227	249	226	191	160	156	157	2312	0.0072	72
22	150	157	161	151	169	213	208	199	160	133	135	155	2037	0.0063	52
23	177	181	180	192	219	243	249	225	209	171	162	178	2443	0.0076	77
24	184	184	209	203	227	261	269	235	209	171	181	180	2565	0.0079	101
25	199	201	191	212	229	249	259	246	192	157	176	182	2520	0.0078	107
26	196	212	201	212	260	282	274	260	217	173	170	187	2701	0.0084	87
27	173	188	176	191	227	232	245	238	212	176	169	162	2430	0.0075	67
28	130	134	136	155	187	206	214	197	177	139	132	132	1961	0.0061	35
29	132	154	139	141	162	213	205	188	164	133	128	136	1917	0.0059	43
30	157	142	134	140	164	180	195	181	161	123	130	160	1890	0.0058	64
31	146	149	140	141	168	186	200	180	154	124	130	118	1854	0.0057	42
32	102	106	100	102	125	129	133	116	108	81	86	98	1303	0.004	26
33	185	185	189	184	204	225	235	204	178	151	153	170	2301	0.0071	57
34	161	182	170	187	220	229	240	218	178	136	142	157	2245	0.0069	82
35	149	173	166	174	221	225	236	209	174	146	138	145	2175	0.0067	62
36	148	168	152	165	198	204	222	199	178	138	124	139	2069	0.0064	45
37	112	122	117	129	149	178	178	169	131	111	114	112	1638	0.0051	33
38	121	125	132	139	161	181	188	164	141	111	109	122	1716	0.0053	29
39	76	69	78	69	83	95	101	99	72	64	62	59	937	0.0029	7
40	97	104	99	98	121	147	147	134	118	94	82	87	1349	0.0042	24
41	201	189	194	208	248	284	300	294	248	212	206	221	2861	0.0088	111
42	208	232	188	226	241	281	291	285	252	209	197	225	2882	0.0089	118
43	120	118	114	106	128	148	151	145	130	118	112	125	1554	0.0048	51
44	174	170	182	175	204	239	267	240	197	169	190	187	2434	0.0075	75
45	160	159	150	154	205	224	245	239	192	171	164	166	2272	0.007	86
46	215	207	193	203	222	254	278	271	244	222	194	212	2763	0.0085	107
47	190	215	205	207	240	281	291	288	243	217	206	213	2837	0.0088	110
48	132	120	114	100	127	143	149	141	128	114	122	122	1532	0.0047	51
49	151	156	143	131	142	173	182	162	151	138	151	148	1867	0.0058	49
50	101	89	75	79	85	103	108	94	87	77	84	88	1097	0.0034	30
51	130	129	120	114	124	144	142	136	126	92	100	116	1499	0.0046	37
52	86	90	85	86	100	102	122	101	94	79	84	96	1133	0.0035	26
53	168	177	152	152	188	231	252	237	188	159	166	167	2263	0.007	69
54	186	179	187	190	231	285	301	281	244	205	189	201	2725	0.0084	95
55	118	107	104	110	126	133	146	149	124	101	107	117	1471	0.0045	55
56	77	92	88	73	97	104	104	108	85	78	86	86	1107	0.0034	24
AV.	156.	160.	156.	158.	184.	207.	215.	199.	173.	146.	145.	155.	2091	0.01	65.98
S.D.	37.64	38.00	37.68	41.26	45.68	51.22	53.43	50.41	44.40	39.03	36.25	38.61	509.27	0.00	26.70
S.E.	5.03	5.08	5.03	5.51	6.10	6.84	7.14	6.74	5.93	5.22	4.84	5.16	68.05	0.00	3.57
S.E./AV	3.21%	3.16%	3.21%	3.48%	3.31%	3.30%	3.32%	3.37%	3.42%	3.57%	3.33%	3.33%	3.25%	3.26%	5.41%

TABLE 5.2 NUMBER OF CRACK INTERCEPTS AT DIFFERENT ANGLES (UNSMOOTHED

image	0°	15°	30°	45°	60°	75°	90°	105°	120°	135°	150°	165°	Total	Sv	% A*	Nodes
1	115	145	150	154	185	203	189	189	163	158	134	140	1925	0.006	4.48	104
2	170	188	167	172	186	217	198	203	177	169	167	169	2183	0.0068	5.66	145
3	134	137	134	155	163	182	172	172	145	118	125	134	1771	0.0055	3.99	83
4	212	231	238	219	276	288	281	270	238	214	212	211	2890	0.0089	6.74	134
5	217	210	220	204	232	252	253	245	212	193	212	217	2667	0.0082	6.17	127
6	127	147	128	131	148	161	167	156	154	110	130	148	1707	0.0053	4.03	66
7	249	255	250	249	290	302	309	282	247	211	221	245	3110	0.0096	7.04	162
8	244	261	257	261	269	299	301	285	268	243	230	260	3178	0.0098	7.37	147
9	170	192	201	205	222	258	266	250	217	184	161	155	2481	0.0077	6.11	120
10	203	188	213	199	239	250	261	253	216	192	191	188	2593	0.008	5.82	117
11	164	195	180	172	200	220	230	208	180	138	165	175	2227	0.0069	5.06	101
12	217	223	212	225	258	278	258	272	245	197	209	204	2798	0.0087	6.17	130
13	190	206	204	213	243	286	291	268	261	202	207	184	2755	0.0085	6.16	132
14	212	196	216	229	256	282	301	281	253	216	191	194	2827	0.0087	6.68	109
15	221	221	224	230	256	279	285	287	230	200	199	210	2842	0.0088	6.67	149
16	184	219	215	221	250	262	259	245	218	173	195	206	2647	0.0082	6.36	124
17	187	186	194	189	213	241	235	213	188	162	167	187	2362	0.0073	5.33	104
18	184	180	197	212	234	271	256	251	211	189	178	194	2557	0.0079	5.89	117
19	188	199	202	186	225	254	231	223	210	173	178	196	2465	0.0076	5.24	95
20	252	257	248	232	275	308	297	286	273	219	221	245	3113	0.0096	6.70	146
21	192	218	228	216	252	265	277	249	219	188	186	185	2675	0.0083	6.05	134
22	178	183	194	175	220	257	250	245	191	174	153	183	2403	0.0074	5.53	103
23	216	237	209	235	258	290	280	282	248	194	193	202	2844	0.0088	6.75	142
24	216	224	249	268	269	303	296	287	245	201	201	219	2978	0.0092	6.64	157
25	232	247	246	264	267	296	290	273	220	203	200	226	2964	0.0092	6.30	162
26	231	256	273	269	301	335	342	317	256	205	191	239	3215	0.0099	7.12	165
27	205	219	214	207	252	277	268	279	249	199	187	202	2758	0.0085	6.15	124
28	155	166	167	174	218	223	225	219	197	153	148	155	2200	0.0068	4.81	80
29	158	169	175	177	198	221	232	210	194	153	158	156	2201	0.0068	4.84	81
30	173	171	172	151	181	212	213	204	175	159	139	169	2119	0.0066	4.61	90
31	163	171	162	167	183	202	220	198	186	139	145	126	2062	0.0064	4.48	67
32	124	119	130	125	130	149	149	133	120	97	96	109	1481	0.0046	3.24	38
33	191	219	216	205	242	251	250	242	219	177	170	203	2585	0.008	5.53	101
34	192	220	214	211	242	264	273	243	207	158	175	186	2585	0.008	6.18	125
35	168	209	176	198	245	258	260	228	219	167	153	151	2432	0.0075	5.54	99
36	168	197	192	187	246	261	244	233	189	173	139	176	2405	0.0074	5.17	106
37	134	137	137	159	174	198	192	185	152	126	128	126	1848	0.0057	4.09	72
38	148	152	149	155	170	202	208	186	165	151	134	155	1975	0.0061	3.66	59
39	93	82	98	93	100	110	115	109	95	85	79	83	1142	0.0035	2.04	33
40	112	115	117	126	145	167	168	155	130	127	108	100	1570	0.0049	3.22	50
41	247	259	241	262	307	340	354	350	303	264	260	275	3462	0.0107	8.10	185
42	248	257	228	244	293	338	345	332	300	242	249	255	3331	0.0103	7.80	161
43	136	132	144	125	166	180	192	184	176	157	138	156	1886	0.0058	4.54	88
44	207	220	221	207	250	283	299	280	239	215	214	229	2864	0.0089	6.34	135
45	198	169	186	200	230	265	272	282	236	212	193	197	2640	0.0082	6.36	121
46	241	241	232	251	270	305	314	319	281	276	254	255	3239	0.01	7.42	156
47	221	234	239	251	285	338	351	329	289	255	236	248	3276	0.0101	7.71	171
48	139	137	136	119	147	163	167	161	149	135	145	142	1740	0.0054	4.18	58
49	180	175	170	155	175	206	201	201	174	163	171	185	2156	0.0067	5.10	64
50	118	108	99	95	115	125	126	121	101	109	96	111	1324	0.0041	2.93	43
51	149	151	155	128	140	169	172	162	139	121	122	151	1759	0.0054	4.22	53
52	101	97	115	108	122	124	128	109	111	102	95	103	1315	0.0041	3.12	46
53	188	208	198	202	237	281	281	263	221	194	198	201	2672	0.0083	5.91	115
54	224	215	216	238	306	322	343	327	292	258	231	228	3200	0.0099	7.29	166
55	140	128	135	129	155	168	173	178	162	138	141	126	1773	0.0055	3.99	103
56	97	123	96	95	115	118	119	137	115	106	126	111	1358	0.0042	2.90	52
AV.	180.	189.	188.	189.	218.	242.	243.	233.	204.	175.	172.	181.	2420	0.01	5.49	109.
S.D.	42.4	45.6	44.5	48.1	54.2	59.8	61.2	59.1	51.7	44.1	42.4	45.3	582.	0.00	1.40	38.9
S.E.	5.67	6.10	5.96	6.44	7.25	8.00	8.19	7.90	6.91	5.89	5.67	6.06	77.8	0.00	0.19	5.20
S.E./AV	3.1%	3.2%	3.1%	3.3%	3.3%	3.3%	3.3%	3.3%	3.3%	3.3%	3.2%	3.3%	3.2%	3.20%	0.03	4.7%

* Percentage of Cracked Area

5.5 Modeling Using Discontinuous Deformation Analysis with Finite Element Mesh

5.5.1 Introduction

With the advent of digital computers, converting a continuous problem to a discrete one becomes possible. In the process of developing general discretization procedures of continuous problems posed by mathematically defined statements, Clough[1,2] appears to be the first one to use the term *finite element (FE)* and apply this unified standard method to stress analysis in 1960. In the early 1960s, the use of FEM made an important contribution in numerical analysis solving scientific and engineering problems; thus, leading the computational mechanics into a new age.

Discretization is the fundamental concept of FEM. Assuming a structure is discretized into several members with known properties, it can be treated as an assemblage of "elements". Each element has *nodes* on the boundaries of elements that play important roles to (1) connect each element to fulfill the compatibility condition that makes FEM a continuous model; (2) act as unknown displacement variables to solve the simultaneous equilibrium equations; (3) depict the boundaries of the elements for the integration of the stresses and external loads; and (4) create the shape function of the element through the displacement function. Polynomials are often used as approximating functions to describe the displacement field of the element. Any point within the element can be interpolated by nodal displacements. Also FEM satisfies the equilibrium condition by minimizing the total potential energy of the entire structure, then solves linear algebraic simultaneous equations to arrive at the results. Shi[3] stated: "FEM was a revolution, it shifted from differential equations to integral equations; from the smooth functions to the piecewise smooth functions. The general shaped mesh of FEM can give good results for continuous materials."

After the birth of FEM, practical discontinuity problems were also taken into account in numerical analysis. In 1968, Goodman, Taylor and Brekke[4] developed the **Jointed Element** and applied it in rock engineering extensively. After three years, Cundall introduced the Distinct Element Method, which is now widely used for jointed or blocky rock [5,6,7]. Unlike FEM, these two methods are force methods which incorporate fictitious forces to reach the convergence criteria of block overlapping and sometimes reach equilibrium. In 1988, the displacement based method - Discontinuous Deformation Analysis - was developed by Shi[8]. The primary function of DDA is to solve large displacements and deformations of discontinuous block system. For each block, displacements, deformations, and strains are permitted for the entire block system. Sliding, opening and closing of block interfaces are also allowed. Like FEM, this method uses minimization of total potential energy to reach equilibrium in the forward model. In backward model, it uses a "least square" minimization to back calculate the global configuration of the block system from measured data.

DDA deals with discontinuous problems and FEM solves continuous ones, the difference between a 'block' in DDA and an 'element' in FEM has to be distinguished. As mentioned earlier, FEM uses nodes to link the elements. Common nodes are shared between two adjacent elements, which makes FEM a continuous model. In DDA, all blocks are isolated and bounded by preexisting discontinuities. When blocks are in contact, Coulomb's law applies to the contact surface, and the simultaneous equilibrium equations are selected and solved for each loading or time increment. The geometry of blocks in DDA can be any convex or concave shape, or even multiconnected polygons with holes, whereas FEM only encompasses standard shaped elements.

The stability of whole systems in the real world comes mainly from inertia forces and friction forces. DDA follows these laws and places them within the realm of mechanical analysis; thus, stabilizing the numerical computation. When forces of inertia are taken into account, the time parameter is considered as well. Therefore, DDA is truly a dynamic model in numerical analysis. Since the assumption of infinitesimal displacement theory needs to be fulfilled in linear elastic mechanics, choosing very small time intervals can satisfy this assumption. When the total potential energy of all the stresses and external forces is minimized, the submatrices of the inertia force terms have the following properties: (1) they are two orders of magnitude higher than internal stress or stiffness submatrices; (2) the coefficient terms of such matrices are proportional to ($1/\text{time}^2$) ; and (3) they are concentrated at the diagonal positions in the global coefficient or stiffness matrix. Thus, large numbers are distributed in all diagonal terms in the global stiffness or coefficient matrix, and the above assumption is fulfilled. In addition to having the dominant influence in the global stiffness matrix, forces of inertia also play another important role in resisting the rigid body movement of the continuum, which is indispensable in dealing with discontinuous block system. When two blocks lose contact, they will depart from each other with each other with high speed if no inertia force term is considered in numerical analysis. Thus, the assumption of infinitesimal displacement theory will not be satisfied. Also, divergence will occur in numerical calculations. In addition, Shi[8] derived the exact analytical integration of the all the submatrices that reduces the error caused by the approximation of Gaussian integration in FEM.

The uniqueness of DDA is the block system kinematics, which regulates the movements of all the blocks or finds the locations of all contacts among the blocks. Since the infinitesimal displacement theory is assumed, the rigid body movements and the deformations of each block can be approximated using coordinate dependent linear functions which are described below. If the locations of all contact forces are found, then the governing equations become simultaneous linear equations in the block system. Shi's block system kinematics is the method to find the locations with two constraints: no tension and no penetration between blocks. The mathematical descriptions of both constraints are given by a set of inequalities. Although minimizing the total potential energy with inequality constraints is a difficult nonlinear programming problem, Shi found some important factors that can break through the numerical impasse. When the block system moves and deforms, the blocks are in contact only along the boundary and the non-penetration inequalities can be transformed into the equations when two blocks are in contact.

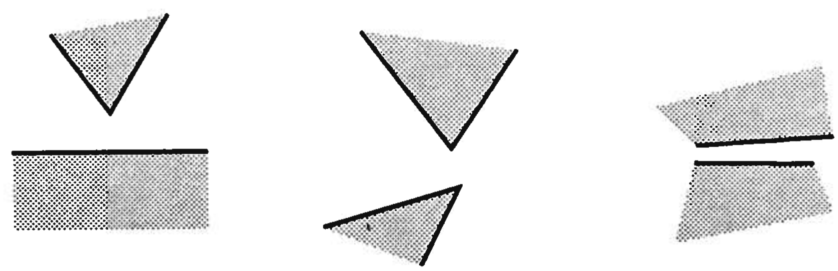

a. angle to edge b. angle to angle c. edge to edge

Figure 5.10.
Three different kinds of contacts

There are three different kinds of contacts between blocks in two dimensional case, angle-to-edge, angle-to-angle, and edge-to-edge (Fig. 5.10). The edge-to-edge case can be transformed to two angle-to-edge contacts. An angle and an edge defined to be in contact has to satisfy the following two conditions: (1) the distance from the angle vertex to the edge is less than two times the maximum displacements of points of all blocks; and (2) there is no overlapping when the angle vertex translates to the edge without rotation. Two angles defined to be in contact also need to fulfill two conditions: (1) the distance between the vertices of two angles is less than two times the maximum displacements of points of all blocks; and (2) there is no overlapping when two angles are translated without rotation until the vertices coincide. Therefore, the contact problem is reduced to point-line crossing inequalities. When the case of inter-penetration occurs at a given position, a "lock" is applied. One stiff spring is added from the point and lies along the directions normal to the reference line. Coulomb's law will determine whether to add or remove the other spring which is parallel to the reference line. By adding very stiff springs or penalties to lock the movements in one or two directions for inter-penetrated positions, the constrained equations can be imposed on the global equations. The physical meaning of applying stiff springs is to push back the invading angle along the shortest path. Accordingly, if a tensile contact force occurs between two blocks, both blocks will separate after removal of the locks. Hence, the non-tension constraining inequalities can be reduced to fixing or losing the locks. Therefore, the so-called open-close iterations repeatedly select the locked positions, or unlock the constraining ones until the condition of no penetration and no tension are satisfied for all the contacts among the blocks. All the penalty submatrices are then imposed into the global stiffness matrix.

In DDA, the Coulomb's law is used to calculate contact forces and is the criterion to evaluate the sliding or locking between the blocks. When the displacement of the point normal to the reference line is positive, the normal component of the contact force is tensile, no lock or stiff spring is applied and the contact is opened. If the above displacement is negative, the normal contact force is compressive and the contact is closed. When the shear component of the contact force is large enough to cause sliding, a stiff spring normal to the reference line is applied to allow the sliding to take place along the reference edge. In contrast, if the shear component of the contact force is less than that calculated from Coulomb's law, the contact spring will be fixed in both directions and no sliding is permitted. Friction forces between the interfaces of blocks are obtained from the result of open-close iterations of block kinematics in the block system, and represent the only energy consumption in DDA.

Statics is defined as the ultimate stable condition of the system in mechanics. Although DDA considers both statics and dynamics, the only difference between these two cases is that the static computation assumes that the velocity is zero at the beginning of each time step, while the dynamic computation inherits the velocity from the previous step. In the process of step-by-step calculations, each step begins with the deformed block shapes and positions from the previous step. The equilibrium equations are solved for updated geometry and updated initial conditions such as velocities, initial stresses, etc. Large displacements and deformations of the blocks are obtained by the accumulation of small displacements and deformations in each time step. This is the reason why DDA is characterized step-by-step linear kinematics. This method indeed makes the best of the spirit of Calculus which originated-from inspecting the motion of celestial bodies and was developed by Newton. As the blocks move or deform, the updating block shapes and positions will produce different block contacts and interactive forces. Thus, the whole block system will be changed and the modes of failure will be affected in a way more sensitive than those in continuum mechanics.

In FEM, the displacement function of a basic three-node triangular element is described by a complete first order polynomial function in two-dimensional case. The displacement field for this element is:

$$u = a_1 + a_2x + a_3y$$
$$v = b_1 + b_2x + b_3y$$

where u, v are displacements in x and y directions. And six variables need to be determined. A triangular element with three node on its vertices has also six degrees of freedom,

$$(u_1\ u_2\ u_3\ v_1\ v_2\ v_3\ )$$

The displacement function of the triangular element can be described as a function of six nodal displacements through a transformation. Therefore, the complete first order polynomial function best describes the characteristics of the three-node element in FEM. The strains and stresses in that element are constant, in the structural mechanics literature this kind of element is often referred to as the constant stress/strain triangle, or simply the *CST*. It was one of the first finite elements conceived and is still widely used[9,10,11].

In DDA, this complete first-order polynomial function is also chosen as the displacement function of a block. Shi transformed these six variables into another six essential variables,

$$(u_0\ v_0\ r_0\ \varepsilon_x\ \varepsilon_y\ \gamma_{xy}\ )$$

where (uo, vo) is the rigid body translation of a specific point (xo, yo) within the block; ro is the rotation angle of the block with the rotation center at (xo, yo); and ε_x ε_y γ_{xy} are the normal and shear strains of this block. Since the infinitesimal displacement theory is assumed, the displacement function of the block can be represented by the coordinate dependent linear function. It is written as:

$$\begin{pmatrix} u \\ v \end{pmatrix} = \begin{pmatrix} 1 & 0 & -(y-y_0) & (x-x_0) & 0 & (y-y_0)/2 \\ 0 & 1 & (x-x_0) & 0 & (y-y_0) & (x-x_0)/2 \end{pmatrix} \begin{pmatrix} u_0 \\ v_0 \\ r_0 \\ \varepsilon_x \\ \varepsilon_y \\ \gamma_{xy} \end{pmatrix}$$

where (xo, yo) is chosen as the center of gravity of that block.

The advantages of choosing (u_0 v_0 r_0 ε_x ε_y γ_{xy}) as block displacement variables are :

1. every block displacement variable has obvious physical meaning as a parameter of mechanics; and
2. the simplest energy formula can be obtained with respect to these variables. The equilibrium equations derived from minimizing total potential energy are simple and have obvious physical meaning.

Although the forward analysis of DDA is a discontinuous model which solves large displacements and deformations and FEM is a continuous model, they have three properties in common:

1. both are displacement-based methods;
2. both establish the equilibrium equations by minimizing the total potential energy; and
3. both add stiffness, loading, and mass submatrices to the global stiffness matrix of the simultaneous equations.

The method of putting a finite element mesh into each block is presented next. The idea of adding nonlinear material behavior is outlined afterward. Then the basic equations will be given. The FORTRAN computer program of this combined model was built on the foundation of Shi's original DDA BASIC program. It uses graphic input and output and is demonstrated by several examples.

5.5.2. Combination of DDA with Finite Element Mesh

The main purpose of placing a finite element mesh in each block is to improve the deformation ability of the block. Although in DDA the geometry of the block can be convex or concave, even with holes in it, the stress and strain in each block is constant which is not realistic for a big block. Thus, the idea of adding a finite element mesh in each block was formulated. Not only the movements of the block system will be depicted by DDA, but the stress distributions of the blocks can also be obtained.

Here the finite element mesh of constant strain elements is chosen, and the complete first order polynomial displacement function are used to describe the triangular element's behavior. There are six nodal displacements

$$(u_1\ u_2\ u_3\ v_1\ v_2\ v_3)$$

to be chosen as unknown variables. The function of the geometry of the blocks is used as the contact boundaries for the purpose of block kinematics in the block system. Thus, the shape of the block need not be triangular. That is the reason why the characteristic of block system kinematics is unique in discontinuous computation.

Suppose there is a three-node element and the boundary of the element is drawn along the nodes in certain directions, then a three-edge block with the same size as the element is obtained, this kind of the *element block* is called the *three-node element* block-a block with nodal displacements as unknowns. If a three-node element is extended to an n-node element mesh, and again, by drawing the outer boundary along the nodes of this mesh, we have an *element-mesh block* with n nodes. In general, a block can be as small as an element or as large as an element mesh. Different meshes can also be put into different blocks if conditions permit.

In the computer program, the meshes of the elements and the boundaries of the blocks need to be input separately. Then, element meshes and blocks are merged with same nodal numbers between the elements, but with different nodal numbers between the boundaries of the blocks. The basic element in this numerical model is triangular element. For the convenience of putting the mesh in each block, four-node element meshes are generated first in the mesh program. Then, a condense five-node element-a quadrilateral element with four nodes on its vertices and one additional node inside it that forms four triangular elements-is used for forward model computations.

From the idea of element-mesh blocks, the mesh in FEM is just one block in DDA. By adding the finite element mesh into each block, we can take advantage of the continuous properties in FEM and discontinuous characteristics of DDA, and thereby being able to approach engineering problems more closely. This significant contribution was first made by Shyu[12].

5.5.3. Adding Nonlinear Material Behavior

In structural mechanics literature, a problem is called nonlinear if the stiffness matrix or the load vector depends on the displacements. In structures, nonlinearity can be classified as (1) material nonlinearity which is associated with changes in material properties, as in plasticity; and (2) geometric nonlinearity which is associated with changes in configuration, as in large displacements or deformations of the structures. The geometric nonlinearity is well solved by Shi's DDA. The material nonlinearity is discussed and solved in the same way as in DDA.

DDA uses a step-by-step approach. Each step starts with the deformed shape and positions from previous step, and the stresses from the previous step are considered as the initial stresses at the current step. After adopting the updated geometry, contact positions, velocities, and stresses from the previous time step, the computation for the current step is independent from the data of the previous step. All the deformability constants, loading, initial stresses, and boundary conditions can be changed at the current step. Since the time interval of each time step is very small, the displacement, deformations, and the changes of stresses are very small, the tangent modulus of the stress-strain relationship at the current step is very close to the secant modulus of the stress-strain curve. Thus, the arc-length method (Fig. 5.11) can be used to calculate the piecewise linear modulus based on the updated values of stresses and strains for nonlinear constitutive behavior of materials.

The use of line segments to depict the nonlinear behavior of the material step by step is another way to show that the step-by-step linear approach may solve nonlinear problems in both materials and geometry. Trying to solve nonlinear material problems with only one step may violate the infinitesimal displacement theory. When finite element meshes and blocks are combined to get the distributions of the stresses or to improve the deformation ability of the block was accomplished, the use of line segments to solve material nonlinearity step by step would allow us to approach the physical meaning of engineering problems successfully. An isotropic material is chosen here as the simplest case in the computer program. The deformability constants Young's Modulus E and Poisson's ratio v change with strains. The more line segments that are chosen to approach the curve of stress and strain, the more accurate Young's modulus and Poisson's ratio are obtained in each time step.

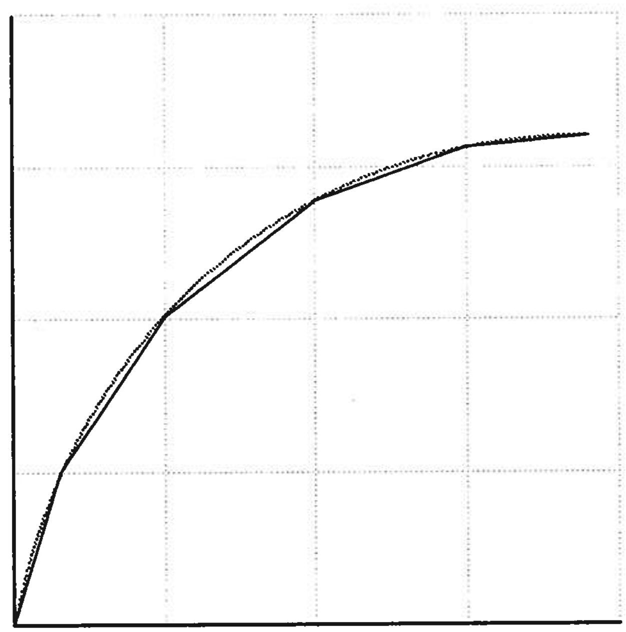

Arc-length Method

Fig: 5.11

5.5.4.0 Simultaneous Equations

The simultaneous equilibrium equations derived by minimizing the total potential energy Π have the following form:

$$\begin{pmatrix} [K_{11}] & [K_{12}] & [K_{13}] & \dots & [K_{1n}] \\ [K_{21}] & [K_{22}] & [K_{23}] & \dots & [K_{2n}] \\ [K_{31}] & [K_{32}] & [K_{33}] & \dots & [K_{3n}] \\ \vdots & \vdots & \vdots & \ddots & \vdots \\ [K_{n1}] & [K_{n2}] & [K_{n3}] & \dots & [K_{nn}] \end{pmatrix} \begin{pmatrix} \{D_1\} \\ \{D_2\} \\ \{D_3\} \\ \vdots \\ \{D_n\} \end{pmatrix} = \begin{pmatrix} \{F_1\} \\ \{F_2\} \\ \{F_3\} \\ \vdots \\ \{F_n\} \end{pmatrix}$$

Like FEM, nodal displacements are chosen as unknown variables in the new model and each node has two degrees-of-freedom in the two-dimensional case. Thus, $[K_{ij}]$ is a 2×2 submatrix in the coefficient or global stiffness matrix, $\{D_i\}$ and $\{F_i\}$ are 2×1 submatrices with respect to unknown displacements and loading matrices.

5.5.5.0 Displacement Function

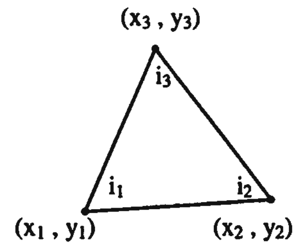

Figure 5.11 Triangular Element

A complete first order polynomial approximation is assumed in the new model. The displacement field for a triangular element(Fig. 3) can be described as:

$$\begin{aligned} u &= a_1 + b_1 x + c_1 y; \\ v &= a_2 + b_2 x + c_2 y. \end{aligned} \tag{0.1}$$

Since

$$\begin{pmatrix} a_1 \\ b_1 \\ c_1 \end{pmatrix} = \begin{pmatrix} 1 & x_1 & y_1 \\ 1 & x_2 & y_2 \\ 1 & x_3 & y_3 \end{pmatrix}^{-1} \begin{pmatrix} u_1 \\ u_2 \\ u_3 \end{pmatrix};$$

$$\begin{pmatrix} a_2 \\ b_2 \\ c_2 \end{pmatrix} = \begin{pmatrix} 1 & x_1 & y_1 \\ 1 & x_2 & y_2 \\ 1 & x_3 & y_3 \end{pmatrix}^{-1} \begin{pmatrix} v_1 \\ v_2 \\ v_3 \end{pmatrix}.$$

where (x_i, y_i) are the coordinates of nodes and (u_i, v_i) are the related nodal displacements; and $i = 1, 2, 3$.

Then,

$$u = \begin{pmatrix} 1 & x & y \end{pmatrix} \begin{pmatrix} 1 & x_1 & y_1 \\ 1 & x_2 & y_2 \\ 1 & x_3 & y_3 \end{pmatrix}^{-1} \begin{pmatrix} u_1 \\ u_2 \\ u_3 \end{pmatrix}, \tag{0.2}$$

and

$$v = \begin{pmatrix} 1 & x & y \end{pmatrix} \begin{pmatrix} 1 & x_1 & y_1 \\ 1 & x_2 & y_2 \\ 1 & x_3 & y_3 \end{pmatrix}^{-1} \begin{pmatrix} v_1 \\ v_2 \\ v_3 \end{pmatrix}. \tag{0.3}$$

Set:

$$\begin{pmatrix} f_1 & f_2 & f_3 \end{pmatrix} = \begin{pmatrix} 1 & x & y \end{pmatrix} \begin{pmatrix} 1 & x_1 & y_1 \\ 1 & x_2 & y_2 \\ 1 & x_3 & y_3 \end{pmatrix}^{-1},$$

and

$$\begin{pmatrix} f_{11} & f_{12} & f_{13} \\ f_{21} & f_{22} & f_{23} \\ f_{31} & f_{32} & f_{33} \end{pmatrix} = \begin{pmatrix} 1 & x_1 & y_1 \\ 1 & x_2 & y_2 \\ 1 & x_3 & y_3 \end{pmatrix}^{-1}; \qquad \Delta = \begin{vmatrix} 1 & x_1 & y_1 \\ 1 & x_2 & y_2 \\ 1 & x_3 & y_3 \end{vmatrix}.$$

Then

$$\begin{pmatrix} f_{11} & f_{12} & f_{13} \\ f_{21} & f_{22} & f_{23} \\ f_{31} & f_{32} & f_{33} \end{pmatrix} = \frac{1}{\Delta} \begin{pmatrix} x_2y_3 - x_3y_2 & x_3y_1 - x_1y_3 & x_1y_2 - x_2y_1 \\ y_2 - y_3 & y_3 - y_1 & y_1 - y_2 \\ x_3 - x_2 & x_1 - x_3 & x_2 - x_1 \end{pmatrix}, \tag{0.4}$$

and

$$\begin{pmatrix} f_1 \\ f_2 \\ f_3 \end{pmatrix} = \begin{pmatrix} f_{11} + f_{21}x + f_{31}y \\ f_{12} + f_{22}x + f_{32}y \\ f_{13} + f_{23}x + f_{33}y \end{pmatrix}. \tag{0.5}$$

Since

$$u = (\,f_1 \quad f_2 \quad f_3\,) \begin{pmatrix} u_1 \\ u_2 \\ u_3 \end{pmatrix}; \qquad v = (\,f_1 \quad f_2 \quad f_3\,) \begin{pmatrix} v_1 \\ v_2 \\ v_3 \end{pmatrix},$$

then

$$\begin{aligned} \begin{pmatrix} u \\ v \end{pmatrix} &= \begin{pmatrix} f_1 & 0 & f_2 & 0 & f_3 & 0 \\ 0 & f_1 & 0 & f_2 & 0 & f_3 \end{pmatrix} \begin{pmatrix} u_1 \\ v_1 \\ u_2 \\ v_2 \\ u_3 \\ v_3 \end{pmatrix} \\ &= [T_e]\{D_e\}, \end{aligned} \tag{0.6}$$

where

$$[T_e] = (\,[T_1] \quad [T_2] \quad [T_3]\,); \qquad \{D_e\} = \begin{pmatrix} \{D_1\} \\ \{D_2\} \\ \{D_3\} \end{pmatrix},$$

and

$$[T_i] = \begin{pmatrix} f_i & 0 \\ 0 & f_i \end{pmatrix}; \qquad \{D_i\} = \begin{pmatrix} u_i \\ v_i \end{pmatrix}, \qquad i = 1, 2, 3.$$

5.5.6.0 Submatrices

In this numerical model, a complete first order polynomial is approximated in the formulations of the forces and displacements within an element. The derivatives of total potential energy with respect to the variables of a triangular element are computed. The corresponding submatrices are formed separately and will be introduced next. The global simultaneous equations are obtained by adding the individual submatrices to the global stiffness matrix.

5.5.6.1 Stiffness Submatrix

A linearly step-by-step approach to discretize the stress-strain curve can simplify a material nonlinearity problem. For an isotropic inelastic material, the stress-strain relationship is assumed to be linear in each time step and can be described as:

$$\begin{pmatrix} \sigma_x \\ \sigma_y \\ \tau_{xy} \end{pmatrix} = \frac{E}{1-\nu^2} \begin{pmatrix} 1 & \nu & 0 \\ \nu & 1 & 0 \\ 0 & 0 & \frac{1-\nu}{2} \end{pmatrix} \begin{pmatrix} \epsilon_x \\ \epsilon_y \\ \gamma_{xy} \end{pmatrix} = [E] \begin{pmatrix} \epsilon_x \\ \epsilon_y \\ \gamma_{xy} \end{pmatrix} \tag{1.1}$$

in plane stress condition, where

$$[E] = \frac{E}{1-\nu^2} \begin{pmatrix} 1 & \nu & 0 \\ \nu & 1 & 0 \\ 0 & 0 & \frac{1-\nu}{2} \end{pmatrix};$$

and $Eand\nu$ are Young's modulus and Poisson's ratio, respectively. And

$$\begin{pmatrix} \epsilon_x \\ \epsilon_y \\ \tau_{xy} \end{pmatrix} = \begin{pmatrix} \frac{\partial}{\partial x} & 0 \\ 0 & \frac{\partial}{\partial y} \\ \frac{\partial}{\partial y} & \frac{\partial}{\partial x} \end{pmatrix} \begin{pmatrix} u \\ v \end{pmatrix} = \begin{pmatrix} \frac{\partial}{\partial x} & 0 \\ 0 & \frac{\partial}{\partial y} \\ \frac{\partial}{\partial y} & \frac{\partial}{\partial x} \end{pmatrix} [T_e]\{D_e\},$$

then

$$\begin{pmatrix} \epsilon_x \\ \epsilon_y \\ \tau_{xy} \end{pmatrix} = \begin{pmatrix} f_{21} & 0 & f_{22} & 0 & f_{23} & 0 \\ 0 & f_{31} & 0 & f_{32} & 0 & f_{33} \\ f_{31} & f_{21} & f_{32} & f_{22} & f_{33} & f_{23} \end{pmatrix} \begin{pmatrix} u_1 \\ v_1 \\ u_2 \\ v_2 \\ u_3 \\ v_3 \end{pmatrix}. \tag{1.2}$$

Let

$$[B_e] = ([B_1] \quad [B_2] \quad [B_3]); \tag{1.3}$$

where

$$[B_i] = \begin{pmatrix} f_{2i} & 0 \\ 0 & f_{3i} \\ f_{3i} & f_{2i} \end{pmatrix}, \qquad i = 1, 2, 3. \tag{1.4}$$

Then

$$\begin{pmatrix} \epsilon_x \\ \epsilon_y \\ \tau_{xy} \end{pmatrix} = [B_e]\{D_e\} = \left([B_1] \quad [B_2] \quad [B_3] \right) \begin{pmatrix} \{D_1\} \\ \{D_2\} \\ \{D_3\} \end{pmatrix}. \tag{1.5}$$

The strain energy Π_e stored by the stresses of element e is:

$$\begin{aligned}
\Pi_e &= \iint_A \frac{1}{2} \left(\epsilon_x \quad \epsilon_y \quad \gamma_{xy} \right) \begin{pmatrix} \sigma_x \\ \sigma_y \\ \tau_{xy} \end{pmatrix} dx\, dy \\
&= \frac{1}{2} \iint_A \{D_e\}^T [B_e]^T [E][B_e]\{D_e\}\, dx\, dy \\
&= \frac{1}{2}\{D_e\}^T \left[\iint_A [B_e]^T [E][B_e]\, dx\, dy \right] \{D_e\} \\
&= \frac{1}{2}\{D_e\}\left(S^e [B_e]^T [E][B_e] \right)\{D_e\},
\end{aligned} \tag{1.6}$$

where S^e is the area of the element.

Therefore,

$$S^e [B_e]^T [E][B_e] = S^e \begin{pmatrix} [B_1]^T \\ [B_2]^T \\ [B_3]^T \end{pmatrix} [E]\Big([B_1] \quad [B_2] \quad [B_3] \Big), \tag{1.7}$$

is the element stiffness matrix.

Then

$$S^e [B_r]^T [E][B_s] \quad \rightarrow \quad [K_{i(r)i(s)}]; \qquad r, s = 1, 2, 3; \tag{1.8}$$

where

$$i(\ell) = \begin{cases} i_1, & \ell = 1; \quad \text{first node} \\ i_2, & \ell = 2; \quad \text{second node} \\ i_3, & \ell = 3; \quad \text{third node} \end{cases}.$$

The matrix of Eqn. (1.8) is added to the submatrix $[K_{ii}]$ in the simultaneous equations.

5.5.6.2 Point Loading Matrix

The point loading force $\left(F_x \quad F_y \right)^T$ acts on point (x, y) of element e, and

$$\begin{pmatrix} u \\ v \end{pmatrix} = \begin{pmatrix} u(x, y) \\ v(x, y) \end{pmatrix}.$$

The potential energy due to the point loading is

$$\begin{aligned}
\Pi_p &= -\left(u \quad v \right) \begin{pmatrix} F_x \\ F_y \end{pmatrix} \\
&= -\{D_e\}^T [T_e(x, y)]^T \begin{pmatrix} F_x \\ F_y \end{pmatrix}.
\end{aligned} \tag{2.1}$$

Therefore,

$$[T_e]^T \begin{pmatrix} F_x \\ F_y \end{pmatrix} = \begin{pmatrix} [T_1]^T \\ [T_2]^T \\ [T_3]^T \end{pmatrix} \begin{pmatrix} F_x \\ F_y \end{pmatrix}. \tag{2.2}$$

is the load matrix.

Then

$$[T_r]^T \begin{pmatrix} F_x \\ F_y \end{pmatrix} \quad \rightarrow \quad \{F_{i(r)}\}; \qquad r = 1, 2, 3. \tag{2.3}$$

The matrix of Eqn. (2.3) is added to the submatrix $[F_i]$ in the simultaneous equations.

5.5.6.3 Forces of Inertia Matrix

Denote $(\,u(t) \quad v(t)\,)^T$ as the time-dependent displacements of any point (x, y) of element e. The force of inertia per unit area is

$$\begin{pmatrix} f_x \\ f_y \end{pmatrix} = -\mathcal{M}\frac{\partial^2}{\partial t^2}\begin{pmatrix} u(t) \\ v(t) \end{pmatrix} = -\mathcal{M}[T_e]\frac{\partial^2\{D_e(t)\}}{\partial t^2}. \tag{3.1}$$

where $\mathcal{M}$ = mass per unit area.

The potential energy of the inertia force of element e is

$$\begin{aligned} \Pi_i &= -\iint_A (\,u \quad v\,)\begin{pmatrix} f_x \\ f_y \end{pmatrix} dx\,dy \\ &= \iint_A \mathcal{M}(\,u \quad v\,)[T_e]\frac{\partial^2\{D_e(t)\}}{\partial t^2}\,dx\,dy. \end{aligned} \tag{3.2}$$

Assume $\{D_e(0)\} = \{0\}$ as the displacements at the beginning of the time step, $\{D_e(\Delta)\} = \{D_e\}$ as the displacements at the end of the time step, Δ as time interval of this time step. Then

$$\begin{aligned} \{D_e\} = \{D_e(\Delta)\} &= \{D_e(0)\} + \Delta\frac{\partial\{D_e(0)\}}{\partial t} + \frac{\Delta^2}{2}\frac{\partial^2\{D_e(0)\}}{\partial t^2} \\ &= \Delta\frac{\partial\{D_e(0)\}}{\partial t} + \frac{\Delta^2}{2}\frac{\partial^2\{D_e(0)\}}{\partial t^2}; \end{aligned} \tag{3.3}$$

$$\frac{\partial^2\{D_e(0)\}}{\partial t^2} = \frac{2}{\Delta^2}\{D_e\} - \frac{2}{\Delta}\frac{\partial\{D_e(0)\}}{\partial t} = \frac{2}{\Delta^2}\{D_e\} - \frac{2}{\Delta}\{V_e(0)\}, \tag{3.4}$$

where

$$\{V_e(0)\} = \frac{\partial\{D_e(0)\}}{\partial t}, \tag{3.5}$$

is the velocity at the beginning of the time step.

Then the potential energy becomes:

$$\mathcal{M}\{D_e\}^T\left[\iint_{\mathcal{A}}[T_e]^T[T_e]\,dx\,dy\right]\left(\frac{2}{\Delta^2}\{D_e\}-\frac{2}{\Delta}\{V_e(0)\}\right). \tag{3.6}$$

Therefore,

$$-\left[\iint_{\mathcal{A}}[T^e]^T[T_e]\,dx\,dy\right]\left(\frac{2\mathcal{M}}{\Delta^2}\{D_e\}-\frac{2\mathcal{M}}{\Delta}\{V_e(0)\}\right) \tag{3.7}$$

is the load matrix.

Thus,

$$\begin{aligned}&\frac{2\mathcal{M}}{\Delta^2}\left[\iint_{\mathcal{A}}[T_e]^T[T_e]\,dx\,dy\right]\\ &=\frac{2\mathcal{M}}{\Delta^2}\left[\iint_{\mathcal{A}}\begin{pmatrix}[T_1]^T\\ [T_2]^T\\ [T_3]^T\end{pmatrix}\left([T_1]\quad[T_2]\quad[T_3]\right)dx\,dy\right]\quad\rightarrow\quad[K_e],\end{aligned} \tag{3.8}$$

and

$$\begin{aligned}&\frac{2\mathcal{M}}{\Delta}\left[\iint_{\mathcal{A}}[T_e]^T[T_e]\,dx\,dy\right]\{V_e(0)\}\\ &=\frac{2\mathcal{M}}{\Delta}\left[\iint_{\mathcal{A}}\begin{pmatrix}[T_1]^T\\ [T_2]^T\\ [T_3]^T\end{pmatrix}\left([T_1]\quad[T_2]\quad[T_3]\right)dx\,dy\right]\{V_e(0)\}\quad\rightarrow\quad\{F_e\}.\end{aligned} \tag{3.9}$$

Then

$$\frac{2\mathcal{M}}{\Delta^2}\left[\iint_{\mathcal{A}}[T_r]^T[T_s]\,dx\,dy\right]\quad\rightarrow\quad[K_{i(r)i(s)}];\qquad r,s=1,2,3. \tag{3.10}$$

$$\frac{2\mathcal{M}}{\Delta}\left[\iint_{\mathcal{A}}[T_r]^T[T_s]\,dx\,dy\right]\{V_s(0)\}\quad\rightarrow\quad\{F_{i(r)}\};\qquad\begin{cases}\mathrm{r}&=1,2,3;\\ \mathrm{s}&=\text{tensor sum},\end{cases} \tag{3.11}$$

where

$$\{V_s(0)\}=\frac{\partial}{\partial t}\begin{pmatrix}u_s(0)\\ v_s(0)\end{pmatrix}.$$

In the following we compute:

$$\begin{aligned}&\iint_{\mathcal{A}}[T_r]^T[T_s]\,dx\,dy\\ &=\iint_{\mathcal{A}}\begin{pmatrix}f_rf_s&0\\ 0&f_rf_s\end{pmatrix}dx\,dy=\begin{pmatrix}t_{rs}&0\\ 0&t_{rs}\end{pmatrix};\end{aligned}$$

where

$$t_{rs} = \iint_A f_r f_s \, dx\, dy$$
$$= \iint_A (f_{1r} + f_{2r}x + f_{3r}y)(f_{1s} + f_{2s}x + f_{3s}y)\, dx\, dy,$$

and

$$\begin{aligned} t_{rs} = f_{1r}f_{1s}S^e &+ (f_{1r}f_{2s} + f_{1s}f_{2r})S^e_x \\ &+ (f_{1r}f_{3s} + f_{1s}f_{3r})S^e_y \\ &+ (f_{2r}f_{3s} + f_{2s}f_{3r})S^e_{xy} \\ &+ f_{2r}f_{2s}S^e_{xx} + f_{3r}f_{3s}S^e_{yy}, \end{aligned} \tag{3.12}$$

where

$$S^e = \iint_A dx\, dy; \tag{3.13}$$

$$S^e_x = \iint_A x\, dx\, dy; \tag{3.14}$$

$$S^e_y = \iint_A y\, dx\, dy. \tag{3.15}$$

$$S^e_{xy} = \iint_A xy\, dx\, dy; \tag{3.16}$$

$$S^e_{xx} = \iint_A x^2\, dx\, dy; \tag{3.17}$$

$$S^e_{yy} = \iint_A y^2\, dx\, dy. \tag{3.18}$$

The analytical solutions of equations (3.13) to (3.18) are in the following:

$$S^e = \frac{1}{2}\begin{vmatrix} 1 & x_1 & y_1 \\ 1 & x_2 & y_2 \\ 1 & x_3 & y_3 \end{vmatrix}; \tag{3.19}$$

$$S^e_x = \frac{S^e}{3}(x_1 + x_2 + x_3); \tag{3.20}$$

$$S^e_y = \frac{S^e}{3}(y_1 + y_2 + y_3); \tag{3.21}$$

$$\begin{aligned} S^e_{xy} = \frac{S^e}{12}&(2x_1y_1 + 2x_2y_2 + 2x_3y_3 + x_1y_2 \\ &+ x_2y_1 + x_1y_3 + x_3y_1 + x_2y_3 + x_3y_2); \end{aligned} \tag{3.22}$$

$$S^e_{xx} = \frac{S^e}{6}(x_1^2 + x_2^2 + x_3^2 + x_1x_2 + x_1x_3 + x_2x_3); \tag{3.23}$$

$$S^e_{yy} = \frac{S^e}{6}(y_1^2 + y_2^2 + y_3^2 + y_1y_2 + y_1y_3 + y_2y_3). \tag{3.24}$$

Then the final formula is

$$\frac{2\mathcal{M}}{\Delta^2}(t_{rs})\begin{pmatrix}1 & 0\\ 0 & 1\end{pmatrix} \quad \longrightarrow \quad [K_{i(r)i(s)}]; \qquad r,s=1,2,3, \tag{3.25}$$

$$\frac{2\mathcal{M}}{\Delta}(t_{rs})\begin{pmatrix}1 & 0\\ 0 & 1\end{pmatrix}\{V_s(0)\} \quad \longrightarrow \quad \{F_{i(r)}\}; \qquad \begin{cases}\mathrm{r} & = 1,2,3;\\ \mathrm{s} & = \text{tensor sum}.\end{cases} \tag{3.26}$$

The matrix of Eqns (3.25) and (3.26) are added to $[K_{ii}]$ and $[F_i]$ in the simultaneous equations.

5.5.6.4 Fixed Point Matrix

As a boundary condition, some of the elements are fixed at specific points. The constraint can be applied by using two very stiff springs. Assume the fixed point is (x, y) at element e with the displacements

$$\begin{pmatrix}u(x,y)\\ v(x,y)\end{pmatrix} = \begin{pmatrix}0\\ 0\end{pmatrix}.$$

The computed displacements are $(u \quad v)^T$.

There are two springs which are along the x and y directions, respectively. The stiffness of the springs is p. The spring forces are

$$\begin{pmatrix}f_x\\ f_y\end{pmatrix} = \begin{pmatrix}-pu\\ -pv\end{pmatrix}.$$

The strain energy of the spring is Π_m, then

$$\begin{aligned}\Pi_m &= \frac{p}{2}(u^2+v^2)\\ &= \frac{p}{2}\left(\begin{pmatrix}u & v\end{pmatrix}\begin{pmatrix}u\\ v\end{pmatrix}\right)\\ &= \frac{p}{2}\{D_e\}^T[T_e]^T[T_e]\{D_e\}.\end{aligned} \tag{4.1}$$

Then

$$p[T_e]^T[T_e] = p\begin{pmatrix}[T_1]^T\\ [T_2]^T\\ [T_3]^T\end{pmatrix}\begin{pmatrix}[T_1] & [T_2] & [T_3]\end{pmatrix}. \tag{4.2}$$

is the $[K_e]$ matrix.

Therefore,

$$pf_rf_s\begin{pmatrix}1 & 0\\ 0 & 1\end{pmatrix} \quad \longrightarrow \quad [K_{i(r)i(s)}]; \qquad r,s=1,2,3. \tag{4.3}$$

The matrix of Eqn. (4.3) is added to $[K_{ii}]$ in the simultaneous equations.

5.5.6.5 Normal Contact Matrix

A spring is assumed to be connected between vertex P_4 of element i and reference line $\overline{P_5P_6}$ of elemet j. The coordinates and displacement increment of point P_i are (x_i, y_i) and (u_i, v_i), respectively, $i = 4, 5, 6$. If a contact happens between two blocks, the no-penetration requirement must be satisfied, thus, the contact problem reduces to the relationship between point P_4 and reference line $\overline{P_5P_6}$(Fig. 4).

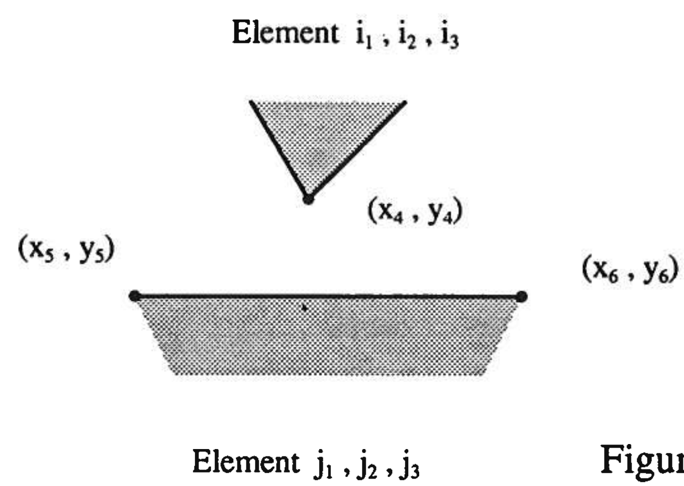

Figure 4.

When inter-penetration pushes the point P_4 back to reference line $\overline{P_5P_6}$, the distance from point P_4 to line $\overline{P_5P_6}$ should be zero after the displacement increment is applied.

$$d = \frac{\Delta}{l} = \frac{1}{l}\begin{vmatrix} 1 & x_4 + u_4 & y_4 + v_4 \\ 1 & x_5 + u_5 & y_5 + v_5 \\ 1 & x_6 + u_6 & y_6 + v_6 \end{vmatrix} = 0, \tag{5.1}$$

and

$$l = \sqrt{(x_5 - x_6)^2 + (y_5 - y_6)^2}.$$

Let

$$S_0 = \begin{vmatrix} 1 & x_4 & y_4 \\ 1 & x_5 & y_5 \\ 1 & x_6 & y_6 \end{vmatrix},$$

and

$$\Delta \approx S_0 + \begin{vmatrix} 1 & u_4 & y_4 \\ 1 & u_5 & y_5 \\ 1 & u_6 & y_6 \end{vmatrix} + \begin{vmatrix} 1 & x_4 & v_4 \\ 1 & x_5 & v_5 \\ 1 & x_6 & v_6 \end{vmatrix}, \tag{5.2}$$

where the determinant

$$\begin{vmatrix} 1 & u_4 & v_4 \\ 1 & u_5 & v_5 \\ 1 & u_6 & v_6 \end{vmatrix}$$

is the second order term which can be neglected as an infinitesimal.

Then

$$\begin{aligned} \Delta = S_0 &+ \left((y_5 - y_6) \quad (x_6 - x_5) \right) \begin{pmatrix} u_4 \\ v_4 \end{pmatrix} \\ &+ \left((y_6 - y_4) \quad (x_4 - x_6) \right) \begin{pmatrix} u_5 \\ v_5 \end{pmatrix} \\ &+ \left((y_4 - y_5) \quad (x_5 - x_4) \right) \begin{pmatrix} u_6 \\ v_6 \end{pmatrix}, \end{aligned} \tag{5.3}$$

and

$$\begin{pmatrix} u_4 \\ v_4 \end{pmatrix} = [T_i(x_4, y_4)]\{D_i\},$$

$$\begin{pmatrix} u_5 \\ v_5 \end{pmatrix} = [T_j(x_5, y_5)]\{D_j\},$$

$$\begin{pmatrix} u_6 \\ v_6 \end{pmatrix} = [T_j(x_6, y_6)]\{D_j\},$$

then

$$\begin{aligned} \Delta = S_0 &+ \left((y_5 - y_6) \quad (x_6 - x_5) \right) [T_i(x_4, y_4)]\{D_i\}, \\ &+ \left((y_6 - y_4) \quad (x_4 - x_6) \right) [T_j(x_5, y_5)]\{D_j\}, \\ &+ \left((y_4 - y_5) \quad (x_5 - x_4) \right) [T_j(x_6, y_6)]\{D_j\}, \end{aligned} \tag{5.4}$$

Set

$$\{H\} = \frac{1}{l}[T_i(x_4, y_4)]^T \begin{pmatrix} y_5 - y_6 \\ x_6 - x_5 \end{pmatrix}, \tag{5.5}$$

$$\begin{aligned} \{G\} = &\frac{1}{l}[T_j(x_5, y_5)]^T \begin{pmatrix} y_6 - y_4 \\ x_4 - x_6 \end{pmatrix} \\ &+ \frac{1}{l}[T_j(x_6, y_6)]^T \begin{pmatrix} y_4 - y_5 \\ x_5 - x_4 \end{pmatrix}, \end{aligned} \tag{5.6}$$

then

$$\begin{aligned} \{H\} &= \begin{pmatrix} \{H_1\} \\ \{H_2\} \\ \{H_3\} \end{pmatrix} \\ &= \frac{1}{l} \left([T_{i1}]^T(x_4, y_4) \quad [T_{i2}]^T(x_4, y_4) \quad [T_{i3}]^T(x_4, y_4) \right)^T \begin{pmatrix} y_5 - y_6 \\ x_6 - x_5 \end{pmatrix}; \end{aligned}$$

$$
\begin{aligned}
\{G\} &= \begin{pmatrix} \{G_1\} \\ \{G_2\} \\ \{G_3\} \end{pmatrix} \\
&= \frac{1}{l}\left([T_{j1}]^T(x_5, y_5) \quad [T_{j2}]^T(x_5, y_5) \quad [T_{j3}]^T(x_5, y_5) \right)^T \begin{pmatrix} y_6 - y_4 \\ x_4 - x_6 \end{pmatrix} \\
&\quad + \frac{1}{l}\left([T_{j1}]^T(x_6, y_6) \quad [T_{j2}]^T(x_6, y_6) \quad [T_{j3}]^T(x_6, y_6) \right)^T \begin{pmatrix} y_4 - y_5 \\ x_5 - x_4 \end{pmatrix};
\end{aligned}
$$

where

$$
\begin{aligned}
\{H_r\} &= \frac{1}{l}\begin{pmatrix} f_{4r} & 0 \\ 0 & f_{4r} \end{pmatrix} \begin{pmatrix} y_5 - y_6 \\ x_6 - x_5 \end{pmatrix} \\
\{G_r\} &= \frac{1}{l}\begin{pmatrix} f_{5r} & 0 \\ 0 & f_{5r} \end{pmatrix} \begin{pmatrix} y_6 - y_4 \\ x_4 - x_6 \end{pmatrix} \\
&\quad + \frac{1}{l}\begin{pmatrix} f_{6r} & 0 \\ 0 & f_{6r} \end{pmatrix} \begin{pmatrix} y_4 - y_5 \\ x_5 - x_4 \end{pmatrix}
\end{aligned}
$$

and

$$
\begin{aligned}
f_{4r} &= f_{1r} + f_{2r}x_4 + f_{3r}y_4 && \text{at element } i; \\
f_{5r} &= f_{1r} + f_{2r}x_5 + f_{3r}y_5 && \text{at element } j; \\
f_{6r} &= f_{1r} + f_{2r}x_6 + f_{3r}y_6 && \text{at element } j.
\end{aligned}
$$

Then Eqn. (5.1) becomes

$$
d = \{H\}^T\{D_i\} + \{G\}^T\{D_j\} + \frac{S_0}{l}. \tag{5.7}
$$

The potential energy of the normal spring is:

$$
\begin{aligned}
\Pi_k &= \frac{p}{2}d^2 \\
&= \frac{p}{2}\left(\{H\}^T\{D_i\} + \{G\}^T\{D_j\} + \frac{S_0}{l}\right)^2 \\
&= \frac{p}{2}\Bigg[\{D_i\}^T\{H\}\{H\}^T\{D_i\} + \{D_j\}^T\{G\}\{G\}^T\{D_j\} + 2\{D_i\}^T\{H\}\{G\}^T\{D_j\} \\
&\quad + 2\left(\frac{S_0}{l}\right)\{D_i\}^T\{H\} + 2\left(\frac{S_0}{l}\right)\{D_j\}^T\{G\} + \left(\frac{S_0}{l}\right)^2\Bigg].
\end{aligned} \tag{5.8}
$$

$$
p\{H\}\{H\}^T = p\begin{pmatrix} \{H_1\} \\ \{H_2\} \\ \{H_3\} \end{pmatrix} \left(\{H_1\}^T \quad \{H_2\}^T \quad \{H_3\}^T \right) \tag{5.9}
$$

$$p\{H\}\{G\}^T = p \begin{pmatrix} \{H_1\} \\ \{H_2\} \\ \{H_3\} \end{pmatrix} \left(\{G_1\}^T \quad \{G_2\}^T \quad \{G_3\}^T \right) \tag{5.10}$$

$$p\{G\}\{H\}^T = p \begin{pmatrix} \{G_1\} \\ \{G_2\} \\ \{G_3\} \end{pmatrix} \left(\{H_1\}^T \quad \{H_2\}^T \quad \{H_3\}^T \right) \tag{5.11}$$

$$p\{G\}\{G\}^T = p \begin{pmatrix} \{G_1\} \\ \{G_2\} \\ \{G_3\} \end{pmatrix} \left(\{G_1\}^T \quad \{G_2\}^T \quad \{G_3\}^T \right) \tag{5.12}$$

are the $[K_e]$ matrices; and

$$-p\left(\frac{S_0}{l}\right)\{H\} = -p\left(\frac{S_0}{l}\right)\begin{pmatrix} \{H_1\} \\ \{H_2\} \\ \{H_3\} \end{pmatrix} \tag{5.13}$$

$$-p\left(\frac{S_0}{l}\right)\{G\} = -p\left(\frac{S_0}{l}\right)\begin{pmatrix} \{G_1\} \\ \{G_2\} \\ \{G_3\} \end{pmatrix} \tag{5.14}$$

are the load matrices.

Then

$$\begin{array}{lcll}
p\{H_r\}\{H_s\}^T & \rightarrow & [K_{i(r)i(s)}]; & r,s = 1,2,3 \\
p\{H_r\}\{G_s\}^T & \rightarrow & [K_{i(r)j(s)}]; & r,s = 1,2,3 \\
p\{G_r\}\{H_s\}^T & \rightarrow & [K_{j(r)i(s)}]; & r,s = 1,2,3 \\
p\{G_r\}\{G_s\}^T & \rightarrow & [K_{j(r)j(s)}]; & r,s = 1,2,3 \\
-p\left(\frac{S_0}{l}\right)\{H_r\} & \rightarrow & \{F_{i(r)}\}; & r = 1,2,3 \\
-p\left(\frac{S_0}{l}\right)\{G_r\} & \rightarrow & \{F_{j(r)}\}; & r = 1,2,3
\end{array}$$

where

$$\text{for element } i \qquad \begin{cases} i(1) = i_1 \\ i(2) = i_2 \\ i(3) = i_3 \end{cases}$$

and

$$\text{for element } j \qquad \begin{cases} j(1) = j_1 \\ j(2) = j_2 \\ j(3) = j_3 \end{cases}$$

Similarly, the submatrices of **Initial Stresses**,**Volume Forces**, **Displacement Constrained in one Direction**, **Shear Contacts**, and **Friction Forces** can be derived in the same way as above.

5.7 Compressive Post-failure Test of a Marble Sample

This case demonstrates post-failure material behavior of a marble sample under compression with a preexisting crack configuration. The marble sample is 1.436 inch long, 1.0625 inch wide and the mesh contains 28 elements and 8 blocks. Figure 5.12 shows the original configuration of the marble sample. The upper and lower rectangular blocks are simulated as the loading block and the base one. Displacement control is used here and the incremental displacement for the loading block is 0.005 inch per second downward. Plane strain condition is assumed. The following data are input:

case : dynamics
time step : 6000
time interval : *0.001 second*
stiffness of penalty : 40,000 kip/in
friction angle : 45
unit mass : 3.241 X 10^{-6} k-slugs/in^3
volume force (v_x, v_y) : (0, -0.00125) kip
initial stress : (0, 0, 0)
yielding strain ($\varepsilon t, \varepsilon c$) for the marble sample: (0.001, -0.001)
range of $\varepsilon 1$ *for(E,, v1)* of the marble sample in compression : (unit of E ksi)
loading case :

range (1) $-0.001 < \varepsilon 1' \leq 0.000$, (El,v1) = (7500,0.30)

range (2) $-0.900 < \varepsilon 1 \leq -0.001$, (El,v1) = (4500,0.35)

unloading case :

range (1) $-0.900 < \varepsilon 1 \leq 0.000$, (El,v1) = (7500,0.30)

(E2,v2) for loading and base blocks(elastic material) : 30, *000 ksi, 0.30*

Figure 5.13 to 5.20 show the results after step 160, 220, 260, 300, 320, 340, 370 and 400, respectively. From the figures shown above one can mainly see the propagation of plastic regions. Figure 5.21 to 5.29 show the results after step 450, 500, 1510, 2000, 3000, 4000, 4500, 5000 and 6000, respectively. The failure mode and the progressive dilation of the marble sample are shown in the figure. Figure 5.30 shows the comparison of deformed and undeformed shapes of the marble sample. Figure 5.31 shows the principal stresses and directions after the final step, with dashed lines representing tension and solid lines for compression. The discontinuous approach provides another way to understand the postfailure effect and global stability of the structure system.

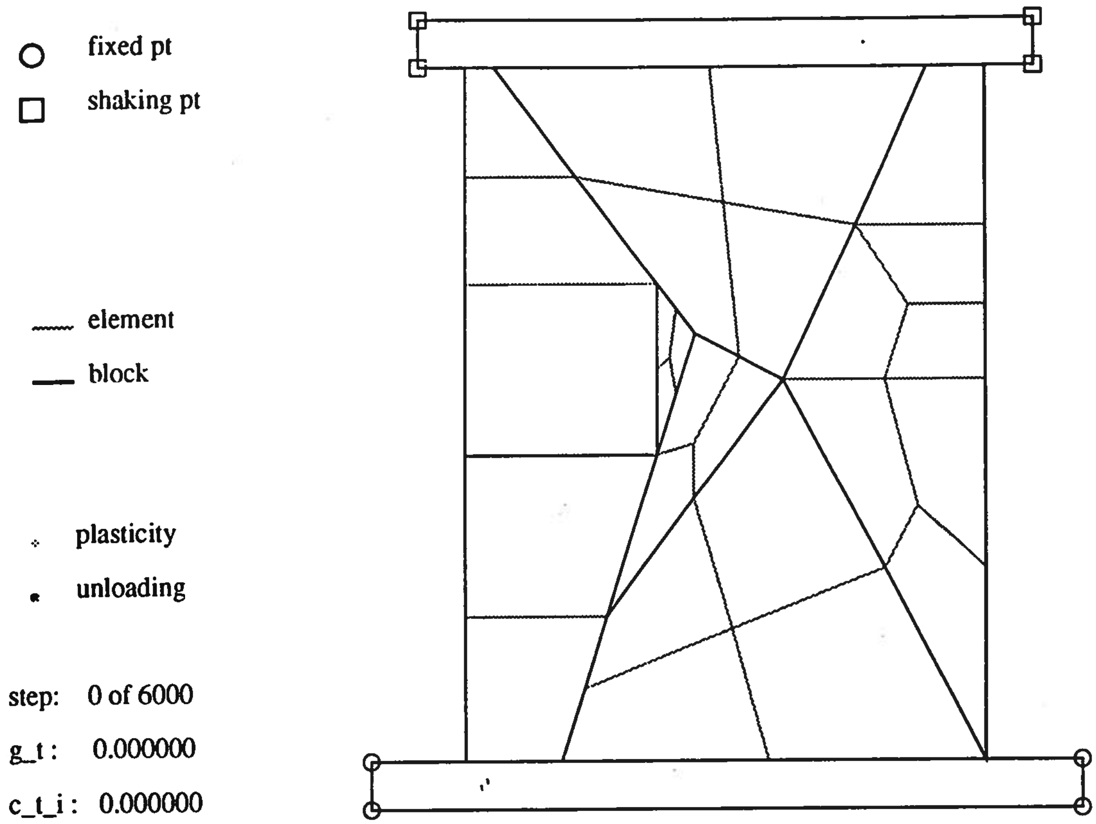

Fig: 5.12

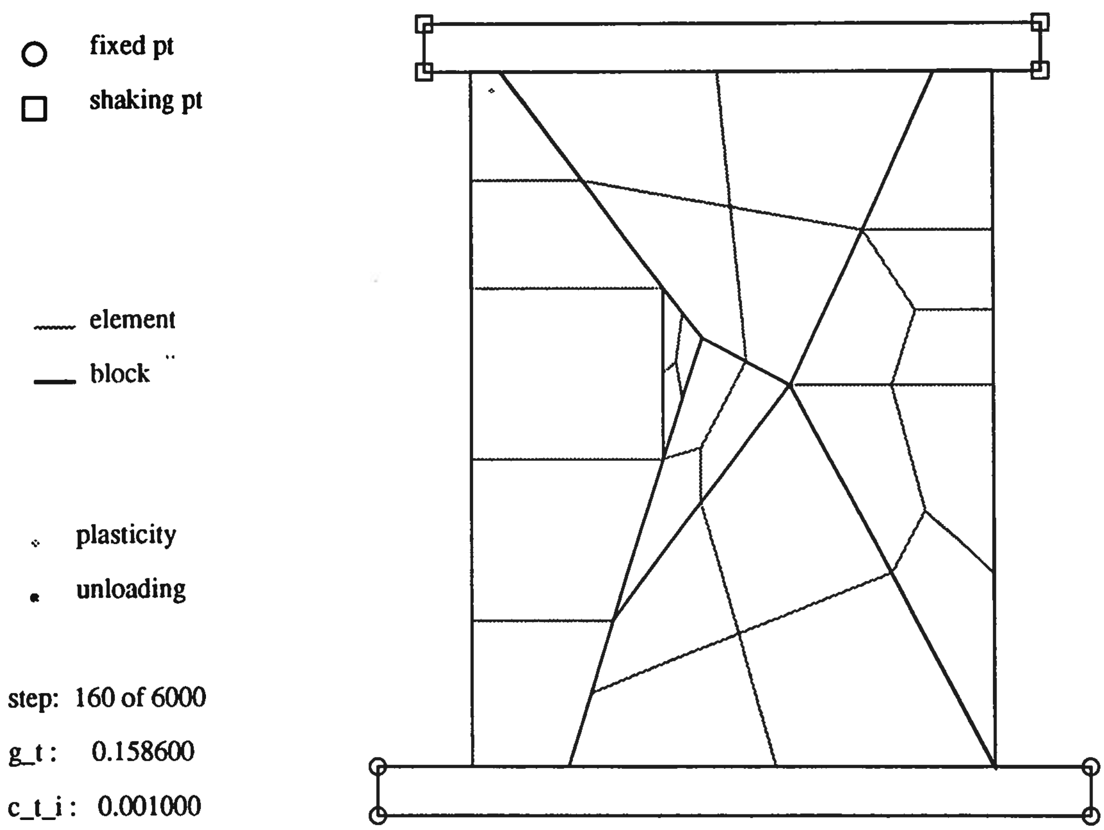

Fig: 5.13

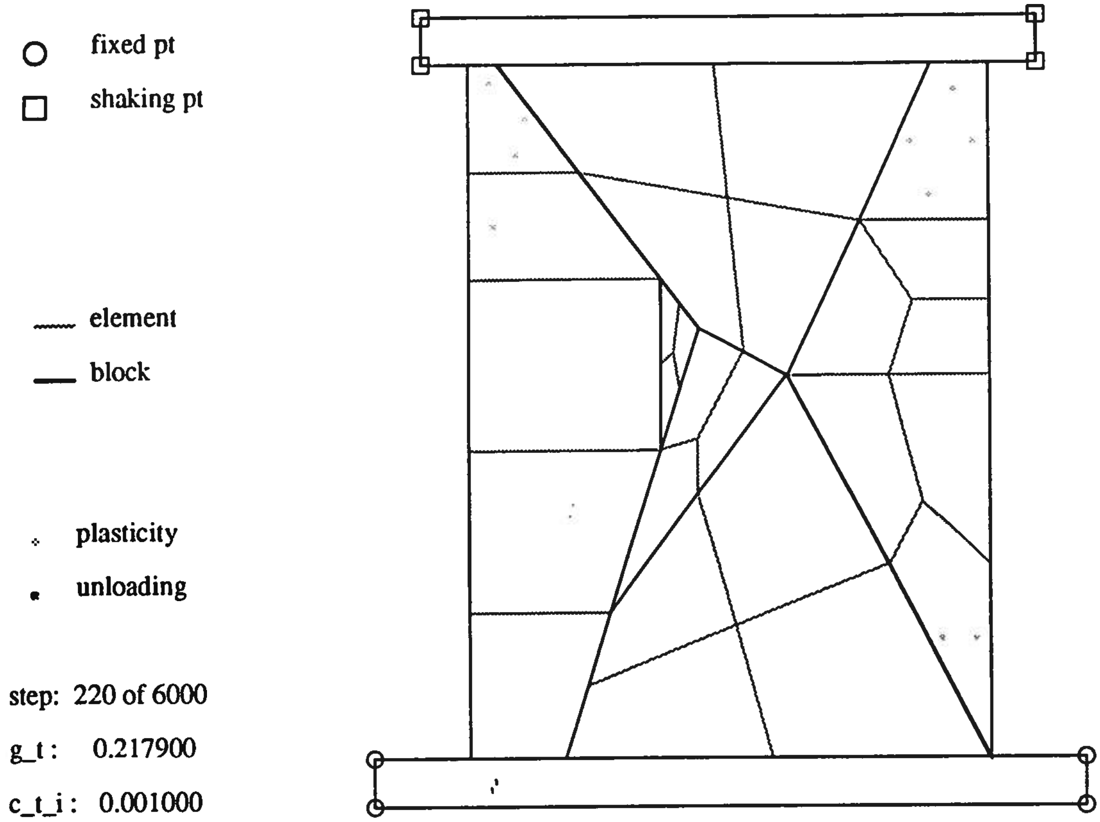

Fig: 5.14

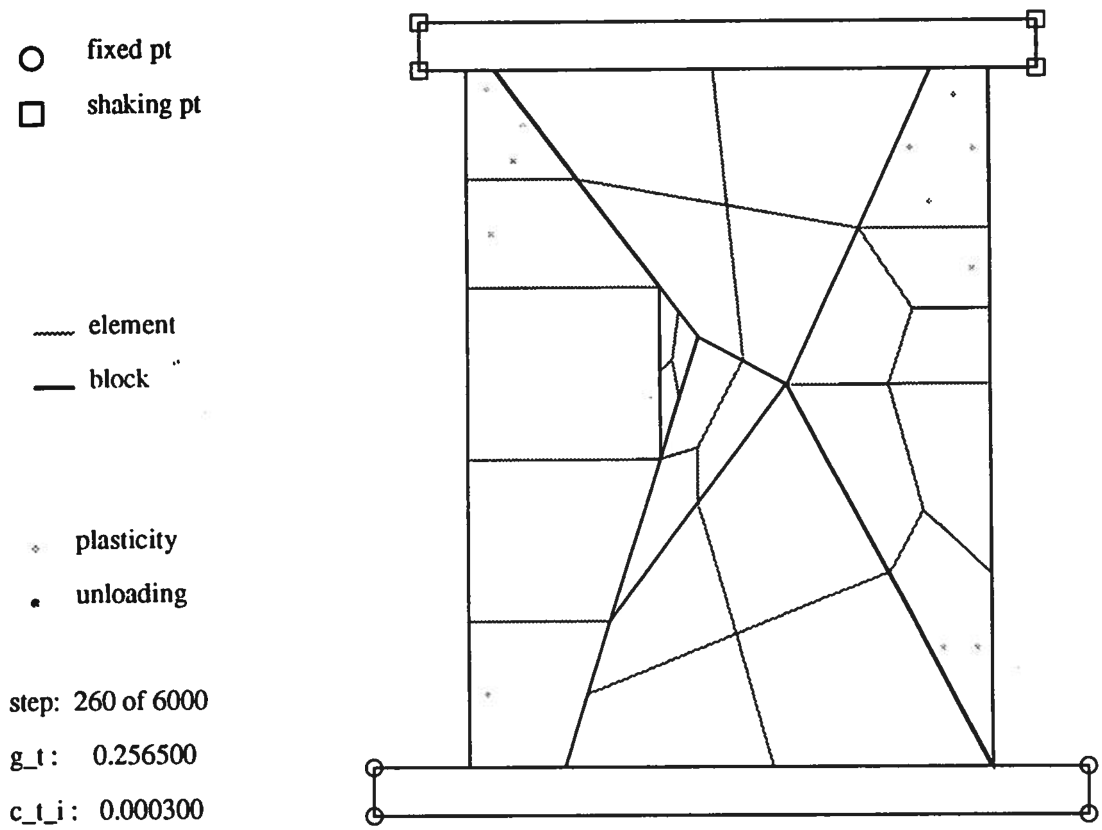

Fig: 5.15

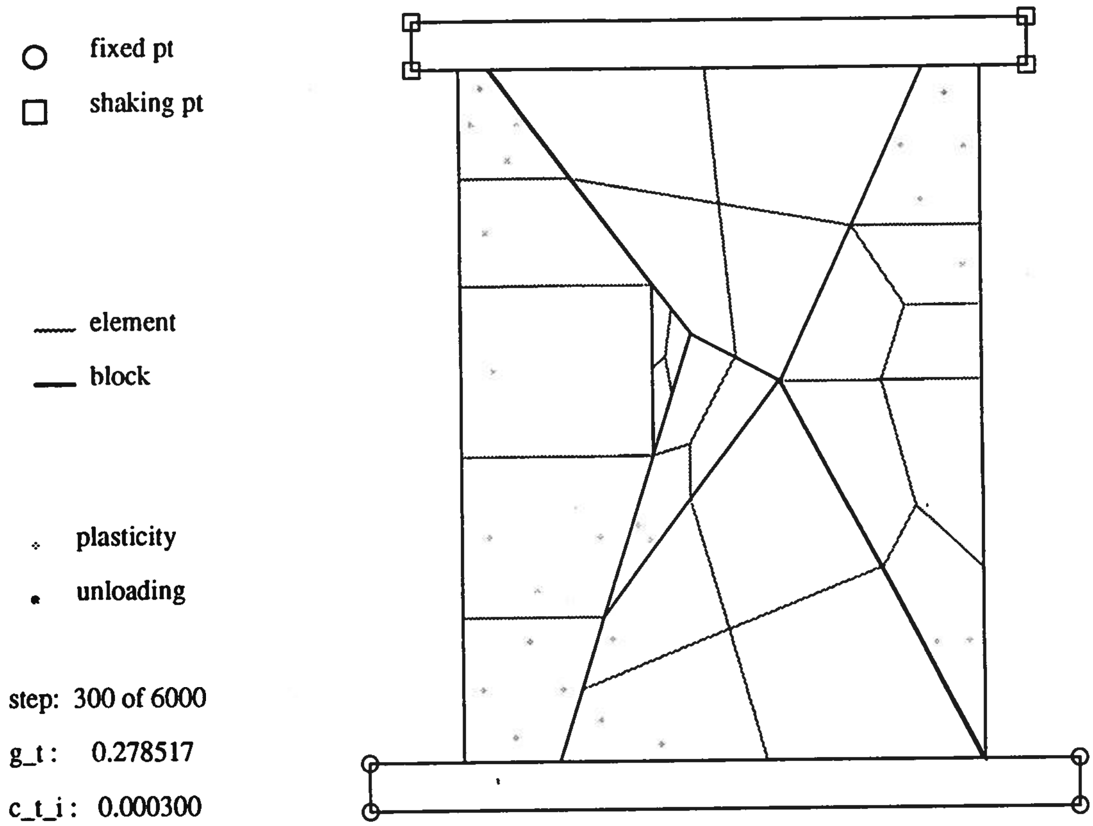

Fig: 5.16

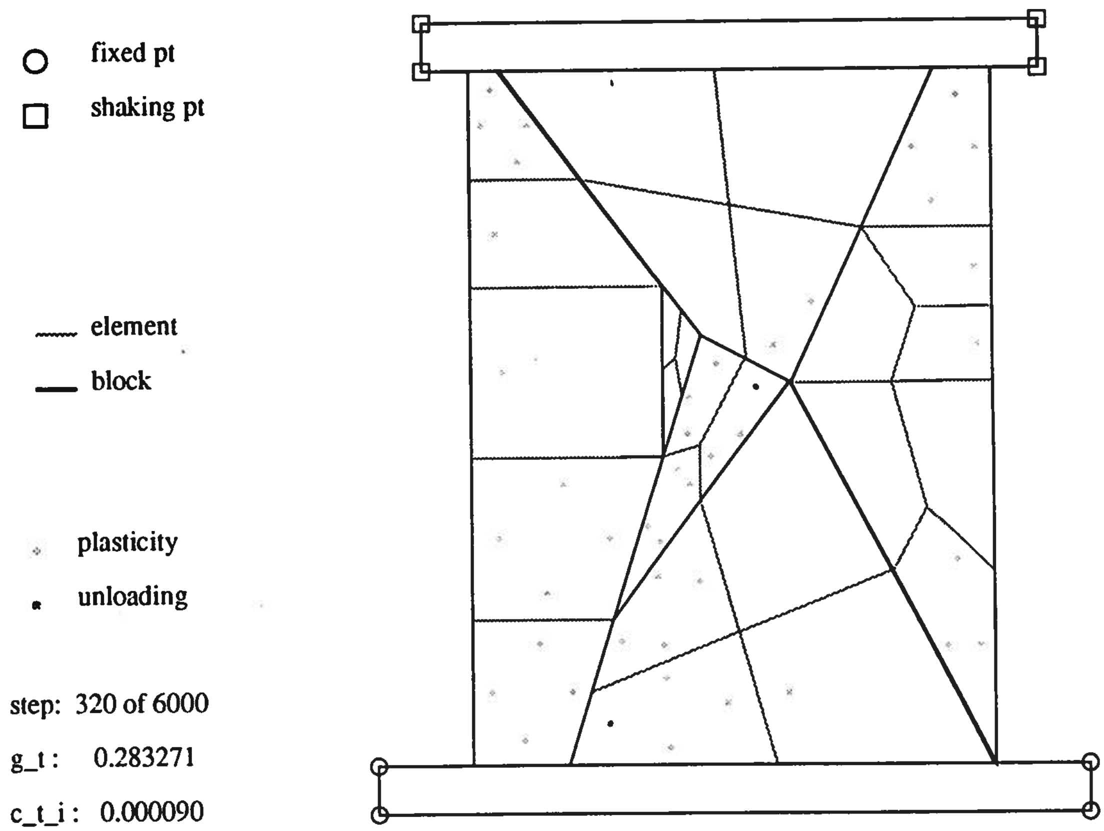

Fig: 5.17

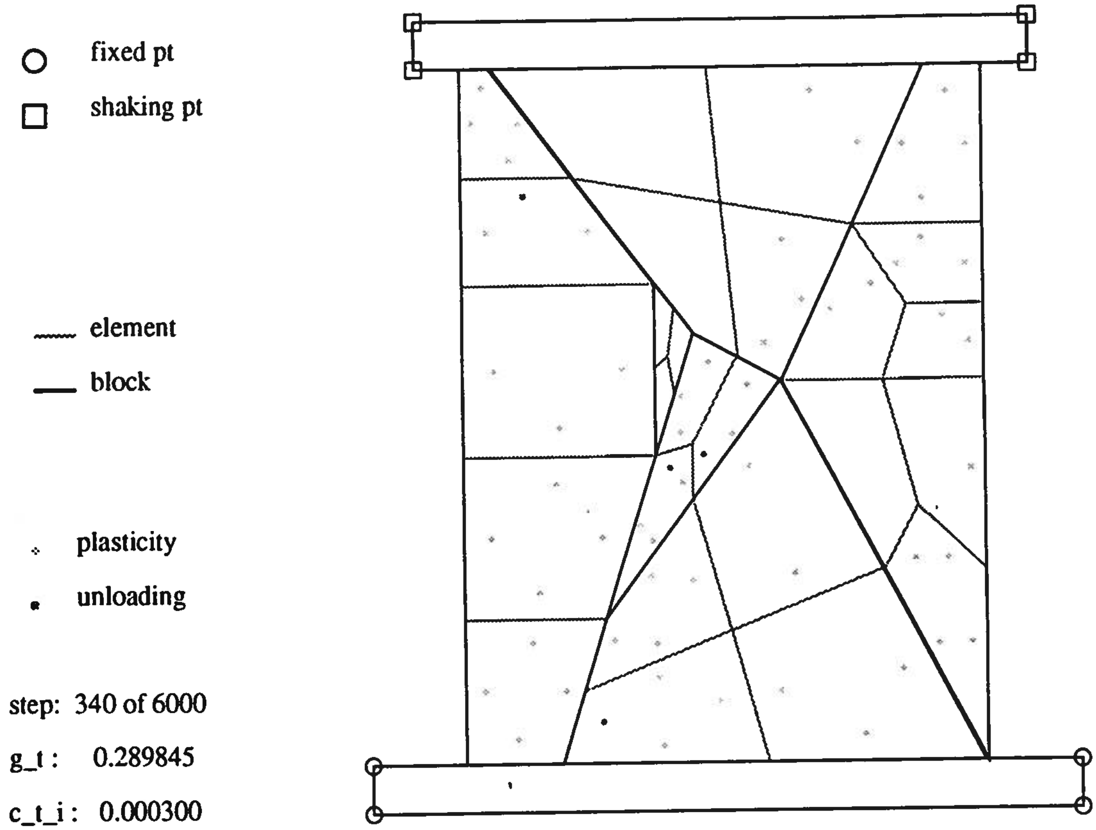

Fig: 5.18

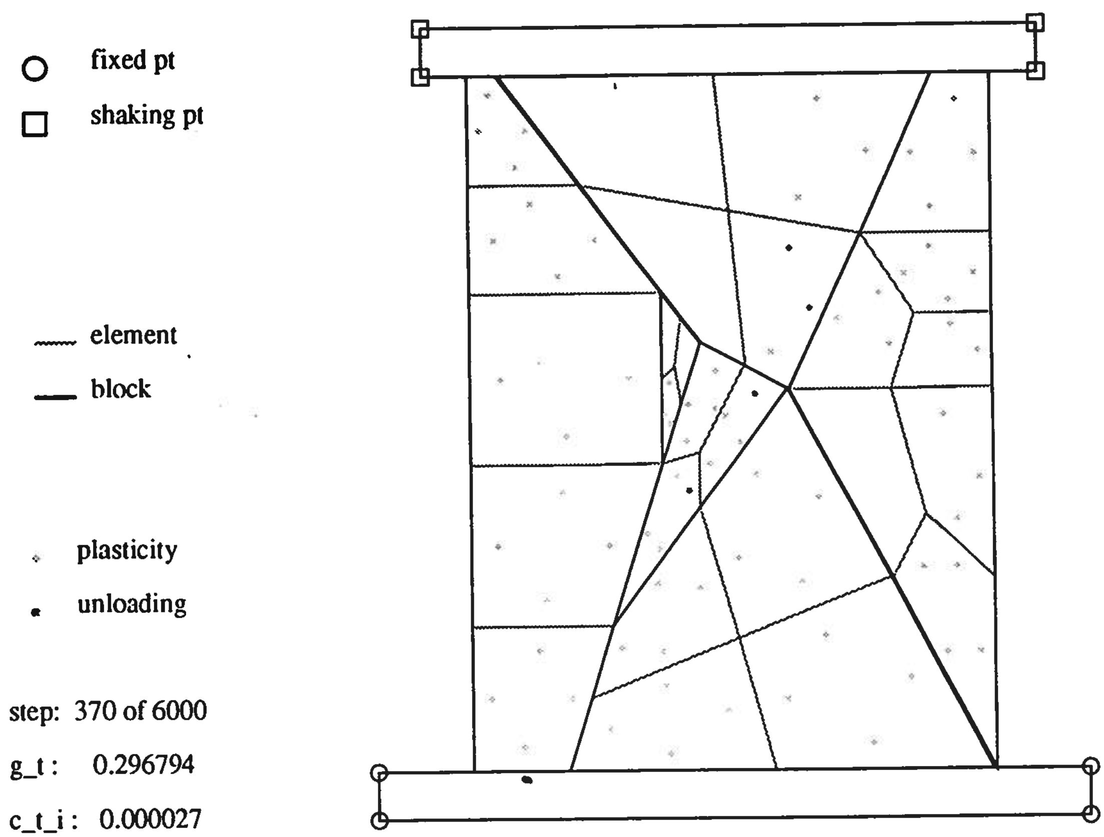

Fig: 5.19

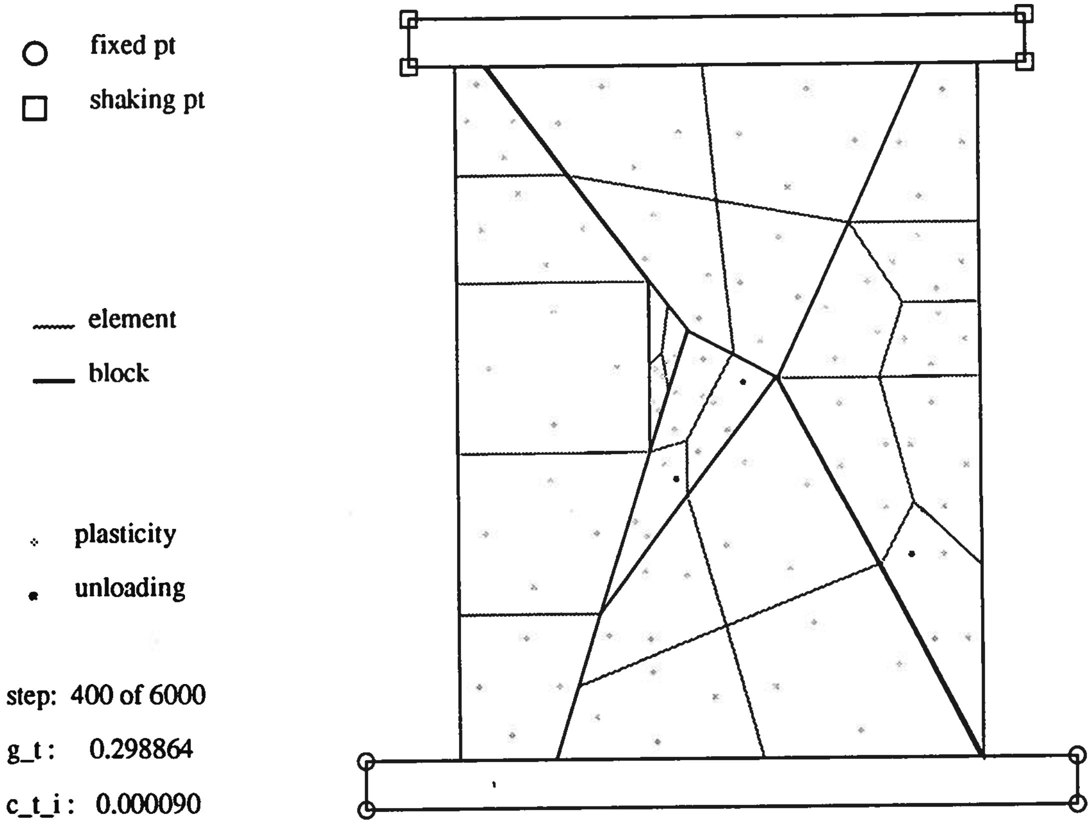

Fig: 5.20

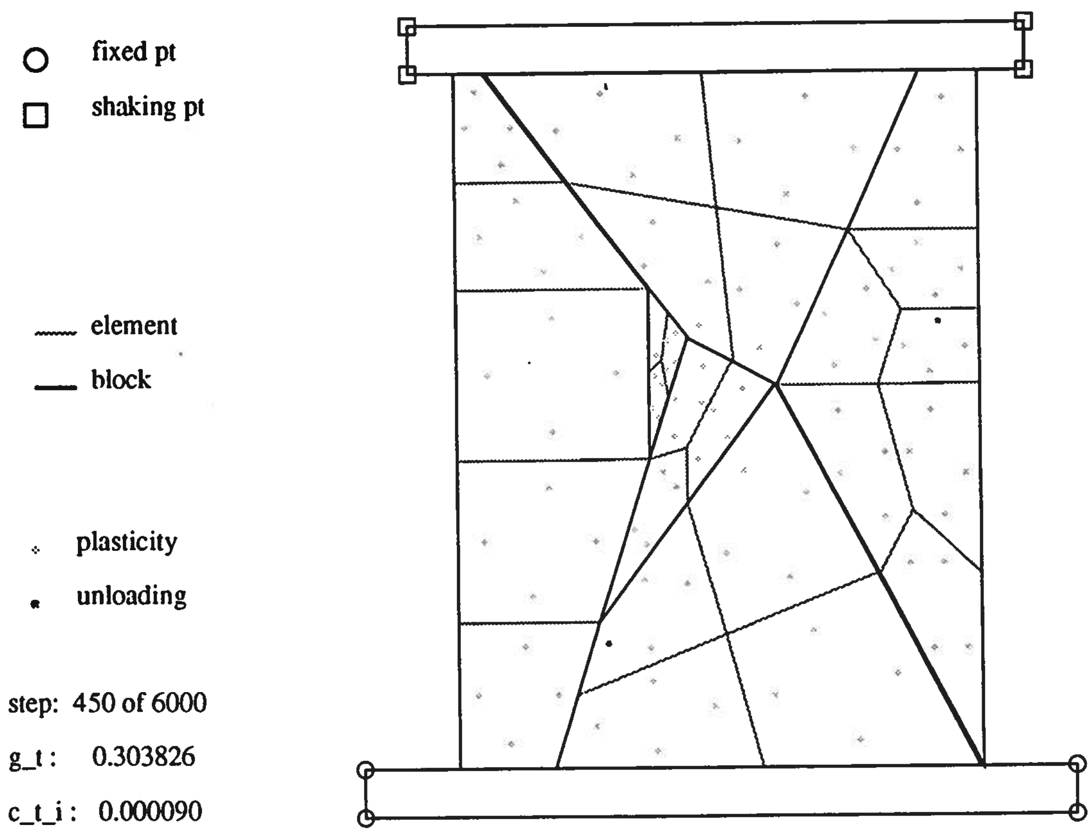

Fig: 5.21

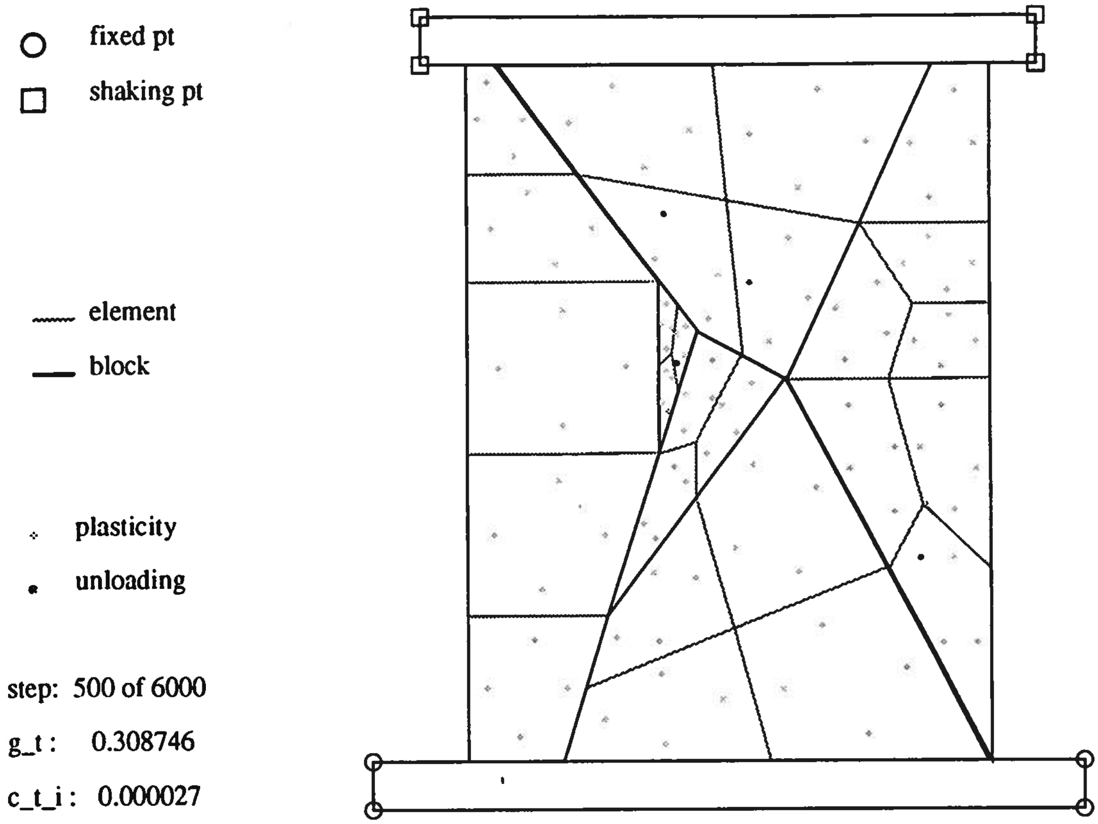

Fig: 5.22

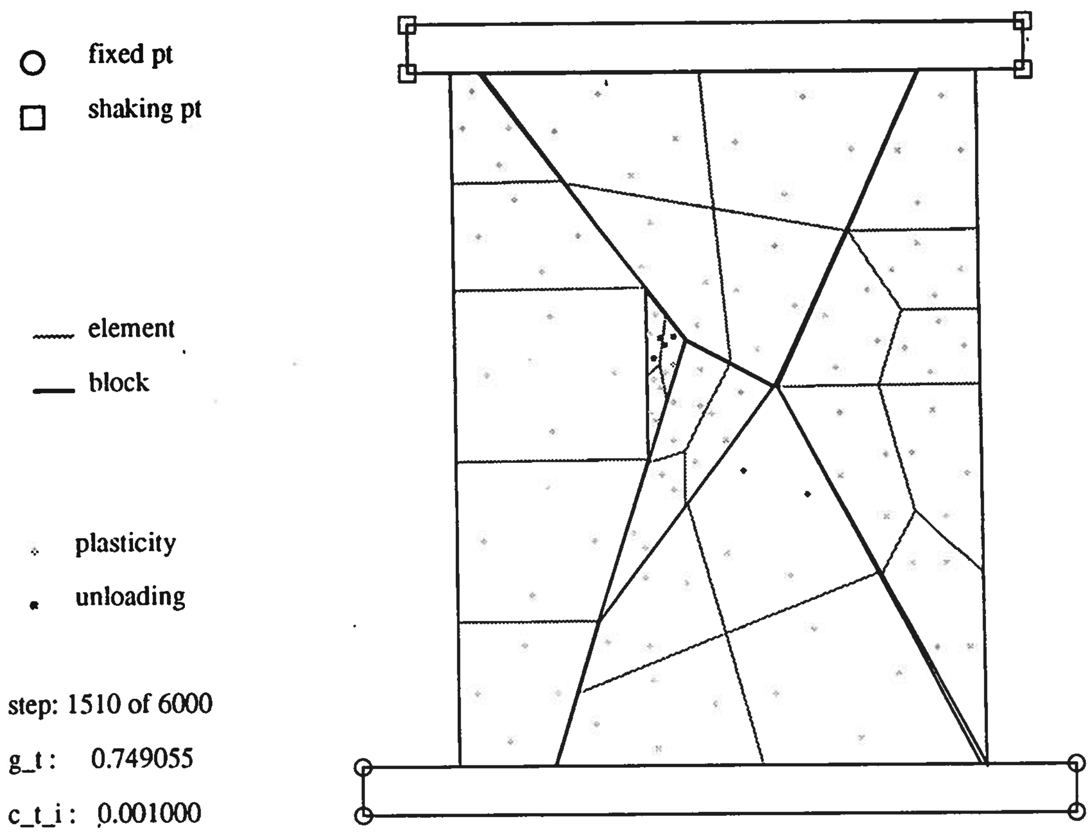

Fig: 5.23

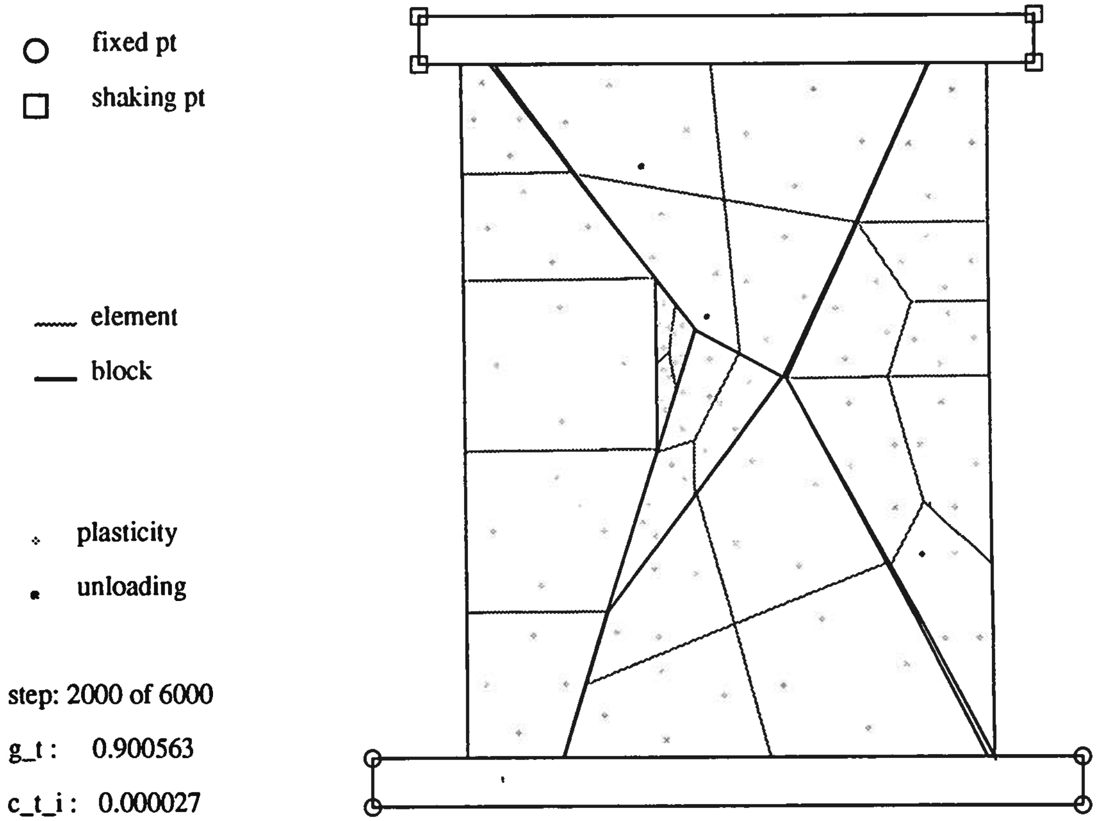

Fig: 5.24

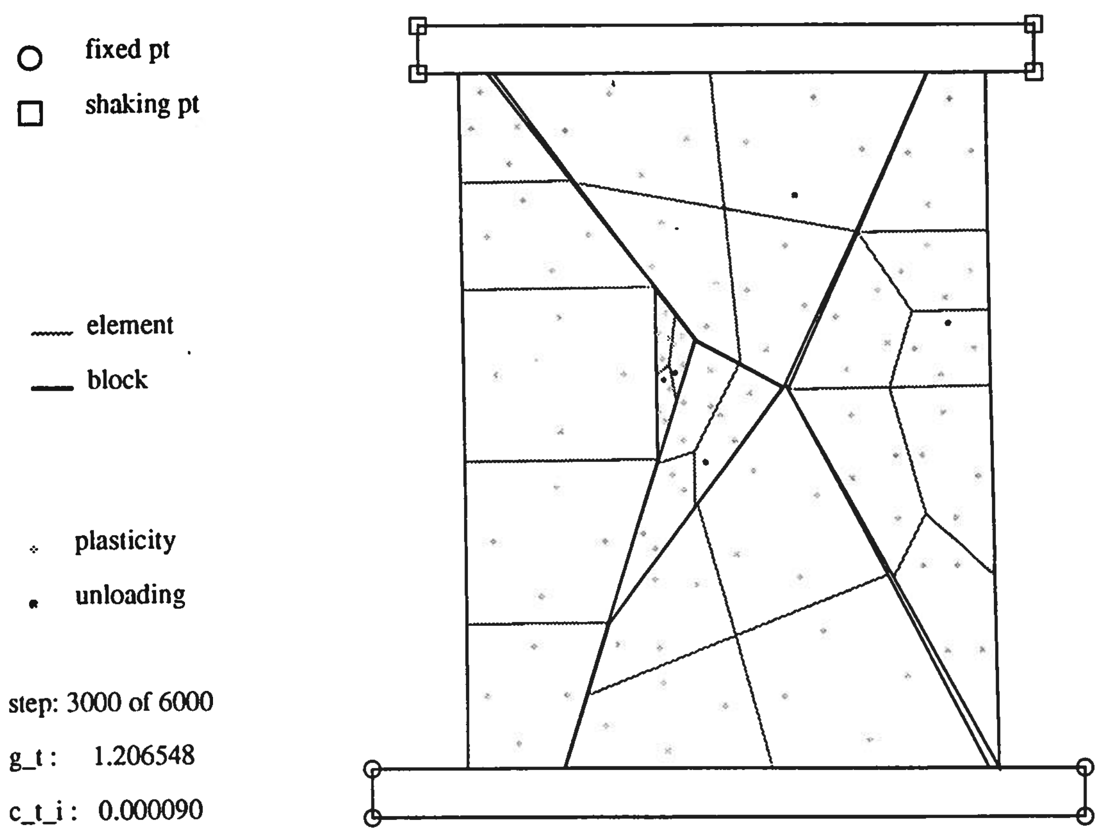

Fig: 5.25

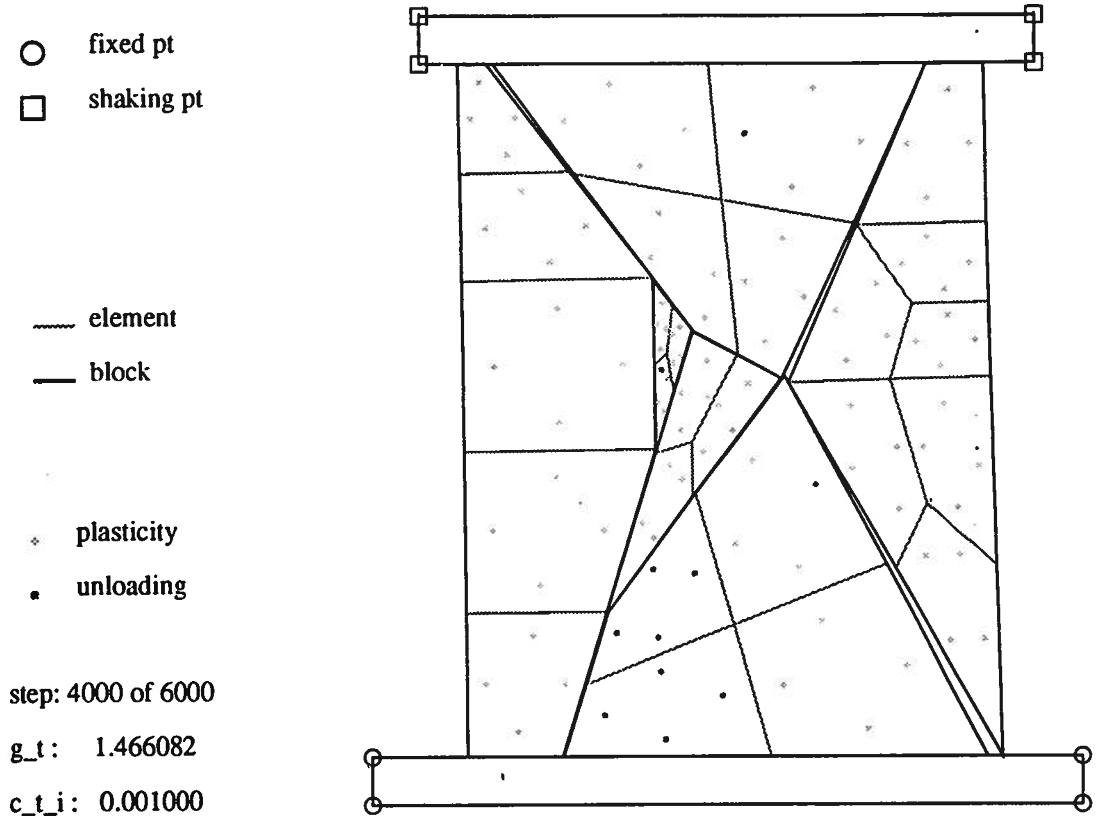

Fig: 5.26

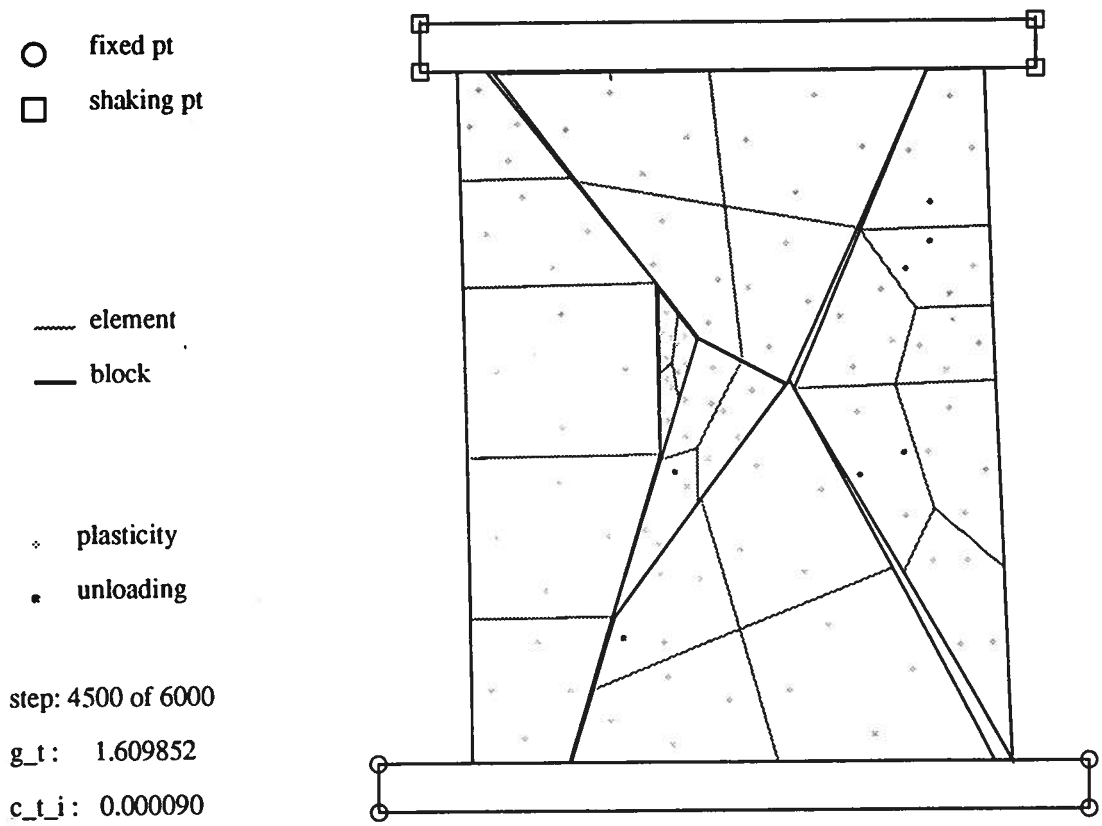

Fig: 5.27

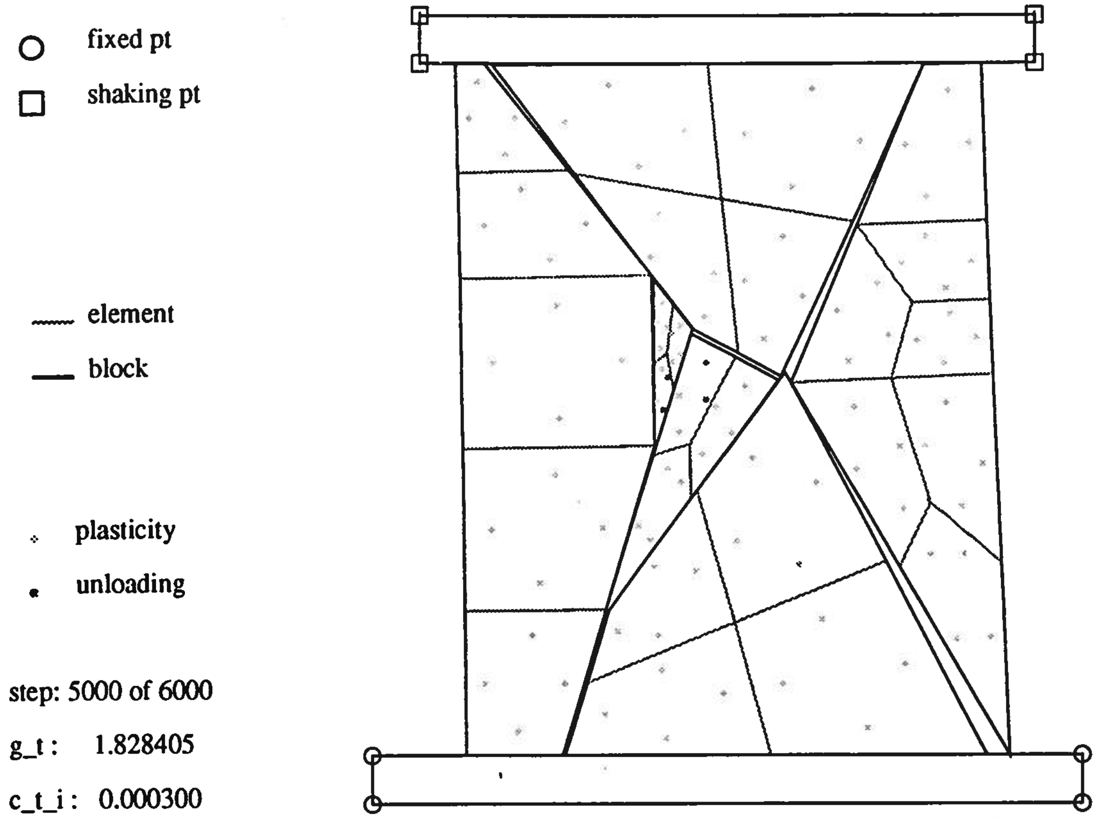

Fig: 5.28

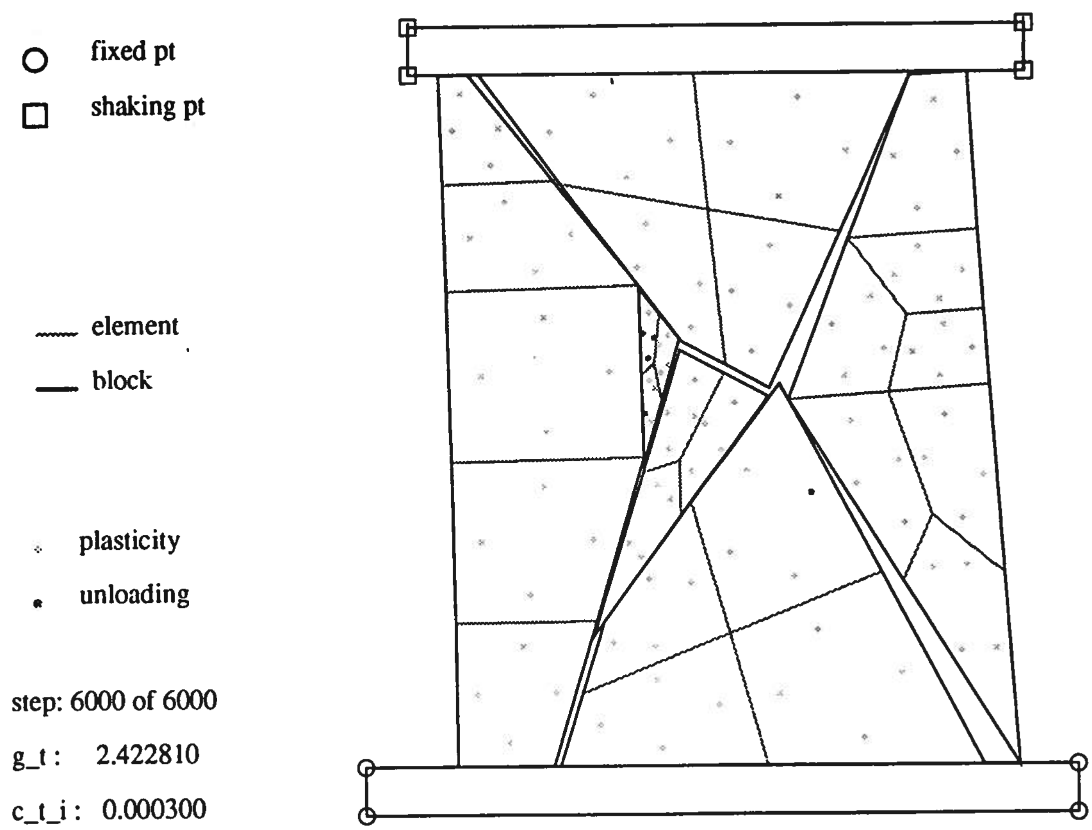

Fig: 5.29

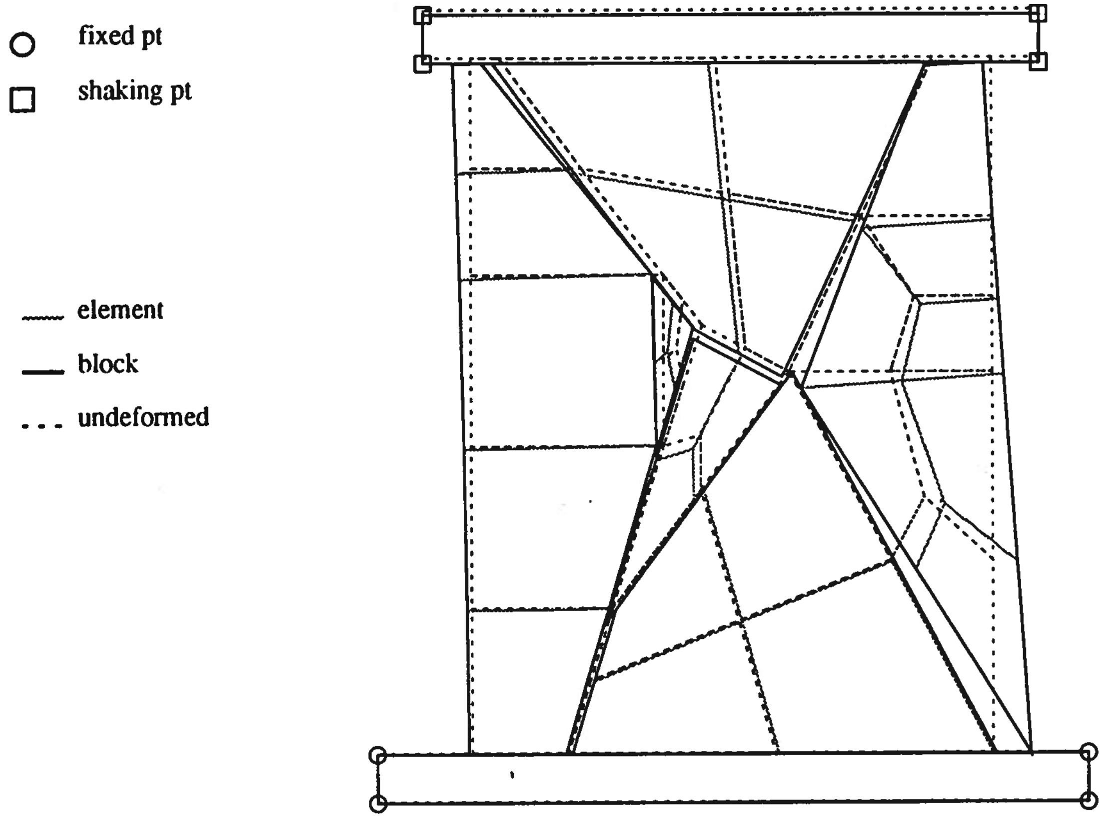

Fig: 5.30

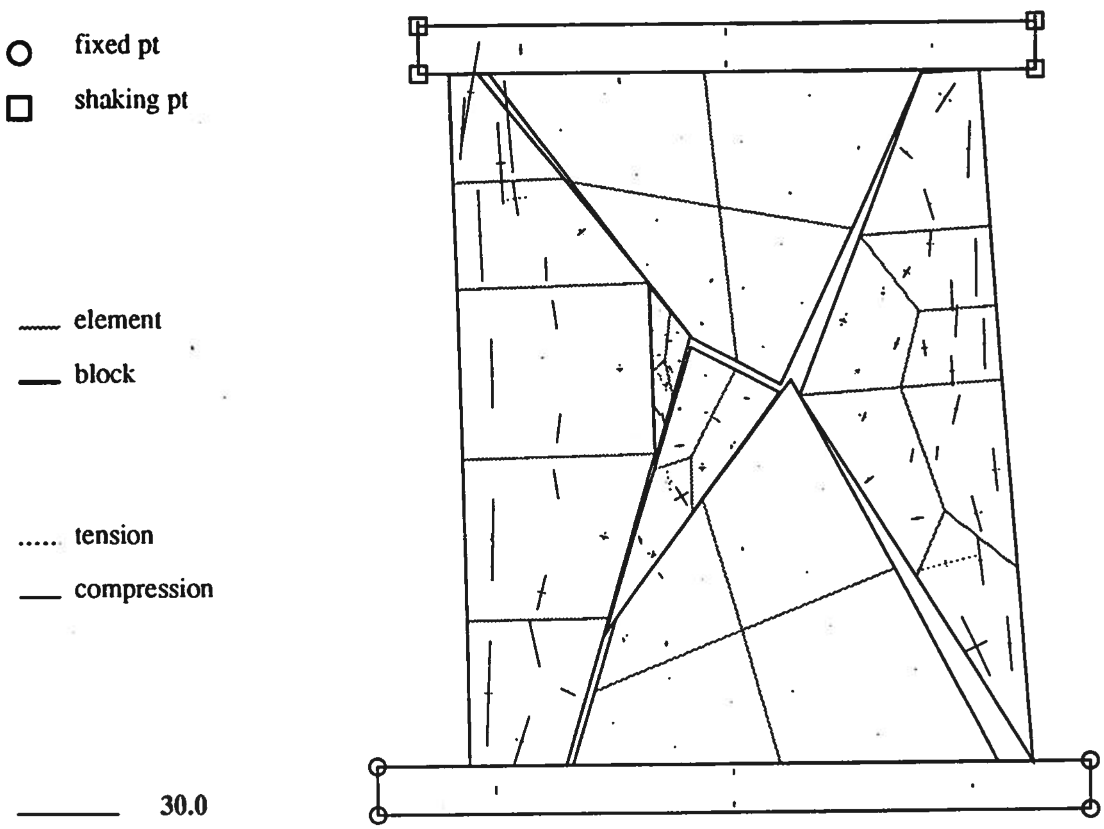

Fig: 5.31

REFERENCES

1. R. W. Clough, "The finite element in plane stress analysis", Proc. 2nd ASCE Conf. on Electronic Computation, Pittsburgh, Pa., Sep. 1960.
2. 0. C. Zienkiewicz and R. L. Taylor, "The Finite Element Method", 4th ed. Vol. 1 McGraw-Hill, London, 1989.
3. G. H. Shi, "Manifold Method of Material Analysis", 19th Army Conf. on Applied Mathematics and Computing, ARO Report 92-1, Mar. 1992.
4. R. E. Goodman, R. Taylor and T.L. Brekke, "A Model for the Mechanics of Jointed Rock." *Journal of the Soil Mechanics & Foundations Dvi.*, ASCE, v.94 pp. 637, 1968.
5. P. A. Cundall, " A Computer Model for Simulating Progressive, Large scale Movements in Blocky Rock Systems" Symposium of International Society of Rock Mechanics Nancy, France. pp. 11-18, 1971.
6. L. J. Lorig, B. H. G. Brady, and P. A. Cundall, "Hybrid Distinct Element - Boundary Element Analysis of Jointed Rock," Int. J. Rock Mech. Mining Sci., V 23 N. 4, pp. 303-312, 1986.
7. T. Maini, P. A. Cundall, J. Marti, Peter Beresford, Nigel Last, and Margaret Asgian, "Computer Modeling of Jointed Rock Masses " Technical Report N-78-4, Dams and Moore, Los Angels, 1878.
8. G. H. Shi, "Discontinuous Deformation Analysis - A New Numerical Model for the Statics and Dynamics of Block Systems ", *Ph. D. Thesis,* Civil Eng., University of California at Berkeley, 1988.
9. R. Courant, "Variational methods for the solution of problems of equilibrium and vibration", Bull. Am. Math. Soc., 49, 1-23, 1943.
10. M. J. Turner, R. W. Clough, H. C. Martin, and L. P. Topp, "Stiffness and Deflection Analysis of Complex Structures", *Journal of Aeronautical Sciences,* 23, no. 9, 805-823, 1956.
11. T. J. R. Hughes, "The Finite Element Method", Prentice-Hall, Englewood Cliffs, N.J., 1987.
12. K. K. Shyu, " Discontinuous Deformation Analysis with Finite Element Mesh", CE299 Report, Civil Eng., University of California at Berkeley, 1991.
13. G. H. Shi and R.E. Goodman, "Discontinuous Deformation Analysis." Proc. 25th U.S. Symposium on Rock Mechanics, pp. 269-277, 1984.
14. G. H. Shi and R.E. Goodman, "Two Dimensional Discontinuous Deformation Analysis." Int. J. Numer. Anal. Methods Geomech., v. 9, pp. 541-556, 1985.

15. J. N. Reddy, "Applied Functional Analysis and Variational Methods in Engineering." McGraw-Hill, New York, 1986.

16. 0. C. Zienkiewicz, and R. L. Taylor, "The Finite Element Method", 4th ed. Vol. 2 McGraw-Hill, London, 1991.

17. R. D. Cook, David S. Malkus, Michael E. Plesha, "Concepts and Applications of Finite Element Analysis", 3rd ed. John Wiley & Sons, N.Y., 1989.

18. P. K. Menta, "Concrete: Structure, Properties, and Materials" Prentice-Hall, 1986.

19. M. Y. H. Bangash, "Concrete and Concrete Structures: Numerical Modeling and Applications", Elsevier Applied Science, London, 1989.

20. G. H. Shi, R. E. Goodman, and J. P. Tinucci, "The Kinematics of Joint InterPenetrations." Proc. 26th U.S. Symposium on Rock Mechanics, pp. 121-130, 1985.

21. G. H. Shi and Goodman, R. E., "Generalization of Two-Dimensional Discontinuous Deformation Analysis for Forward Modeling", International Journal for Numerical and Analytical Methods in Geomechanics, Vol. 13 (4), pp. 359-380, August 1989.

22. W. F. Chen and A. D. Pan, Finite Element and Finite Block Methods in Geome chanics", Proceedings of the Third International Conference on Constitutive Laws for Engineering Materials, ASME Press, pp. 669-675, January 1991

23. W. F. Chen and A. D. Pan, "State-of-the-Art Future Development of the Finite Element Method", Civil Eng., Purdue University, 1991.

24. Irving H. Shames and Francis A. Cozzarelli, "Elastic and Inelastic Stress Analysis", Prentice Hall, Englewood Cliffs, New Jersey, 1992.

25. R. E. Goodman, "Introduction to Rock Mechanics", 2nd ed. John Wiley & Sons, N.Y., 1989.

26. J. C. Jaeger, N. G. W. Cook, "Fundamentals of Rock Mechanics", Methuen & Co LTD, London, 1969.

27. F. C. Tsai, "Generalized Discontinuous Deformation Analysis for Jointed Rock Mass", Mineral Eng., University of California, Berkeley, October, 1992.

CHAPTER 6

THE EFFECTS OF SODIUM SULFATE ON MARBLE

6. 1 Introduction

The effects of various naturally occurring elements on building materials is critical knowledge when deciding on safe and appropriate application. It is well documented that sodium sulfate deteriorates some aggregates and lower strength concrete. Tests indicate that the crystallization pressure created when mirabilite forms in solution is the main cause of the deterioration of concrete and other materials. The purpose of this investigation was to determine the effects on marble when submerged in a sodium sulfate solution that was cycled across the crystallization temperature for mirabilite.

6.2 The sodium Sulfate-Water System

The solubility curves for thenardite (Na_2SO_4), mirabilite ($Na_2SO_4 \cdot 10H_2O$) and heptahydrate ($Na_2SO_4 \cdot 7H_2O$) are shown in Figure 1 [1]. Mirabilite is stable below 32.4 °C when in contact with a saturated solution of sodium sulfate, or when the relative humidity exceeds the critical relative humidity shown in Figure 2 [2]. Mirabilite will dehydrate to form thenardite regardless of humidity if heated above 32.4 °C, or if dried below 32.4 °C at a relative humidity less than indicated in Figure 2. It is not possible to crystallize mirabilite above 32.4 °C at a pressure greater than or equal to atmospheric pressure.

Thenardite is stable above 32.4 °C regardless of relative humidity. Thenardite will hydrate to mirabilite if in contact with a saturated solution of sodium sulfate at temperatures less than 32.4 °C.

Heptahydrate is a meta-stable form of sodium sulfate. A very rapid temperature drop is required to form heptahydrate, and this form of sodium sulfate is unstable in the presence of mirabilite. These factors make the formation of heptahydrate unlikely in all except laboratory conditions.

6.2.1 Hydration

The hydration of thenardite to mirabilite is usually described as a solid-state reaction resulting in hydration pressure. However, this hydration pressure development is relatively slow ; Knacke and von Erdberg [3] found that the solid-state hydration will only transpire if water is supplied at a rate less than 0.015 g H_20 / g thenardite per hour. If the rate of water addition is greater, an impermeable coating results which prevents

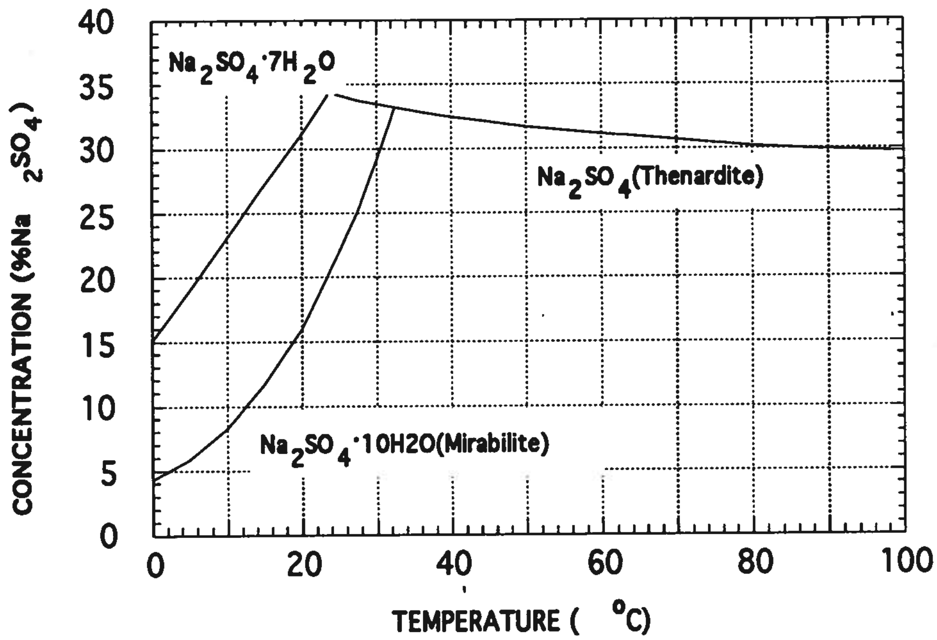

Figure 1. Solubility curves for the sodium sulfates (after Seidell and Linke, 1965)

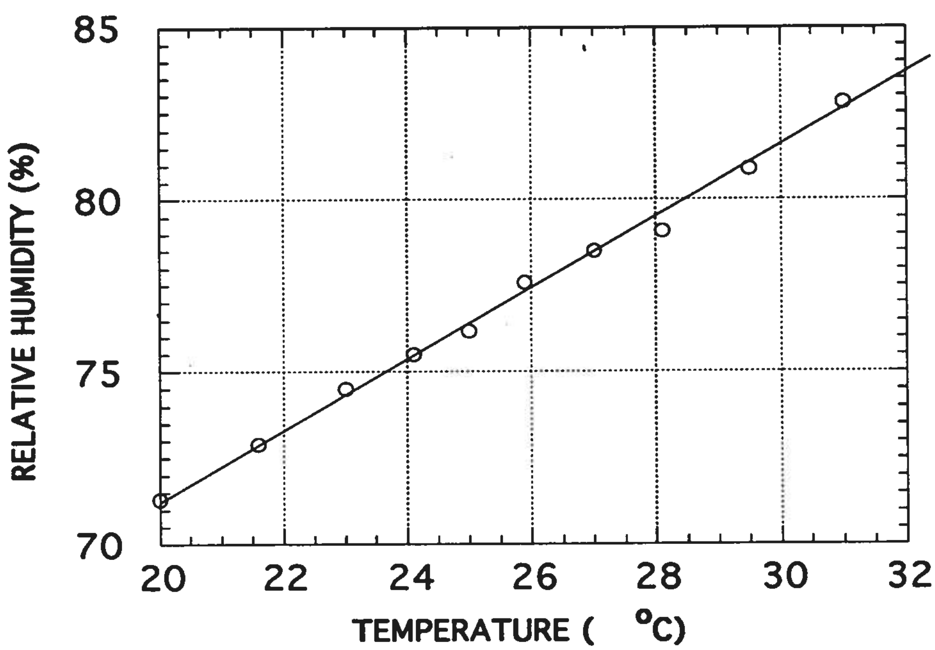

Figure 2. Critical relative humidities for mirabilite at 20-32 °C (after Sperling and Cooke, 1985)

further hydration. Furthermore, thenardite is orthorhombic (dipyramidal) and mirabilite is monoclinic (prismatic) and this difference in crystal structure may in itself prevent rapid solid-state hydration. Thus, the high solubility of thenardite is likely to favor through-solution rather than solid-state hydration to mirabilite, and any resulting pressure should properly be termed "crystallization pressure", rather than "hydration pressure", since it originates from the crystallization of mirabilite from solution. In either case, relatively small volumes of the system are affected during any given time period.

6.2.2 Crystallization of Mirabilite

In addition to thenardite hydrating to mirabilite, mirabilite can be formed directly from solution due to temperature changes or evaporation. As seen in Figure 1, the solubility of mirabilite changes significantly over a range of temperature that corresponds to normal daily temperature changes at the earth's surface. A gradual temperature drop results in a saturated solution and gradual precipitation, affecting only a small percentage of the total system at any time. However, a more rapid temperature drop can result in a supersaturated solution, and eventually rapid crystallization of a large volume of the total system.

Evaporation is a slow process which affects only a small volume during any time period, and supersaturation is unlikely during evaporation because seed crystals typically form at the evaporation front. The rates of evaporation and the volumes affected during evaporation in the field are relatively small and casts doubts on the ability of evaporation alone to cause excessive deterioration of concrete.

6.2.3 Crystallization of Thenardite

Similar to the crystallization of mirabilite, the crystallization of thenardite from solution can be achieved by temperature changes or evaporation. However, unlike mirabilite, the solubility of thenardite decreases with increasing temperature and is relatively insensitive to temperature changes typically encountered in the field. Hence, supersaturation with respect to thenardite is not likely to result from temperature changes or evaporation rates, and any resulting crystallization would only affect a small volume of the system.

6.3 Experimental Methods

6.3.1 Materials

Vermont, Georgia and Italian marbles were used in the experiment. Also concrete samples mixed at 0.3 and 0.7 water to cement ratio were also studied for comparison. Three of each of the marble samples were loaded until cracking developed to analyze the effect of sodium sulfate on fractured samples. The sodium sulfate solutions were 30% by weight (300 g of sodium sulfate in one liter of water for each sample set). The solutions were cooled in a constant temperature (40 deg. F) room and were heated in a hot bath to a temperature of 90 deg. F.

6.3.2 Procedures

The 0.3 and 0.7 water to cement ratio concrete samples were cast in 2"x2" molds. The molds were covered with burlap for 24 hours after that they were demolded and cured under water. Nine samples were cast for each mix.

Nine 2"x2" marble samples were cut from 1'x1' blocks. Three specimens were cycled in the sodium sulfate solution, three specimens were tested to determine the ultimate strength and finally three specimens were loaded until crack developed and then cycled in the sodium sulfate solution. Each set of three similar samples were placed in their own 6"x12" cylinder with a mixture of one liter of water and 300g of sodium sulfate. The samples were continuously covered except when stirred.

The first samples were placed in the 40 deg. room on the 23rd of October. On the 24th they were transferred to a hot bath for an hour and a half. With a little stirring, this was sufficient time to completely dissolve the marbilite. The procedure was continued with the addition of the other samples as indicated on Table 1.

6.4 Results and Discussions

The samples were periodically weighted (wet weight) to monitor deterioration. These results are shown in Table 2. The weight with an asterisk indicates a sample that had broken. The samples with a prime mark were loaded before subjected to cycling (Tables 1 and 2).

Table 2 shows that the marble samples were not affected by sodium sulfate. Even after 77 cycles, the weight of original samples were unchanged. It was interesting that the marble samples with crack induced by external mechanical load were not affected by sodium sulfate even after 52 cycles. The concrete with 0.3 water to cement ratio was equally unaffected by the sodium sulfate cycles, but on the other hand the 0.7 water to cement ratio concrete had a 44% weight loss after 55 cycles (Table 3). The amount of damage is a function of the permeability of the samples. For the marble samples and for the concrete with low water to cement ratio the permeability is low therefore the resulting damage from sodium sulfate cycles is also low.

6.5 References

1. Seidell, A. and Linke, W.F., " Solubilities of Inorganic and Metal-Organic Compounds," American Chemistry Society, Washington, D.C., 1965, p.1122.

2. Sperling, C.H.B, and Cooke, R.U., " Laboratory Simulation of Rock Weathering By Salt Crystallization and Hydration Processes In Hot, Arid Environment," *Earth Surface Processes and Landforms*, Vol. 10, 1985, pp. 541-555.

3. Knacke, O. and von Erdberg, R., " The Crystallization Pressure of Sodium Sulphate Decahydrate," *Berichte der Bunsen-Gesellschaft*, Vol. 79, nr 8, 1975, pp. 653-657.

Date	# Cycles	Vt/Ga/It	Vt'/Ga'/It'	0.3 Concrete	0.7 Concrete
October					
23	1	x			
24	1	x			
26	1	x			
28	2	x			
29	2	x			
30	1	x			
31	2	x			
November					
1	2	x			
2	2	x			
3	2	x			
4	2	x			
5	2	x			
6	2	x			
8	1	x			x
9	2	x			x
11	2	x	x	x	x
12	2	x	x	x	x
13	1	x	x	x	x
14	1	x	x	x	x
15	1	x	x	x	x
16	2	x	x	x	x
17	1	x	x	x	x
18	2	x	x	x	x
19	1	x	x	x	x
20	1	x	x	x	x
21	1	x	x	x	x
22	1	x	x	x	x
23	1	x	x	x	x
24	2	x	x	x	x
25	1	x	x	x	x
30	1	x	x	x	x
December					
2	2	x	x	x	x
3	1	x	x	x	x
4	1	x	x	x	x
5	1	x	x	x	x
6	1	x	x	x	x
7	1	x	x	x	x
8	2	x	x	x	x
9	1	x	x	x	x
10	1	x	x	x	x
14	2	x	x	x	x
15	1	x	x	x	x
16	2	x	x	x	x
17	1	x	x	x	x
18	1	x	x	x	x
19	1	x	x	x	x
20	1	x	x	x	x
22	1	x	x	x	x
23	2	x	x	x	x
24	1	x	x	x	x
26	1	x	x	x	x
27	2	x	x	x	x
28	1	x	x	x	x
29	1	x	x	x	x
30	2	x	x	x	x
Total Cycles		77	52	52	55

Table 1

Sample	Initial Weight (g)	Weight (g) 12/9	Final Weight (g) 1/12
Vt1	310.41	310.54	HCl
Vt2	341.88	341.79	341.72
Vt3	338.65	338.73	338.66
Ga1	368.13	368.32	HCl
Ga2	372.85	373.09	373
Ga3	387	387.1	387.05
It1	306.1	306.27	HCl
It2	317.69	317.8	317.78
It3	315.5	315.6	315.54
Vt1'	343.56	343.93	343.85
Vt2'	343	337.63*	331.18*
Vt3'	376.34	376.4	373.43*
Ga1'	337.09	311.59*	321.09*
Ga2'	344.77	344.6	344.04
Ga3'	333.47	332.36	332.24
It1'	355.7	355.25	354.2
It2'	363.75	364.2	364.27
It3'	356.89	357.32	357.26
0.3C1	324.9	327	324.66
0.3C2	325.97	328.18	326.65
0.3C3	324.53	326.46	324.7
0.7C1	287.17	244.66	166.08
0.7C2	300.68	223.15	163.29
0.7C3	286.08	220.1	160.33

Table 2

Sample	Weight Loss (%)
Vermont Marble	0
Georgia Marble	0
Italian Marble	0
0.3 w/c Concrete	0
0.7 w/c Concrete	44

Table 3

CHAPTER 7

CONCLUSIONS

The use of fracture mechanics can provide scientific basis for the design of marble elements. This research suggested a new test method for the measurement of the fracture toughness of different types of marble. The test is based on the traditional "Brazilian" or splitting test performed under constant strain rate. The experimental procedure is extremely simple and it does not require polishing of the sample; indeed extracted cores can be tested directly. The drawback of the test is that no close form solution for the stress intensity factor is available. This work presented the use of the finite element method for the calculation of the stress intensity factors and describes an experimental program developed to calculate the toughness of different types of marble. Four types of marble were tested in a Brazilian test under controlled strain rate. The test was fully controlled as it can be observed by the stable crack growth that originates the strain softeneing once the maximum load is achieved. Using the results obtained from the finite element methods it was possible to compute the fracture toughness of the various types of marble. It was found that there is an inverse relationship between fracture toughness and crystal size.

The sensitivity of marble samples to slow crack growth was investigated. It is well-known that for many structural materials the strength is dependent on how fast the stress is applied. Brittle materials such as glass, mortar, and concretes are very sensitive to the load rate. Comparatively little study has been performed on the sensitivity of marble and how marbles with different grain size behave under different load rate. The fundamental equation relating strength and load rate was derived for the four types of marble studied:

Italian Marble

$$S_f^{46.93} + 1.21\,\dot{\sigma}\,S_f^{43.93} = 2.99\,10^{6}\,\dot{\sigma}$$

Georgia Marble (I)

$$S_f^{33.25} + 0.38\,\dot{\sigma}\,S_f^{29.26} = 1.16\,10^{-4}\,\dot{\sigma}$$

Georgia Marble (II)

$$S_f^{32.26} + 1.84\,\dot{\sigma}\,S_f^{29.26} = 2.60\,10^{10}\,\dot{\sigma}$$

Vermont Marble

$$S_f^{29.41} + 1.74\,\dot{\sigma}\,S_f^{26.41} = 4.17\,10^{9}\,\dot{\sigma}$$

Chinese Marble

$$S_f^{47.62} + 5.56\,\dot{\sigma}\,S_f^{44.62} = 8.96\,10^{14}\,\dot{\sigma}$$

These equations are non-linear so a program was written for Mathematica and the values were computed numerically. It was found that there is a correlation between the value n and the crystal size of the marble.

The preservation of stress-induced structure and the identification of cracks induced by loading and unloading are important to understand the mechanisms for the generation, propagation and interaction of stress-induced microcracks in complex systems such as marble. To preserve the microstructure in marble specimens under load, the voids were filled with a liquid metal alloy called "Wood's metal" during loading, and the alloy was solidified in place before unloading. Cylindrical marble specimens were submerged in the molten metal alloy during the test and the alloy was driven into voids and fractures by pore pressure. With a surface tension of 400 mN/m, the alloy could penetrate into flat cracks with apertures as fine as 0.08 microns under a pore pressure of 1500 psi. Such a technique not only allows one to observe the microcracks as they exist under load, but also facilitates observing the microcracks in three dimensions . A comprehensive image analysis was performed on the cracking pattern developed in the marble samples. Also the propagation of the cracking process was modeled using discontinuous deformation analysis with finite element mesh. The discontinuous approach provides another way to understand the postfailure effect and global stability of the structure system.

The effects of various naturally occurring elements on building materials is critical knowledge when deciding on safe and appropriate application. It is well documented that sodium sulfate deteriorates some rocks. This investigation determined the effects on marble when submerged in a sodium sulfate solution that was cycled across the crystallization temperature for mirabilite. The samples were periodically weighted (wet weight) to monitor deterioration. The marble samples were not affected by sodium sulfate. Even after 77 cycles, the weight of original samples were unchanged. It was interesting that the marble samples with crack induced by external mechanical load were not affected by sodium sulfate even after 52 cycles. The concrete samples with 0.3 water to cement ratio was equally unaffected by the sodium sulfate cycles, but on the other hand the 0.7 water to cement ratio concrete had a 44% weight loss after 55 cycles. The amount of damage is a function of the permeability of the samples. For the marble samples and for the concrete with low water to cement ratio the permeability is low therefore the resulting damage from sodium sulfate cycles is also low.